2023

HOW TGFBR1 SHAPES THE VERTEBRATE POSTERIOR BODY

Molecular mechanisms of Gdf11/Tgfbr1 activity regulating the trunk to tail transition and development of posterior appendages

Anastasiia Lozovska

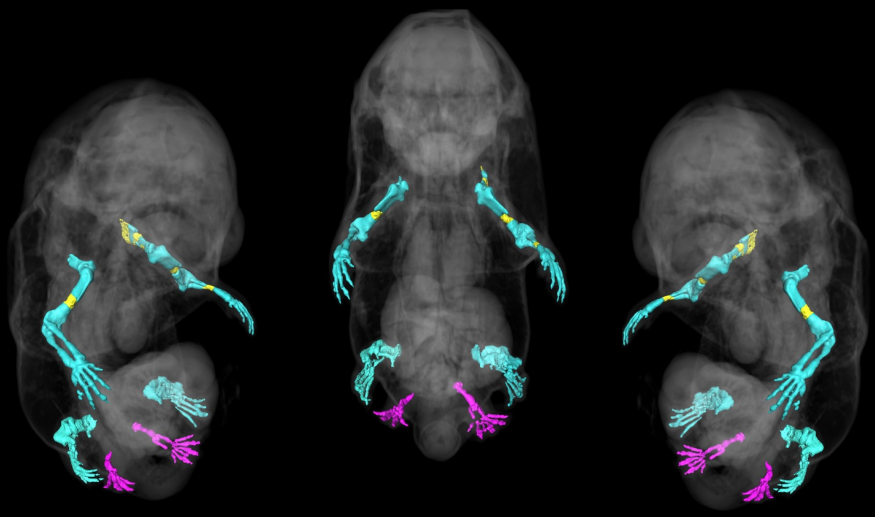

Dissertation presented to obtain the **Ph.D degree in** Integrative Biology and Biomedicine

Oeiras, July, 2023

INSTITUTO DE TECNOLOGIA QUÍMICA E BIOLÓGICA ANTÓNIO XAVIER | UNIVERSIDADE NOVA DE LISBOA

HOW TGFBR1 SHAPES THE VERTEBRATE POSTERIOR BODY

Molecular mechanisms of Gdf11/Tgfbr1 activity regulating the trunk to tail transition and development of posterior appendages.

Anastasiia Lozovska

Dissertation presented to obtain the Ph.D degree in Integrative Biology and Biomedicine

Instituto de Tecnologia Química e Biológica António Xavier | Universidade Nova de Lisboa

Research work coordinated by:

INSTITUTO GULBENKIAN DE CIÊNCIA

Oeiras, July, 2023

ITQB UNIVERSIDADE NOVA DE LISBOA

The work presented in this thesis was supported by FCT grant
PD/BD/128437/2017

FCT Fundação para a Ciência e a Tecnologia

Оксані

яка дуже любила дисертації

TABLE OF CONTENTS

ACKNOWLEDGEMENTS

I would like to thank my colleagues from the Patterning and Morphogenesis lab. Thank you to Moisés, for his enthusiasm for science and this project in particular, and for the immense amount of work that he contributed. I also thank him for his kindness, for showing me how to look at questions from different perspectives, and for encouraging my independent thinking.

Thank you to Ana Casaca and Rita Aires, for patiently teaching me standard laboratory techniques from scratch. A special thank you to Ana Casaca, who helped me resolve many technical difficulties, for always being genuinely interested in finding solutions, and for her willingness to go through volumes of old lab books to find the answer.

Thank you to Ana Nóvoa, for her invaluable input in establishing new mouse models, and also for her caring attitude (and for sharing cookies).

Thank you to André Dias, for his dedication to science, for his input in this work, and for his advice. Thank you to Patrícia Duarte, my tea-mate, for sharing her knowledge of data analysis and then sharing my excitement for the results. Thank you to Artemis Korovesi, for her help at the final stages of this project. I am happy that someone so curious and full of ideas will continue this work. Thank you to Tiago Carneiro for his sympathy and friendship.

Thank you to all members of the lab, past and present, for the amazing environment that we have in the lab. I am grateful for all the help that I received during these years; for the support and advice that you gave me at during times when things did not go smoothly; finally, for your kindness and understanding during the most difficult times.

I want to thank my thesis committee, Vera Martins and Diogo Castro, for following my project throughout all these years and for giving valuable feedback. Thank you for always being supportive and acting in my best interest.

Thank you to everyone involved in the IBB program – to Ana Aranda da Silva, Particia Gomes, Élio Sucena, Alekos Athanasiadis and Jorge Carneiro. A special thank you to Ana Aranda da Silva, who joined IGC the same year as I did, and put in an incredible amount of hard work and dedication to make things right from the start rather than to learn from mistakes. Thank you to Élio Sucena (and the selection committee), for accepting me to this program and giving me the opportunity to work at the special place that IGC is. Thank you to Pedro Fernandes for organizing great training courses and to IGC for the opportunity to freely attend them. Of course, thank you to my PhD cohort IBB 2017, for being my friends, for all the fun moments we shared, and for making IGC more than a workplace.

Thank you to the research support units at IGC. To the mouse facility, especially to Sofia Leocádio, Marília Perreira, Joana Bom and Ana Ribeiro, for the training and technical support that they provided. Thank you to Carla Almada for taking good care of our mouse colonies. To the advanced imaging unit, especially to Gaby Martins for the countless times that he helped with data acquisition and analysis. And also, for his interest and excitement for his work. To Joana Rodrigues and Andrea Mindouro from the histopathology unit for their assistance and for making long hours at the vibratome more pleasant. To the genomics unit, especially to João Sobral, for his willingness to help and for never getting tired of troubleshooting.

I want to thank Portugal for being my home for more than six years, for its kind and welcoming people, and of course for supporting my PhD training from public funding. I also want to thank my home country Ukraine for giving me access to free education. Thank you to my teachers from the University of Kyiv, especially to Tetiana Kutsenko for her excitement for science, for her support and encouragement. Thank you to all the bright people that I met there. Some will hopefully stay my lifelong friends.

Дякую моїй родині за те, що навчили мене цінувати знання. Люсі і Олексі за книжкові лабіринти в дідовому кабінеті. Володі, за те, що дивився зі мною на зірки і пояснював фізику природних явищ. Оксані, за те, що прищепила важливість освіти. Славі, за її любов і підтримку. Сергію, за його любов до природи, і за те, що я стала біологом. Марині, за її допомогу під час пошуку докторської програми. І, звичайно, Микиті, за те, що був поруч зі мною останні 13 років, за те, що був готовий змінити своє життя заради мене і за його безмежну любов і підтримку.

SUMMARY

Signaling pathways regulate multiple aspects of vertebrate embryonic development. Members of Transforming Growth Factor β (Tgfβ) superfamily in particular, are involved in embryogenesis starting from the earliest cell-fate decisions and including establishment and patterning of the main body axis and its appendages. One of Tgfβ family ligands, Growth differentiation factor 11 (Gdf11), is an evolutionary conserved regulator of vertebrate trunk length due to its function as inductor of the trunk to tail transition. In the context of trunk to tail transition Gdf11 activities are mediated by the Tgfbr1 type I receptor: its premature activation in axial progenitors region is sufficient to induce the transition more anteriorly.

Previously trunk to tail transition was mainly studied from the perspective of patterning of the main body axis. Establishment of the boundary between the trunk and tail compartments, however, is associated with multiple vital functions of an organism. Proper development of the caudal trunk region, associated with the trunk to tail transition, ensures realization of reproductive, excretory and locomotory functions of an adult organism as the outlets of digestive and urogenital systems and the hindlimbs are located at this axial level. Trunk to tail transition is, therefore, a complex integrative process involving massive tissue rearrangement and tightly connecting the main and secondary body axes. In this work we studied the mechanisms of Gdf11/Tgfbr1 dependent regulation of the trunk to tail transition.

Trunk most apparently differs from tail by the presence of the lateral plate mesoderm (LPM) derivatives - namely internal organs and body appendages. Vertebrate column, spinal cord, and musculature, on the other hand, are present in both trunk and tail. Moreover, these tissues derive from the continuous population of progenitor cells able to generate paraxial mesoderm and neural tissue – neuro-mesodermal competent cells (NMCs). During the trunk formation, these cells are located in the epiblast, proximally to the lateral plate

mesoderm progenitors. At the time of the trunk to tail transition, LPM progenitors exit resolving epiblast, while NMCs are relocated to the newly formed niche in the tail bud to support tail growth. Both epiblast and tail bud progenitor cell populations, including NMCs and progenitors of the LPM will be referred to as axial progenitors.

First, we investigated how axial progenitors' gene expression profile is changed after the trunk to tail transition and identified genes under the control of *Gdf11* in this context. Our results suggest the pivotal role of *Gdf11* in the downregulation of the trunk related LPM genes and activation of posterior *Hox* genes in the caudal growth zone. Additionally, *Gdf11* regulates many cell adhesion molecules, which possibly reflects rearrangements associated with the progenitors relocation to the tail bud. Our differential gene expression analysis also uncovers *Gdf11's* involvement in activity of multiple other signaling pathways, particularly Wnt, Shh and Fgf-MAPK. Finally, analysis of chromatin accessibility patterns suggest that changes in gene expression following trunk to tail transition are mainly regulated by distal enhancers.

Despite the evident requirement of Gdf11 for the timely transition, apparent redundancy with other Tgf-β ligands leads to delayed, rather than absent, trunk to tail transition in *Gdf11* mutants. Therefore, we dedicated the next part of this work to characterization of the *Tgfbr1* mutant, in which any redundancy is eliminated. Our results confirm Tgfbr1 requirement to realize the trunk to tail transition both on cellular and tissue levels. On the cellular level, we show that axial progenitors in *Tgfbr1* mutants fail to delaminate from the epiblast and therefore, cannot efficiently relocate to the tail bud. Furthermore, axial progenitors are unable to induce tail-specific growth regulators and maintain their population. On the tissue level, *Tgfbr1* mutants fail to properly organize trunk caudal end, most evident by inability to induce hindlimb buds, bring together LPM layers and to form cloaca and pericloacal mesenchyme – precursor of external genitalia. Therefore, we show that Tgfbr1 regulates all the

main aspects of the trunk to tail transition, and we suggest that its activity in the lateral plate mesoderm is realized upstream of *Isl1*.

Finally, in the last part of the thesis we investigated the role of *Tgfbr1* in development of trunk caudal appendages – the hindlimbs and external genitalia – past its requirement to induce these structures. We uncovered remarkable plasticity between precursors of these appendages. In the absence of Tgfbr1, the pericloacal mesoderm generates an extra pair of hindlimbs at the expense of the external genitalia. This striking observation is particularly interesting from the evolutionary perspective: it has been proposed that in ancestral species the hindlimbs and external genitalia share their developmental origin. In mammals, hindlimbs and external genitalia are generated from different primordia, which, nonetheless, share many of their key regulatory factors. Tgfbr1 controls the response to those factors by modulating the chromatin accessibility status of their *cis*-regulatory elements.

In this work we comprehensively studied functions of Gdf11/Tgfbr1 signaling in context of trunk to tail transition and associated appendages development. Our results elaborated the molecular mechanisms driving the trunk to tail transition and expanded our understanding of this process. Additionally, we uncovered a novel mechanism downstream of the Tgfbr1 signaling as a regulator of the tissue specific response to common factors in the hindlimb and genital primordia.

SUMÁRIO

As vias de sinalização regulam vários processos durante o desenvolvimento embrionário dos vertebrados. Por exemplo, os membros da superfamília dos fatores de transformação de crescimento beta (Tgfβ) estão envolvidos em múltiplos contextos embrionários; desde as primeiras decisões sobre o destino celular, até ao estabelecimento e padronização do eixo principal do corpo e dos seus apêndices. Um dos ligandos da família Tgfβ, o fator de diferenciação de crescimento 11 (Gdf11), está descrito como um regulador evolutivamente conservado do comprimento do tronco dos vertebrados, dada a sua função como indutor da transição do tronco para a cauda. Neste contexto, a atividade de Gdf11 é mediada pelo recetor Tgfbr1 tipo I: a sua ativação prematura na região dos progenitores axiais é suficiente para induzir a ocorrência da transição num nível axial mais anterior.

Em estudos anteriores foi analisada a transição do tronco para a cauda, principalmente do ponto de vista da padronização do eixo principal do corpo. Contudo, o estabelecimento da fronteira entre os compartimentos do tronco e da cauda, está também associado a várias funções vitais de um organismo. Deste modo, o desenvolvimento adequado da região caudal do tronco, associado a esta transição, assegura as funções reprodutoras, excretoras e locomotoras de um organismo adulto; uma vez que as saídas dos sistemas digestivo e urogenital, assim como os membros posteriores, se situam a este nível axial. A transição do tronco para a cauda é, por conseguinte, um processo integrativo complexo que envolve uma reorganização geral dos tecidos, ligando os eixos principais e secundários do corpo. Neste trabalho, estudámos os mecanismos de regulação dependentes da via de sinalização Gdf11/Tgfbr1 subjacentes aos aspetos principais da transição do tronco para a cauda.

Essencialmente, o tronco difere da cauda pela presença de derivados da mesoderme da placa lateral (LPM) - nomeadamente, os órgãos internos e os apêndices corporais. Todavia, a coluna vertebral, a espinal medula e a

musculatura dos vertebrados estão presentes tanto no tronco como na cauda. Além disso, estes tecidos derivam de uma população contínua de células progenitoras capazes de gerar mesoderme paraxial e tecido neural – as células neuro-mesodérmicas competentes (NMCs). Durante a formação do tronco, estas células estão localizadas no epiblasto, na proximidade dos progenitores da mesoderme da placa lateral. Na fase da transição do tronco para a cauda, os progenitores da LPM saem do epiblasto em resolução, enquanto as NMCs se deslocam para um nicho recém-formado no botão caudal, promovendo o crescimento da cauda. As populações de células progenitoras do epiblasto e do botão caudal, incluindo as células NMCs e os progenitores da LPM, serão referidas como progenitores axiais.

Inicialmente, investigámos de que modo o perfil de expressão génica dos progenitores axiais é alterado após a transição do tronco para a cauda e identificámos genes sob o controlo de Gdf11 neste contexto. Os nossos resultados sugerem que Gdf11 é essencial na sob expressão dos genes da LPM relacionados com o desenvolvimento do tronco e também na ativação dos genes Hox posteriores, na zona de crescimento caudal. Além disso, Gdf11 regula a expressão de moléculas de adesão celular, o que possivelmente reflete rearranjos associados à relocalização dos progenitores para o botão caudal. A nossa análise de expressão génica diferencial também revelou o envolvimento de Gdf11 na atividade de outras vias de sinalização, particularmente Wnt, Shh e Fgf-MAPK. Finalmente, a análise dos padrões de acessibilidade da cromatina sugere que as alterações na expressão génica após a transição do tronco para a cauda são reguladas principalmente por enhancers distais.

Apesar de Gdf11 ser indispensável para a ocorrência da transição tronco-cauda no momento adequado, a sua redundância aparente com outros ligandos Tgf induz um atraso, em vez da ausência, da transição nos mutantes Gdf11. Assim, na parte seguinte deste trabalho procedemos à caraterização de mutantes Tgfbr1, nos quais qualquer redundância é eliminada. Os nossos resultados confirmam a necessidade do recetor Tgfbr1 para a ocorrência da

transição tronco-cauda, tanto a nível celular como a nível dos tecidos. A nível celular, mostramos que os progenitores axiais, nos mutantes Tgfbr1, não conseguem delaminar do epiblasto e, portanto, não se deslocam eficientemente para o botão caudal. Além disso, os progenitores axiais não são capazes de induzir a expressão de reguladores de crescimento específicos da cauda e de manter a sua população. A nível dos tecidos, os mutantes Tgfbr1 não conseguem organizar corretamente a extremidade caudal do tronco, tornando-se isto evidente pela incapacidade de induzir os botões embrionários dos membros posteriores, de agrupar as camadas da LPM e de formar a cloaca e o mesênquima pericloacal -precursor da genitália externa. Assim, mostramos que Tgfbr1 regula os aspetos principais da transição do tronco para a cauda e sugerimos que a sua atividade na mesoderme da placa lateral ocorre a montante do fator Isl1.

Finalmente, na última parte da tese, investigámos o papel de Tgfbr1 no desenvolvimento dos apêndices posteriores do tronco - os membros posteriores e a genitália externa – para além de ser necessário para induzir estas estruturas, tendo a nossa análise revelado uma plasticidade notável entre os precursores destes apêndices. Na ausência de Tgfbr1, a mesoderme pericloacal gera um par extra de membros posteriores, à custa da genitália externa. Esta observação surpreendente é interessante do ponto de vista evolutivo: é geralmente aceite que nas espécies ancestrais, os membros posteriores e os órgãos genitais externos partilham a mesma origem embrionária. Nos mamíferos, os membros posteriores e os genitais externos são formados a partir de primórdios diferentes, mas que partilham vários fatores reguladores. Tgfbr1 controla esta resposta, pela modulação do estado de acessibilidade à cromatina dos elementos regulatórios em cis destes fatores.

Neste trabalho, estudámos exaustivamente as funções da sinalização Gdf11/Tgfbr1 no contexto da transição do tronco para a cauda e no desenvolvimento dos respetivos apêndices. Os nossos resultados permitiram compreender melhor os mecanismos moleculares que determinam a transição do tronco para a cauda, aprofundando o conhecimento geral sobre este

processo. Adicionalmente, descobrimos um novo mecanismo a jusante da sinalização Tgfbr1, responsável pela regulação da resposta tecidular específica a fatores presentes tanto nos primórdios dos membros posteriores como nos genitais.

Chapter 1

GENERAL INTRODUCTION

Embryonic development is an incredibly complex yet robust process resulting in formation of an entire body from a single cell. During this process limited number of conserved regulatory modules are repurposed and modified to generate variety of different structures. Timely coordination between the main patterning events results in development of an organism with specific phenotypical features. These include, for example, particular length of the main body compartments and shape of the appendages. In this chapter we will follow a mammalian embryo from the first cell divisions up to the time when the main body plan is being established.

Preimplantation development

After fertilization, mammalian embryo starts forming new blastomeres by series of symmetrical divisions which, by embryonic stage (E) 2.5 in the mouse embryo, forms the 8-cell morula (Figure *1-1*). Until this stage all blastomeres are uniform in terms of position, polarity, and cell-cell contact (Frum and Ralston, 2015). At the 8-cell stage, however, blastomeres start polarizing along the apical-basal axis (Johnson and Ziomek, 1981), undergo compaction by forming more cell-cell contacts and acquiring contractile function (Maître et al., 2015). At the same time, morula cells start differentially expressing some lineage specific markers, preparing the embryo for differentiation (Guo et al., 2010; Sasaki, 2015). Closely thereafter, formation of the first fluid-filled lumen – the blastocele – breaks radial symmetry of the morula (Kim and Bedzhov, 2022). These rearrangements lead to blastomeres' reorganization into the outer and inner layers, resulting in the formation of the blastocyst by the 32-cell stage (Figure *1-1*).

At the blastocyst stage the first lineage differentiation event occurs in the embryo: formation of the trophectoderm (TE) from the outer cell layer, and of the inner cell mass (ICM) from the cells located inside. The TE maintains extra embryonic ectoderm (ExE) fate and will eventually form the embryonic portion of the placenta. At the mid-blastocyst stage two cell types become specified

within the ICM to further differentiated into primitive endoderm (PrE) and pluripotent epiblast (Figure *1-1*) (Zhang and Hiiragi, 2018).

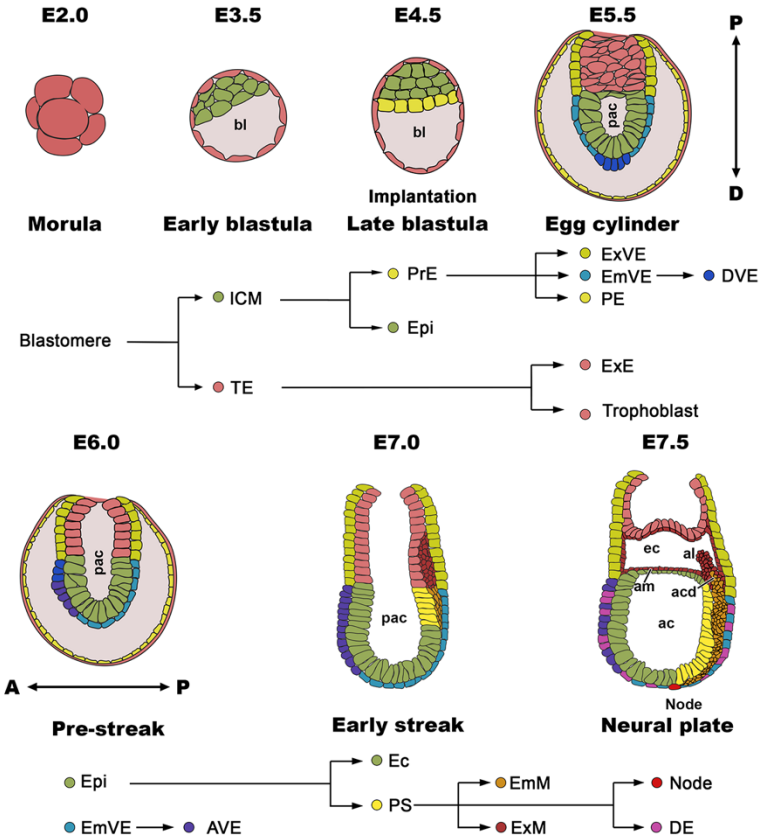

Figure 1-1. Early mouse embryonic development. Schematic representation of mouse development from morula stage to gastrulation. The first cell fate decision in the mouse embryo takes place at E3,5 by blastomeres differentiation into the inner cell mass (ICM) and trophectoderm (TE). Once the embryo implants at E4,5 ICM differentiates into epiblast (Epi) and primitive endoderm (PrE). At E5,5 proximo distal axis (P-D) is formed in the embryo as it acquires cylindrical shape. TE contributes to trophoblast and extraembryonic ectoderm (ExE). PrE gives rise to parietal endoderm (PE), embryonic (EmVE) and extraembryonic (ExVE) visceral endoderm. Distal visceral endoderm (DVE) cells are restricted to distal most part of the cylinder by inhibiting signals from ExE. At E6.0 DVE cells move to the prospective anterior side of the embryo recruiting anterior visceral endoderm (AVE) cells, and thus establishing arterio-posterior (A-P) axis. At E7.0 primitive streak (PS) is formed at the posterior past of epiblast and extraembryonic (ExM) and embryonic (EmM) mesoderm is being formed by ingression through PS. When PS reaches the distal part of the cylinder node is formed on its anterior end. Definitive endoderm (DE) is formed from ingression through PS and is intercalated between EmVE cells. Epiblast forms embryonic and amniotic ectoderm (Ec). bl – blastocele, pac – pre amnionic cavity, ec – exocelom, ac – amniotic cavity, am – amnion, acd – allantois core domain, al – allantois. Adapted from Rivera-Pe´rez and Hadjantonakis, 2015.

Gastrulation and symmetry breaking

Upon implantation (at E4.5) mouse embryo starts acquiring a cylinder shape (Figure *1-1*). First, epiblast cells are anchored to the basal membrane and form a polarized epithelium. Epiblast growth and proliferation pushes it inside the blastocoel. This allows for initiation of lumenogenesis at the apical side of epiblast cells, leading to formation of the proamniotic cavity at the embryo's proximal end (Kim and Bedzhov, 2022). The PrE, which adjoins the epiblast since the blastocyst stage, now expands lining the inner wall of the trophoblast, and thus forming parietal endoderm. The remaining PrE forms the visceral endoderm (VE), which is divided into embryonic (emVE), covering the epiblast, and extra-embryonic (exVE) covering proximally located ExE (Figure *1-1*).

For further differentiation radial symmetry of the embryo is broken to establish the main body axis. In the mouse this process is initiated at the distal side of the emVE. The cylindrical shape of the mouse embryo allows to create a proximo-distal signal gradient. Nodal gradient in the emVE results from inhibition by Bmp4 expressed in the proximally located ExE. Low Nodal in the distal emVE favors generation of the distinct cell population called the distal VE (DVE) (Figure *1-1*) (Ben-Haim et al., 2006; Yamamoto et al., 2009). Shortly thereafter the DVE starts to asymmetrically express the Nodal inhibitors Lefty and Cer1, which reinforce Nodal gradient and initiate DVE migration towards the proximal region following the lower Nodal levels. As the DVE migrates, a distal population of VE cells are recruited to move along, eventually generating a structure known as anterior VE (AVE) (Kumar et al., 2015; Yamamoto et al., 2004). AVE's final location determines the anterior side of the embryo.

The AVE secrets signaling inhibitory factors – including the Nodal inhibitors Lefty1 and Cer1, and the Wnt inhibitor Dkk1 – instructing the epiblast to acquire anterior ectoderm fate (Figure *1-2*B) (Robertson, 2014). Posterior epiblast, in turn, accumulates higher levels of Nodal and Wnt (Figure *1-2*B). Early Nodal expression in the epiblast is required to keep it pluripotent, by maintaining expression of *Oct4* and *Nanog* (Mesnard et al., 2006). These

transcription factors, together with Sox2, are considered to be at the core of the epiblast pluripotency network, in part by repressing lineage specific genes. (Yeh et al., 2021)

Crosstalk between the epiblast and the ExE results in the induction of the primitive streak (PS) at the proximal end of the posterior epiblast adjoining the ExE. Nodal produced from the epiblast reinforces expression of *Bmp4* in the distal ExE, which in turn signals back to the epiblast and induces *Wnt3* expression. *Wnt3* expression in the epiblast induces PS formation, also being required for its maintenance, and subsequent activation of *Brachyury* (now called *Tbxt)*, which becomes a PS marker (Huelsken et al., 2000; Liu et al., 1999; Rivera-Pérez and Magnuson, 2005; Tortelote et al., 2013). Wnt3 also upregulates *Nodal* and its co-receptor *Cripto* in the epiblast, thus generating a positive feedback loop (Figure *1-2*C) (Shen, 2007).

During PS formation epiblast cells lose their basal lamina, polarity, and epithelial junctions to adopt a mesenchymal fate and prepare for migration – a process called epithelial to mesenchymal transition (EMT) (Williams et al., 2012). Switch from E-cadherin to N-cadherin is one of the signature features of EMT. In the PS it is regulated by a set of factors, including the transcription

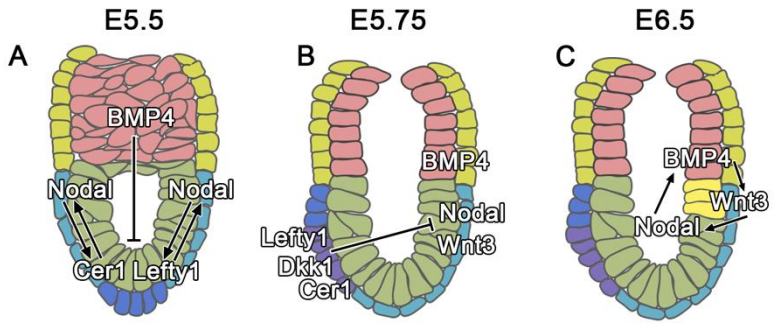

Figure 1-2. Formation of the antero-posterior axis. A. Formation of DVE (blue) at the distal part on the cylinder resulting from Nodal gradient. **B.** Restriction of Nodal and Wnt3 to the posterior end by inhibitory signals from AVE (purple). **C.** Induction of the primitive streak (yellow) at the posterior end of epiblast (green). Adapted from Bardot and Hadjantonakis (2020).

factors Snai1 and Eomes, and FGF signaling (Amack, 2021; Bardot and Hadjantonakis, 2020).

First wave of cells ingressing through PS forms extraembryonic mesoderm, which gives rise to blood islands, yolk sack vasculature, and later the allantois bud (Figure *1-1*) (Downs and Rodriguez, 2020; Robertson, 2014). Similarly, cranial, and cardiac mesoderm are among the first tissues to be formed from posterior epiblast ingression (Bardot and Hadjantonakis, 2020). The definitive endoderm (DE) is also generated from the epiblast early in gastrulation, retaining some epithelial properties, to intercalate into the VE cells and form the gut tube (Figure *1-1*), which also have contribution from the VE cells themselves (Cambray and Wilson, 2002; Kwon et al., 2008; Scheibner et al., 2021; Tzouanacou et al., 2009). As the PS elongates, *Nodal* expression becomes confined to the PS anterior end, eventually forming the node (Figure *1-1*). The node is essential for the formation of the notochordal plate – a DE cell population, which eventually transforms into the notochord, a structure involved in neural tube and gut dorsal-ventral patterning (Balmer et al., 2016).

Neuro mesodermal competent cells

The classical view considering that the whole embryo is derived from the three germ layers formed during gastrulation by cells delaminating from pluripotent epiblast, has been predominant for a long time. Recent discoveries using grafting and lineage tracing experiments have however challenged this view and redefined the concept of germ layers.

First, not all embryonic tissues derive from the epiblast. For example, the posterior part of the gut tube, in addition to the DE cells formed during gastrulation, have significant contribution from the VE (Nowotschin et al., 2019; Peng et al., 2019). Furthermore, lineage differentiation into derivatives of two different germ layers continues after gastrulation has ceased. In particular, a pool of progenitors with the capacity to self-renew and potency to enter either neural or mesodermal fates is present in the epiblast throughout trunk

extension and later in the tail bud (Cambray and Wilson, 2007, 2002; Tzouanacou et al., 2009), indicating that germ layer differentiation persists throughout the process of axial extension and is not confined to gastrulation (Figure *1-3*).

Although often referred to as a single population, these progenitors are not homogeneous, being instead comprised of the mono-fated neuro-mesodermal competent (NMC) cells (Binagui-Casas et al., 2021), capable to give rise to either neural or mesodermal descendants; and of bi-fated neuro mesodermal progenitor cells (NMPs), which upon division generate both neural and mesodermal cell derivatives (Attardi et al., 2019; Binagui-Casas et al., 2021). Correspondingly, these cells are typically characterized by double expression of the neural marker *Sox2* and the mesodermal marker *Tbxt*.

There is a certain level of plasticity within the NMC population. In mouse embryos, cells located closer to the node adopt neural fates, while cells residing more caudally within the node-streak border (NSB) and exposed to higher Wnt3a levels contribute to paraxial mesoderm (Jurberg et al., 2013; Wymeersch et al., 2016). Additionally, Bmp4 was shown to regulate *Tbxt* expression and thus to promote paraxial mesoderm formation (Sharma et al., 2017). Exposure to retinoic acid (RA), on the contrary, prompts NMC cells toward neural fates (Gouti et al., 2017).

NMC cells rely on multiple factors to confer their capacity to self-renew. Transcription factors Cdx2 and Tbxt, and members of the Wnt and FGF signaling pathways seem to be the core elements maintaining the pool of axial progenitors. Embryos deprived of these factors prematurely cease their extension at variable axial levels. *Wnt3a* mutant embryos, for example, are truncated just posterior to the forelimb (Takada et al., 1994), while *Fgf8/Fgf4* double mutants are able to accomplish formation of the trunk but are truncated at the sacral level (Boulet and Capecchi, 2012). Embryos deficient for *Cdx2/4* or *Tbxt* are both characterized by the most severe truncation phenotypes just posterior to occipital somites (Amin et al., 2016; Chawengsaksophak et al., 2004;

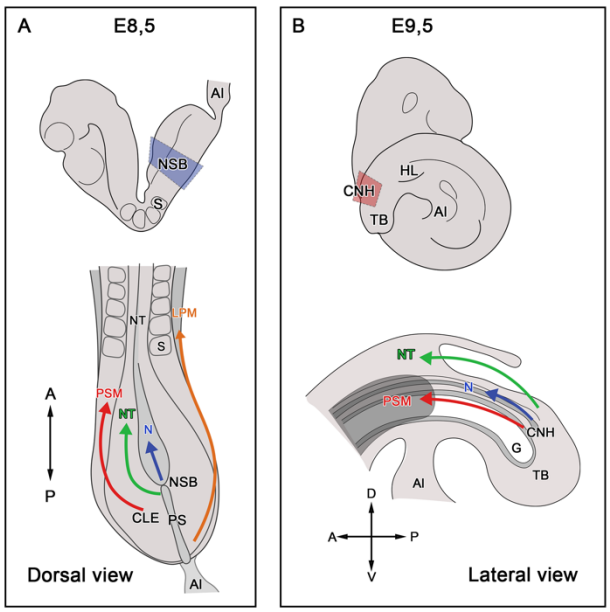

Figure 1-3. Axial progenitors during trunk and tail development. A. Before the trunk to tail transition axial progenitors are located in the epiblast and comprise NMCs located in the node-streak border (NBS – marked by blue shade in the upper panel) with potential to differentiate into neural and mesodermal tissue; notochord (N) progenitors located in the rostral node; and LPM progenitors in the most caudal part of the epiblast and primitive streak (PS). NMCs located more rostrally mainly contribute to the neural tube (NT), while progenitors located more posteriorly in the caudal lateral epiblast (CLE) contribute more to presomitic mesoderm (PSM) due to exposure to higher level of Wnt3a. **B.** After the trunk to tail transition LPM progenitors are depleted in the axial growth niche, while NMCs relocate to the chordo neural hinge (CNH – marked by red shade in the upper panel) in the tail bud (TB). S – somite, Al – allantois, G – gut.

van Rooijen et al., 2012). *In vitro* studies using epiblast stem cells suggest that Cdx2 and Tbxt act to sustain Fgf and Wnt signaling in the axial extension niche (Amin et al., 2016). Additionally, balance between RA activity and its timely clearance by the RA metabolizing enzyme Cyp26a1 is crucial to maintain posterior growth (Abu-Abed et al., 2001). Elevated RA levels are associated with premature cessation of axial extension, likely via inhibition of growth factors activity (Olivera-Martinez et al., 2012).

Timely termination of the axial extension is key to determine the length of an adult organism. In mouse embryos it is associated with activation of *Hox* genes of the paralog group (PG) 13. *HoxPG13* genes likely downregulate *Cyp26a1,* which results in accumulation of RA and block of activities required for growth, including Tbxt and Fgf8/4 (Aires et al., 2019; Olivera-Martinez et al., 2012; Young et al., 2009).

Making the trunk

Three major compartments are placed along the vertebrate antero-posterior axis: head, trunk, and tail. Formation of head structures mostly occurs in the early gastrulating embryo. Trunk and tail development are associated with the process of axial extension, when tissues are laid down from the caudally located progenitors in a sequential manner from anterior to posterior.

The epiblast is the source of progenitor cells for axial extension during trunk development (Wilson et al., 2009). Epiblast cells contribute to the neural tube, paraxial mesoderm, and lateral plate mesoderm (LPM), which eventually form most trunk structures (Wymeersch et al., 2016). The neural tube will develop into the spinal cord; the paraxial mesoderm form somites, which in turn, form organism's axial skeleton and musculature; the LPM contributes to the body wall, internal organs and their lining, as well as to the limb skeleton (Prummel et al., 2020).

Grafting and transcriptomic experiments revealed a fate map for the epiblast according to embryonic lineage contribution (Cambray and Wilson, 2007; Peng et al., 2019; Wymeersch et al., 2019, 2016). Particularly, paraxial mesoderm differentiates from the NMC-populated PS and lateral epiblast regions within the NSB, while cells from the caudal epiblast become the LPM (Figure *1-3*A) (Cambray and Wilson, 2007; Wymeersch et al., 2016). The intermediate mesoderm (IM), which mainly contributes to the urogenital system, is localized medially from the LPM, and have been considered a LPM subdivision (Prummel et al., 2019). Interestingly, a part of IM have been shown to derive from $Tbx6^{+}$ paraxial mesoderm cells, therefore from the NMC cells (Hayashi et al., 2021).

Despite the evident lineage separation of paraxial and lateral mesoderm already in the epiblast, some level of plasticity between the two neighboring tissues still remains: when exposed to high levels of BMP signaling, the somitic mesoderm acquires features characteristic of the LPM (Wijgerde et al., 2005).

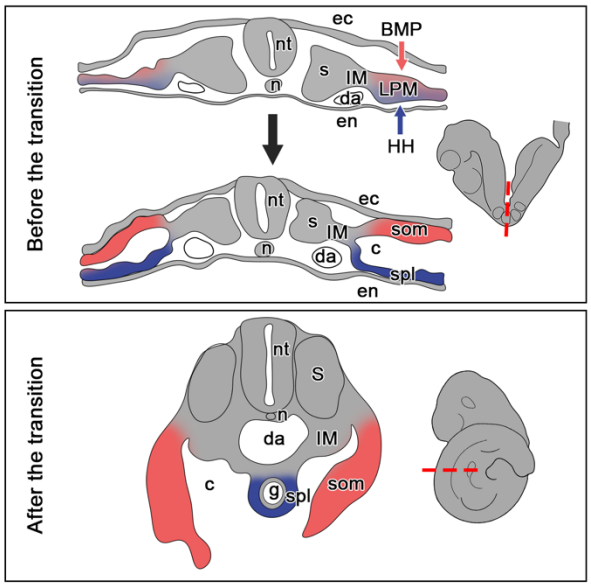

Figure 1-4. Development of the lateral plate mesoderm. Lateral plate mesoderm (LPM) divides into somatic (som) and splanchnic (spl) layers by responding to inductive signals from ectoderm (ec) and endoderm (en), respectively. Separation results in formation of the coelomic cavity (c) between the two LPM layers. After embryo turns, left and right LPM sheets are brought together. Splanchnic LPM surrounds the gut tube and somatic forms the body wall. da – dorsal aorta, nt – neural tube, n – notochord, IM – intermediate mesoderm, s – somite.

Bmp4 signals from LPM also regulate somite medial-lateral patterning and, consequently, influence development of axial skeleton (Tonegawa et al., 1997; Wijgerde et al., 2005).

The primitive LPM contacts with two epithelial layers: dorsal ectodermal and ventral endodermal. By expressing differential cues these epithelia induce dorsal-ventral subdivision of the primitive LPM into somatic and splanchnic layers, respectively, leaving the coelomic cavity between them (Figure *1-4*). Markers of splanchnic and somatic LPM – e.g., *Foxf1* and *Prrx1,* respectively – are first co-expressed in the primitive LPM and become restricted to their respective domains after the induction of subdivision (Funayama et al., 1999; Mahlapuu et al., 2001; Newton et al., 2022). Particularly important is the expression of *Foxf1* in the primitive LPM, necessary for LPM layer separation and thus formation of the coelom (Funayama et al., 1999). Somatopleure is formed in response to Bmp2/Bmp7 cues from the ectoderm, which upregulate *Prrx1* expression and induce expression of the LPM marker *Irx3*. Splanchnopleure, meanwhile, maintains *Foxf1* expression in response to Shh signaling from the endoderm (Astorga and Carlsson, 2007; Funayama et al., 1999; Mahlapuu et al., 2001; Newton et al., 2022).

Correct separation of the LPM into two layers is vital for normal development. The splanchnic layer of LPM forms the mesenchymal and smooth muscle layers of the organs of the gastrointestinal track, as well as the vascularization of all abdominal organs, while the body wall, and the limb skeleton and connective tissue originate from the somatic LPM (Prummel et al., 2020). The role of the LPM is then restricted to trunk formation. During the trunk to tail transition, this tissue is involved in the organization of the terminal part of the trunk by generating the caudal appendages and contributing to the formation of the excretory and digestive system outlets.

The trunk to tail transition

A combination of coordinated events coupled with extensive changes in gene expression leads to reorganization of the embryo caudal end preceding the trunk to tail transition. In the mouse this transition occurs between E8.5 and E9.0 and is characterized by reorganization of the axial extension niche, the establishment of the embryonic-extra embryonic bloodstream connection, the induction of trunk terminal appendages and the organization of excretory system outlets.

Switch of the axial extension niche.

As a final accord of gastrulation, axial progenitors undergo an incomplete EMT (Dias et al., 2020), which allows them to maintain differentiation potential and migrate to their new place of residence in the tail bud to continue axial extension (Figure *1-3*B) (Cambray and Wilson, 2007, 2002; Guillot et al., 2021). Activation of Gdf11 signaling in the posterior embryo at the time of transition is required to protect progenitors from excess RA by upregulating the RA degrading enzyme *Cyp26a1* and to successfully relocate them to the tail bud (Jurberg et al., 2013; Lee et al., 2010). Although axial progenitors are a continuous population contributing to trunk and tail neural tube and paraxial

mesoderm, gene regulatory networks conferring their differentiation potential change after the transition. While during trunk formation progenitors rely on *Oct4* expression to maintain potency and self-renewal capacity, during tail development *Lin28* and *Sall4* genes undertake this function (Aires et al., 2019, 2016; Robinton et al., 2019; Tahara et al., 2019).

Vascular remodeling and the trunk to tail transition.

In mouse embryos the trunk to tail transition is associated with turning. At this time, the main extraembryonic vessels – the umbilical and omphalomesenteric arteries - are brought closer together (Dobreva et al., 2010). The umbilical artery is brought anteriorly along the ventral side of the embryo by movement of the allantois – a finger-shaped structure adjacent to the distal PS during gastrulation (Figure *1-3*A) (Rodriguez et al., 2017; Rodriguez and Downs, 2017). During this process, the embryonic vasculature undergoes dramatic remodeling. Embryonic-extraembryonic bloodstream connection is being established by the vessel of confluence (VOC) located at the proximal end

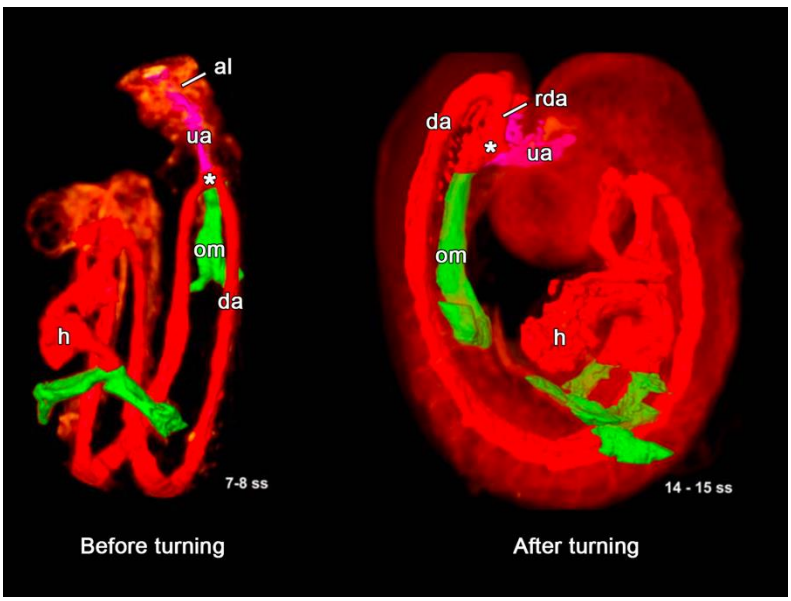

Figure 1-5. Main vascular tree during the trunk to tail transition. VOC (labelled by asterisk) merge with the dorsal aortae (da)and branches to form the recurved dorsal aortae (rda). ua – umbilical artery (magenta), om – omphalomesenteric artery (green). h – heart. Adapted from Walls 2009.

of the allantois (Figure *1-5*). The bifurcated VOC connects to the roots of the dorsal aorta (DA), thus forming its recurved portion (rDA), and sprouts to join umbilical and omphalomesenteric arteries (Rodriguez et al., 2017). Despite its extraembryonic origin, VOC development seems to be regulated by signals coming from the embryo proper. The proper contact between the base of allantois and the caudal PS before the formation of VOC is particularly important for VOC differentiation and development of its derivatives (Rodriguez et al., 2017).

Development of cloaca

The trunk to tail transition and embryo turning coincides with hindgut formation in mouse. As the allantois moves anteriorly its most proximal part eventually forms the hindgut lip – a structure that mediates collective migration of endodermal cells and hindgut invagination (Rodriguez et al., 2017). Shortly after the trunk to tail transition is completed, the hindgut itself undergoes major rearrangements: the cloacal cavity starts to be distinguishable in mouse embryos around E10.5. From E10.5 to E13.5 the cloaca is transformed from a gut widening into separate outlets for the urogenital and digestive systems as

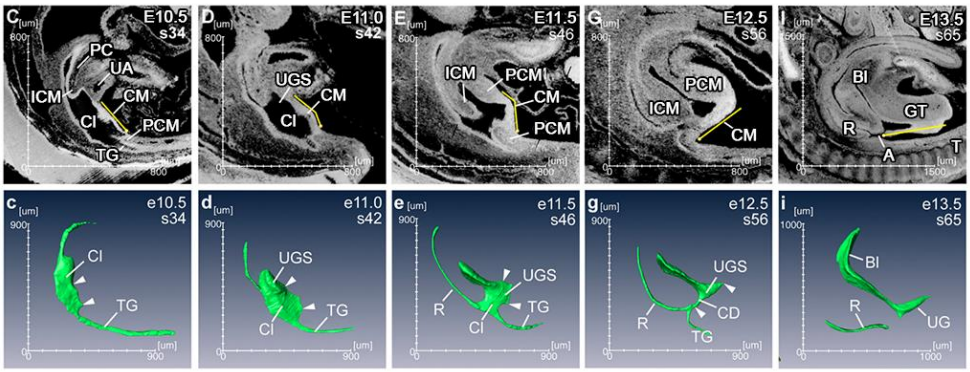

Figure 1-6. Cloaca septation resulting in formation of separate digestive and urogenital system outlets. The midline sagittal view (top) and 3D reconstruction (bottom) of mouse cloaca (Cl) from E10,5 to E13,5. ICM – intra-cloacal, PC – peritoneal cavity, UA – umbilical artery, CM - cloaca membrane (also labelled by yellow line), PCM - pericloacal mesenchyme, TG – tailgut, UGS - urogenital sinus, Bl – bladder, R – rectum, GT – genital tubercle, A – anus, T – tail, CD - cloacal duct, UG - urethral groove. Adapted from Huang 2016.

result of the process called cloacal septation (Figure *1-6*). Despite being perceived mainly as a cavity within gut endoderm, the cloaca also has prominent mesenchymal components deeply involved in its reorganization. The endodermal cloaca is delimited by the intra-cloacal mesenchyme anteriorly, by the posterior cloacal mesenchyme posteriorly, and by the pericloacal mesenchyme at the ventral side.

Cloacal septation is achieved by progressive movement of the intra-cloacal mesenchyme towards posterior end of the embryo (Huang et al., 2016). This movement eventually divides the cloacal cavity into two compartments (Miyagawa et al., 2014; Seifert et al., 2009a; Wang et al., 2013). The endodermal cloaca compartment located ventrally to the intra-cloacal mesenchyme develops into the bladder, while the gut portion dorsal to the intra-cloacal mesenchyme forms rectum (Huang et al., 2016). Disruption of cloacal development can lead to multiple congenital malformations summarily termed anorectal malformations. Several studies have shown the requirement of endodermal Shh signaling for cloacal septation. Accordingly, *Shh*$^{-/-}$ embryos are characterized by persistent cloaca (Haraguchi et al., 2007; Perriton et al., 2002; Seifert et al., 2009a). Canonical Wnt signaling in the intra-cloacal mesenchyme depends on Shh signaling and is required for proper cloaca development (Miyagawa et al., 2009). Particularly, Shh balances the level of the Wnt inhibitor Wif1, whose upregulation produces an increase of apoptosis in the intra-cloacal mesenchyme, leading to anorectal malformations (Ng et al., 2014). Interestingly, both loss and gain of Wnt signaling function led to a similar impaired septation phenotype (Ng et al., 2014). Upregulation of activated β-catenin in the cloacal endoderm ectopically activated BMP signaling, further compromising intra-cloacal mesenchyme growth possibly by acting on cell proliferation (Miyagawa et al., 2014).

Finally, the most conspicuous trunk to tail transition landmarks are the hindlimbs and the genital tubercle (GT). The mechanisms of their induction will be discussed below in their corresponding sections.

Genetic regulation of the trunk to tail transition.

The trunk to tail transition is a complex but highly coordinated process. Genetic studies in the mouse clearly indicate that Tgf-β signaling is a master regulator of this transition. The first evidence for this was provided by embryos deficient in ligands of the Tgf-β/BMP family. In *Gdf11* mutant embryos the trunk region was extended, with 3 to 5 extra thoracic vertebrate and 1-2 extra lumbar elements (Mcpherron et al., 1999). This phenotype was aggravated in the *Gdf11/Gdf8* compound knock out embryos (McPherron et al., 2009). Consequently, all trunk caudal-most structures, including the hindlimbs, the GT, and the cloaca, were displaced posteriorly in these mutants (Jurberg et al., 2013; Lee et al., 2010; McPherron et al., 2009; Mcpherron et al., 1999; Szumska et al., 2008). Gdf11 activity in axial tissues is mediated by the type I receptor Tgfbr1 (or Alk5) together type II receptors Acvr2a-, Acvr2b (Andersson et al., 2006; Lee et al., 2010; Paul Oh et al., 2002). In a complementary set of experiments, Tgfbr1 signaling was prematurely activated in the axial progenitors using a constitutively active form of Tgfbr1, which resulted in the anterior displacement of the transition, significantly shortening the trunk (Jurberg et al., 2013). These experiments further reinforced the involvement of Tgfbr1 signaling in the control of the trunk to tail transition.

In mouse embryos *Gdf11* expression is activated in the posterior epiblast at E8.5, just prior the trunk to tail transition. After the transition the signal concentrates in the tail bud and limb mesenchyme (Nakashima et al., 1999). Importantly, the onset of *Gdf11* expression correlates with initiation of trunk to tail transition throughout the vertebrate clades and an ectopic Gdf11 signal is sufficient to activate posterior *Hox* gene expression in the flank mesoderm and to induce the hindlimb bud (Matsubara et al., 2017), thus indicating evolutionary conservation of the mechanism regulating the transition to tail development. The mechanism by which Tgf-β coordinates the trunk to tail transition is, however, not fully understood. The phenotype of *Gdf11* mutant embryos is, at

least in part, mediated by extended expression of the pluripotency factor *Oct4* in the axial progenitor niche (Aires et al., 2016). Whether Gdf11 directly regulates *Oct4* expression is not clear.

One of the functions of Gdf11 signaling is the regulation of posterior *Hox* gene expression (see Box 1) (Jurberg et al., 2013; Liu, 2006; Mcpherron et al., 1999; Szumska et al., 2008). In *Gdf11* mutant embryos, activation of posterior *Hox* genes (*Hox9* to *Hox13*) was posteriorized, following the position of the hindlimb in these embryos. Conversely, embryos with anteriorized transition induced by expression of the constitutive active Tgfbr1 molecule showed a more anterior activation of posterior *Hox* genes, again following the new hindlimb position (Jurberg et al., 2013). Grafting a Gdf11-saoked bead into chick limb bud

Box 1. Hox genes

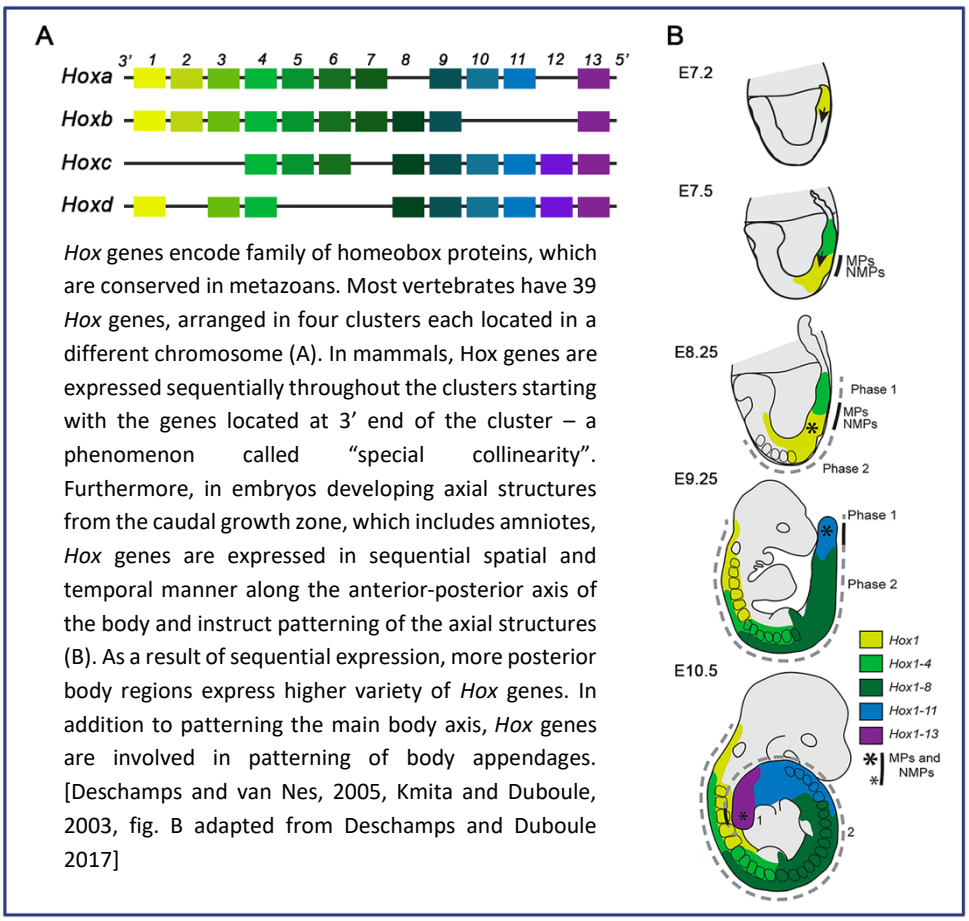

Hox genes encode family of homeobox proteins, which are conserved in metazoans. Most vertebrates have 39 *Hox* genes, arranged in four clusters each located in a different chromosome (A). In mammals, Hox genes are expressed sequentially throughout the clusters starting with the genes located at 3' end of the cluster – a phenomenon called "special collinearity". Furthermore, in embryos developing axial structures from the caudal growth zone, which includes amniotes, *Hox* genes are expressed in sequential spatial and temporal manner along the anterior-posterior axis of the body and instruct patterning of the axial structures (B). As a result of sequential expression, more posterior body regions express higher variety of *Hox* genes. In addition to patterning the main body axis, *Hox* genes are involved in patterning of body appendages. [Deschamps and van Nes, 2005, Kmita and Duboule, 2003, fig. B adapted from Deschamps and Duboule 2017]

induced ectopic expression of *Hoxd11* and *Hoxd13* (Gamer et al., 2001). How this is achieved is still unknown. However, direct activation of *Hoxd11* by canonical SMAD-dependent signaling was reported in mouse (Gaunt et al., 2013). It must be noted, however, that posterior *Hox* genes do not seem to play critical role for induction of the main features of the trunk to tail transition. For example, hindlimbs of the *Hox10* and *Hox11* triple mutants were associated with the vertebrate column at the proper axial level, despite the homeotic transformation in the vertebral column of those mutant embryos (Wellik and Capecchi, 2003).

Isl1, on the other hand, is involved in induction of hindlimbs from the caudal end of the LPM (see below), most likely downstream of Gdf11/Tgfbr1 (Jurberg et al., 2013). Indeed, *Isl1* is sufficient to ectopically induce these structures when prematurely expressed in the axial progenitors. However, still much is left to understand about how Gdf11/Tgfbr1 signaling regulates and integrates all processes associated with the trunk to tail transition.

Appendage induction and growth

Tetrapod limbs are paired appendages that had contributed to the animal's adaptation to terrestrial life. Forelimbs and hindlimbs share their core growth and patterning program, despite eventually acquiring significant morphological differences, also varying significantly across species (McQueen and Towers, 2020). Generally, several distinct stages can be distinguished during limb development. These are: limb bud initiation; early limb bud growth and establishment of distal and posterior signaling centers; establishing the different sections along the proximal distal axis, namely the stylopod, zeugopod and autopod; digit patterning within the autopod; and, finally, termination of limb bud growth. For the purpose of this study, I will mainly focus on hindlimb bud initiation and early limb bud development.

Hindlimb induction

Limbs are initiated from the somatic layer of the LPM (Gros and Tabin, 2014; Takeuchi et al., 2003; Tanaka, 2016). Although the LPM stretches throughout the length of the trunk, limbs do not appear out of context, but require inductive signals at the appropriate axial level.

Anterior *Hox* genes instruct the positioning of the forelimbs along the main body axis by direct activation of the Tbx5 – a gene essential for the forelimb induction (Nishimoto and Logan, 2016). Posterior *Hox* genes, however, do not seem to play major role in defining hindlimb position. While posterior *Hox* genes of groups 9 and 10 are expressed at the lumbo-sacral axial level their expression does not seem to be the main regulator of the hindlimb induction. When expressed prematurely in axial progenitors they fail to dramatically change the hindlimb position (Jurberg et al., 2013). Hindlimb induction is coupled with the trunk to tail transition, and therefore hindlimb position is mostly defined by Gdf11/Tgfbr1 signaling (Jurberg et al., 2013; Matsubara et al., 2017).

Hindlimb buds are characterized by early expression of specific marker genes. *Tbx4*, a hindlimb-specific paralog of *Tbx5*, alone seems not to be essential for hindlimb induction (Naiche and Papaioannou, 2003), despite being sufficient to rescue forelimb induction in *Tbx5* mutants (Minguillon et al., 2005). Another early hindlimb specific marker *Pitx1* is also dispensable for hindlimb bud initiation but defines hindlimb morphological identity (Duboc and Logan, 2011; Logan et al., 1998; Minguillon et al., 2005; Szeto et al., 1999) and possibly the anterior-posterior dimension of the hindlimb field (Marcil et al., 2003). There is apparent redundancy between the *Tbx4* and *Pitx1* – compound mutants deficient in both of these genes are unable to initiate the hindlimbs (Naiche and Papaioannou, 2003).

Another gene vital for the hindlimb induction is *Isl1* (Kawakami et al., 2011). *Isl1* is transiently expressed in the somatic LPM eventually generating the hindlimb field. After hindlimb bud initiation, *Isl1* expression is progressively shifted posteriorly by anterior inhibition from *Gata6*, and eventually is excluded

from the hindlimb bud (Tahara et al., 2018). Early embryonic lethality of the *Isl1* mutants makes evaluation of the hindlimb phenotype in these embryos challenging. Conditional deletions showed that embryos deficient for *Isl1* in the LPM failed to initiate hindlimb buds (Itou et al., 2012; Kawakami et al., 2011). A complementary gain of function approach proved that *Isl1* expression is sufficient to induce hindlimb buds (Jurberg et al., 2013). In the hindlimb bud *Isl1* is required for expression of *Tbx4*, but not *Pitx1* (Kawakami et al., 2011). Therefore, additional factors are likely involved in hindlimb induction downstream of *Isl1*. *Isl1* activity in the hindlimb is mediated by accumulation of nuclear β-catenin (Kawakami et al., 2011) At least in forelimb, subcellular β-catenin reorganization in the somatopleure is concomitant to EMT preceding limb initiation (Gros and Tabin, 2014). Whether the same applies to the hindlimb have not been tested.

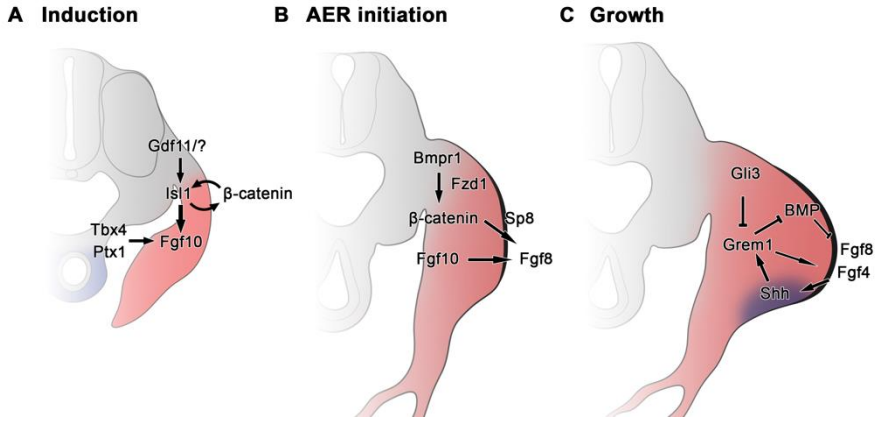

Figure 1-7. Hindlimb development. A. Hindlimb bud induction from the somatic layer of LPM (pink). **B.** AER (thick black line) induction at the dorsa-ventral interface of limb bud ectoderm. **C.** Positive feedback loop between limb bud mesenchyme and AER maintaining limb bud distal growth. ZPA is labelled in dark blue.

Establishment and maintenance of the apical ectodermal ridge

Limb induction ultimately leads to activation of the Fgf10 – an essential factor starting the limb outgrowth cascade (Sekine et al., 1999). *Fgf10* expression in limb mesenchyme is required for formation of the apical

ectodermal ridge (AER) – a major signaling center required for regulation of the limb distal growth and mesenchymal cells' survival (Barrow et al., 2002; Fernandez-Teran et al., 2013; Satoh et al., 2004; Saunders, 1948; Sekine et al., 1999).

Fgf10 activates expression of *Fgf8* – the main marker of the AER, required for normal distal growth of the limb (Lewandoski et al., 2000; Mahmood et al., 1995). Several other FGF ligands, including *Fgf4, Fgf9, Fgf17*, are also expressed later in the AER. Although dispensable for limb growth (Mariani et al., 2008; Moon et al., 2000; Sun et al., 2000) they are capable to compensate for *Fgf8* loss to a large extent (Lu et al., 2005) by maintaining cell survival in a dose-dependent manner (Mariani et al., 2008). *Fgf4* seems to be the next most important of the AER's FGFs: early double *Fgf8/Fgf4* KO in the limb AER results in limb bud truncation and complete limb skeleton agenesis (Boulet et al., 2004; Sun et al., 2000).

Together with Fgf10, Wnt/β-catenin signaling is involved in formation and maintenance of the AER (Barrow et al., 2002; Kawakami et al., 2001; Kengaku et al., 1998; Lin et al., 2008; Lu et al., 2008; Soshnikova et al., 2003; Zhu et al., 2014). Wnt/β-catenin acts upstream of the *Sp8* gene, which modulates *Fgf8* expression, and is essential for the maintenance of the AER and limb growth (Figure 1-7B) (Bell et al., 2003; Kawakami et al., 2004; Lin et al., 2013; Treichel et al., 2003).

Early BMP activity in the limb bud is indispensable for AER development and maintenance. Mouse embryos deficient for the receptor Bmpr1 display severe limb truncation and disruption of AER (Ahn et al., 2001). The BMP receptor Bmpr1 aids Wnt signaling transduction by positively regulating expression of the membrane receptor Fzd1 and subsequent β-catenin release (Pajni-Underwood et al., 2007; Soshnikova et al., 2003). Notably, due to limitations of genetic models, all data regarding the role of Bmpr1 in AER formation was obtained from the conditional gene knock out (KO) in the hindlimbs. Bmpr1 requirement for AER development is ectoderm specific, as

conditional inactivation of mesenchymal Bmpr1 caused limb truncation, with relatively intact AER (Ovchinnikov et al., 2006), or even, in case of *Isl1-Cre* driver, ventral overgrowths expressing AER markers (Yang et al., 2006). Interestingly, simultaneous conditional removal of *Bmp2/Bmp4/Bmp7* or of BMP/Tgfβ downstream effector Smad4 from early limb ectoderm failed to recapture the *Bmpr1* mutant phenotype in the AER, only causing digit patterning defects (Benazet and Zeller, 2013; Choi et al., 2012). These reports reflect the complexity of BMP signaling activity in the regulation of limb development.

Constructing limb axes

Anterior-posterior limb patterning

Antero-posterior patterning of the limb is coordinated by finely tuned balance of the activities of anterior and posterior factors. Shh activity is a key element in this process (Riddle et al., 1993). HH signaling activity is mediated by Gli transcription factors (see Box 2). In mammals, the Gli family is composed of three members, Gli1-Gli3. In the context of limb development, Gli3 seems to play the most important role in digit patterning as *Gli3* mutant embryos are characterized by severe polydactyly (Hui and Joyner, 1993), whereas *Gli1* mutants appear normal and *Gli1/Gli2* double mutants show phenotypes compatible with *Shh* loss in some tissue like lung, gut, spinal cord, but only have a minor phenotype in the limbs (Park et al., 2000). Regardless of its developmental significance, *Gli1* is activated in the limb bud tissues in response to Shh (Panman et al., 2006) and routinely used, alongside with the membrane receptor Ptch1, as a readout of the Shh signaling response.

Shh expression is activated in the posterior part of the limb bud mesenchyme, in the so-called zone of polarizing activity (ZPA) by Hand2 (Charité et al., 2000; Galli et al., 2010) and 5'*Hox* genes (Kmita et al., 2005; Tarchini et al., 2006). Hand2 interacts with Hoxd13 and in a complex binds to the ZPA regulatory sequence (ZRS), which controls *Shh* expression specifically in limb buds (Capellini et al., 2006; Galli et al., 2010; Lettice, 2003). Early

transient expression of *Etv2* in the posterior limb mesenchyme primes the future ZPA cells to respond to Hand2/Hoxd13 by opening the ZRS chromatin (Koyano-Nakagawa et al., 2022).

Hand2 is activated in the posterior mesenchyme by *Isl1* (Itou et al., 2012) and after the onset of *Shh* its posterior domain is maintained by Gli3-R-mediated anterior repression (Lex et al., 2022; Welscher et al., 2002). However, additional factors should also be involved in regulating *Hand2* spatial distribution, as a certain level of *Hand2* posterior restriction is still observed in *Gli3* mutant limb buds (Deimling et al., 2018; Lex et al., 2022; Litingtung et al., 2002).

Due to their reciprocal expression domains and shared genome binding sites, Gli3 and Hand2 were considered to prepattern developing limb bud into anterior and posterior regions, consistent with the anterior and posterior expression of their target genes, like *Alx4* and *Tbx3*, respectively (Osterwalder et al., 2014; Welscher et al., 2002). This model considers Gli3 repression as a default mode throughout the limb bud, which is relieved by *Shh* expression in

Box 2. HH signaling pathway

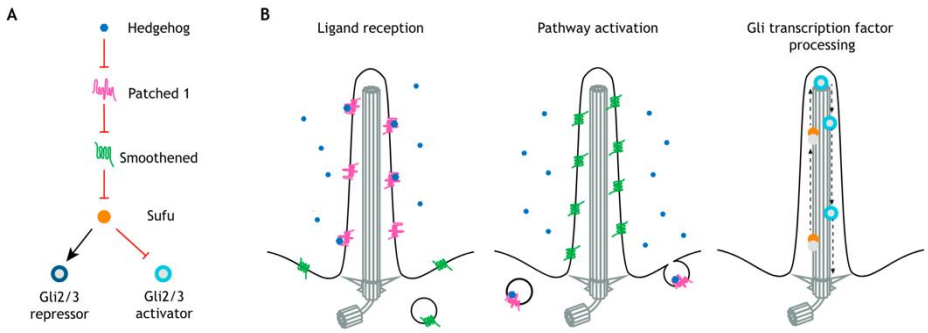

Hedgehog (HH) signaling response in vertebrates occurs in ciliated cells, which includes some limb bud ectoderm and mesenchyme cells (Ashe et al., 2012; Lex et al., 2022). Respectively, syndromes associated with ciliopathies often cause skeletal deformations including polydactyly (McInerney-Leo et al., 2013; Ashe et al., 2012). The HH signaling pathway involves several components, including the cell membrane receptor Patched (Ptch), the pathway activator Smoothered (Smo) and the Gli transcriptional regulators. In the absence of HH Ptch1 is concentrated in the cilia, where it inhibits Smo, thus keeping the pathway silent. Under these conditions full length Gli is cleaved, which generates the Gli repressor form (Gli-R) (Wang et al., 2000). Upon ligand binding, Ptch1 leaves the cilia releasing Smo inhibition, which turns Gli factors to the activator state (Gli-A). Gli-A enter nucleus and activate target expression genes (scheme from Ho and Stearns, 2021).

the posterior mesenchyme and subsequent conversion of Gli3-R to Gli3-A. The Gli3 prepatterning activity has recently been challenged by a study showing Gli3 relevance in HH-response only at the stages after the onset of Shh activity in the limb bud, but not before that (Lex et al., 2022). Nonetheless, the finding that the limb phenotype of *Shh/Gli3* double mutants is identical to that of *Gli3* single mutants indicates the absolute requirement of Gli3 downstream of Shh (Litingtung et al., 2002).

Shh signaling from the ZPA was considered to be the main regulator of posterior digit identity. Classical experiments showed that anterior induction of a ZPA caused posterior mirror image polydactyly (Masuya et al., 1995; Tickle et al., 1975). Conversely, loss of Shh causes severe autopod degeneration, with only one - presumably d1 - digit present (Chiang et al., 1996; Zhu et al., 2008). The truncated limb development of *Shh* mutants results from interference with ZPA/AER interactions affecting global limb growth, as will be discussed below. A recent genetic study showed that transient early expression of *Shh* from the ZPA is sufficient to specify all digits when cell survival is maintained in the autopod (Zhu et al., 2022). The observation that in the *Shh/Gli3* double mutants, the digits in their severe polydactyl autopods have no sing of specific digit identity further indicates an important role of the Shh/Gli3 system to specify anterior-posterior limb polarity (Litingtung et al., 2002).

Less is known about the specification of the anterior digit identity. Most of the described anterior factors (e.g., Alx4) are involved in anterior restriction of *Shh* activity rather than in generation of anterior skeletal elements (Kuijper et al., 2005). Recently, two factors have been shown to be implicated in early specification of anterior limb progenitors and in formation of anterior limb elements. The transcription factor Sall4 is reportedly required in early limb progenitors (particularly in the hindlimb) to activate *Gli3* expression and to establish an anterior limb field (Akiyama et al., 2015). Similarly, somatic LPM markers *Irx3/5* are involved in *Gli3* activation in the anterior mesenchyme, and

consequent restriction of *Hand2* to posterior part of the limb bud (D. Li et al., 2014).

ZPA/AER interactions

Shh is involved in mesoderm – ectoderm interactions, which play an important role in maintenance of the AER and thus in the control of limb growth. The so-called Shh-Fgf positive feedback loop "starts" with Shh activation of *Grem1* (gene encoding Gremlin1 protein) by Gli-A binding to multiple enhancers located 5' from *Grem1*, within the *Formin1* gene (Q. Li et al., 2014; Malkmus et al., 2021; Zúñiga et al., 2004). Gremlin1 is a secreted factor, which inhibits BMP signaling by direct interaction with the ligand (Ali and Brazil, 2014; Brazil et al., 2015) leading to reduced activation of the BMP downstream cascade and consequent downregulation of its targets in the limb bud (Figure 1-7C) (Norrie et al., 2014). As mentioned above, multiple BMP ligands are expressed in distal limb bud mesenchyme and participate in autopod patterning.

Interestingly, low concentrations of Bmp2 expressed in the posterior limb mesenchyme and the AER have been shown to activate *Grem1* independently of Shh in a paracrine fashion (Nissim et al., 2006). BMP signaling modulates AER dimension and persistence by negative regulation of the *Fgf8* and *Fgf4* expression (Bandyopadhyay et al., 2006; Bénazet et al., 2012, 2009; Pajni-Underwood et al., 2007; Selever et al., 2004). Gremlin1 acts by antagonizing BMP inhibition of FGFs and, therefore, maintaining the proper AER size (Khokha et al., 2003; Niswander et al., 1994; Zúñiga et al., 1999). Consistently, *Grem1* KO embryos are characterized by zeugopod and autopod hypoplasia (Khokha et al., 2003; Zúñiga et al., 2004), while conditional *Grem1* overexpression in the limb bud causes overgrowth of AER and polydactyly (Norrie et al., 2014). Spatial regulation of *Grem1* expression is, therefore, an important mechanism modulating BMP-dependent regulation of the anterior and posterior extension of the AER, and, consequently, limb field dimensions. Interestingly, high concentrations of both Shh and Bmp2 in the posterior limb bud inhibit *Grem1*

expression in this area (Nissim et al., 2006). Spatial restriction of *Grem1* expression – both at the anterior and posterior margins - is, at least in part, regulated via BMP-dependent activation of *Tbx2* (Farin et al., 2013). Such pattern allows for BMP inhibition of FGFs in the anterior- and posterior-most margins of the limb bud, preventing polydactyly and potential limb field expansion.

In addition to indirect maintenance of FGF levels in the AER via repression of BMP signaling, *Grem1* positively regulates *Fgf4* expression (Zúñiga et al., 1999), and *Fgf4* is excluded from the anterior AER by Gli3-R-mediated repression of *Grem1* (Litingtung et al., 2002; Welscher et al., 2002). *Fgf4* expression in posterior AER positively regulates *Shh* expression, thus keeping the positive feedback loop active (Figure 1-7C) (Bénazet et al., 2012; Niswander et al., 1994; Ros et al., 1996; Watson et al., 2018; Yang and Niswander, 1995).

Dorsal-ventral limb patterning

Dorsal-ventral patterning of the limb bud is dependent on specific gene expression in the ectoderm. It is also tightly connected with proximal-distal and anterior-posterior patterning, as ectodermal signals serve to establish the dorsal-ventral AER boundary (Crossley and Martin, 1995; Cygan et al., 1997; Ros et al., 1996), and many characterized compound mutants acquire limb phenotypes beyond dorsal-ventral deviations (Chen and Johnson, 2002; Y. Wang et al., 2022). Dorsal ectodermal *Wnt7a* activates mesenchymal expression of the transcription factor *Lmx1b*, which regulates expression of multiple mesenchymal genes (Cygan et al., 1997; Feenstra et al., 2012; Gu and Kania, 2010; Haro et al., 2017). *Lmx1b* is required to generate limb dorsal features, as *Lmx1b* inactivation in mouse embryos causes ventralization of the dorsal side of the limb (Chen et al., 1998; Qiu et al., 2009). *Bmpr1* expression in early mesoderm of, at least, the hindlimb bud and expression of *Sp6* and *Sp8* in the AER are required for *En1* expression in the ventral ectoderm and consequent

Wnt7a/Lmx1b restriction to dorsal limb bud (Ahn et al., 2001; Haro et al., 2014; Yang et al., 2006).

Proximal-distal limb growth and patterning

Three major skeletal compartments are defined along the proximo-distal axis of the limb: stylopod, represented by the humerus in the forelimb and the femur in the hindlimb; zeugopod, consisting of two bones - ulna and radius in the forelimb and tibia and fibula in the hindlimb; and finally, the autopod, consisting of the wrist and fingers in the forelimb and the ankle and toes in the hindlimb.

The control of proximal-distal patterning of the limb is a complex process that depends on timely expression of the compartment specific genes. Early onset of expression and proximal restriction of the *Meis* transcription factors in the developing limb suggested their importance for stylopod development. Indeed, elimination of *Meis1/2* in the limb bud precursor cells from the mouse LPM, caused limb proximal defects (Delgado et al., 2021, 2020). Conversely, overexpression of *Meis1/2* in the distal limb buds of chicken and mouse embryos disrupted zeugopod and autopod development, suggesting a role for *Meis* genes as specifically proximal patterning factors (Capdevila et al., 1999; Mercader et al., 2009, 1999).

Hox genes play a key role in the patterning of the different limb sections (Zakany and Duboule, 2007). *Hox* genes are expressed in dynamic spatial and temporal pattern in developing limb (Nelson et al., 1996). *Hox11* paralogs are associated with zeugopod development based on their expression pattern in early limb mesenchyme and, more relevantly, the triple *Hox11* KO mouse phenotype that resulted in strong reductions of the zeugopod (Koyama et al., 2010; Nelson et al., 2008; Wellik and Capecchi, 2003). Similarly, *Hox10* genes are important for stylopod development as revealed by the limb phenotypes of the triple *Hox10* mutant mice, although the effect seemed more evident in the hindlimb (Wellik and Capecchi, 2003). Finally, *Hox13* genes are expressed in the

distal limb mesenchyme and are critical for autopod growth (Fromental-Ramain et al., 1996; Lu et al., 2008) possibly by modulating distal-specific gene expression via changes in chromatin state of their regulatory elements (Sheth et al., 2016).

Multiple signaling pathways are involved in regulation of limb's proximo-distal axis. For instance, FGF signaling from the AER serves to establish limb bud's distal domain by inhibiting proximal genes (Mariani et al., 2008). *Wnt5a* is also related to distal limb development. It is expressed in the distal limb bud and its activity regulates autopod growth (Oishi et al., 2003; Yamaguchi et al., 1999; Zhu et al., 2012) by promoting directional cell division and distal movement (Gao et al., 2018; Gros et al., 2010).

Limb proximo-distal patterning network, however, cannot be reduced to linear sequence of activation and repression of corresponding genes along the axis as it is intertwined with development of other axes. The best studied case is the connection with anterior-posterior patterning processes, to a large extent related to Shh activity in the ZPA (Riddle et al., 1993). Indeed, *Shh* mutant limb buds are smaller than those of wild type controls and, in addition to lacking most of the autopod elements they fail to generate posterior zeugopod elements in both fore- and hindlimb (Chiang et al., 1996; Zhu et al., 2008). FGF signaling from the AER and *Hox13* gene activity in the limb mesenchyme are critical for both distal limb growth and its interaction with antero-posterior patterning (Mariani et al., 2008; Zákány et al., 2004). Indeed, 5'- *Hoxa* and *Hoxd* genes are expressed in biphasic manner, the first being required for the development of more proximal limb elements and to induce *Shh* in the ZPA, and later to regulate autopod antero-posterior patterning, essential to establish digit identity (Pérez-Gómez et al., 2018). Likewise, early LPM expression of main regulators of anterior autopod identity, *Sall4* and *Irx3/5,* is necessary for the growth of proximal-anterior skeletal elements in the hindlimb: femur, tibia, and for anterior digits development in the autopod (Akiyama et al., 2015; D. Li et al., 2014).

Genital tubercule induction and development

Mammalian external genitalia development is divided into an early androgen independent phase (from E10 to E15 in mouse), when male and female genitalia develop according to the same scheme, and a late androgen-dependent stage. Recent single cell gene expression studies, however, found clusters of cells differential between sexes as early as E14.5 (Armfield and Cohn, 2021). For the purpose of this work, I will focus on the early external genitalia development.

GT initiation

Signaling from the embryonic cloaca is crucial for external genitalia development. Before cloaca emergence, a small part of embryo's hindgut contacts with the ventral ectoderm, forming the cloacal membrane. The pericloacal mesenchyme is positioned laterally on either side of this endoderm-ectoderm junction. Slightly later, after cloaca initial widening, two symmetrical swellings emerge from the pericloacal mesenchyme (Haraguchi et al., 2007). These swellings grow further and merge to form a single GT. At the same time the cloacal membrane is maintained in the form of the urethral epithelium (UE). Its distal part (dUE) gives rise to urethral plate, an endodermal grove extending along with GT distal growth, which eventually is engulfed by the expanding mesenchyme, resulting in the formation of the urethral canal (Penington and Hutson, 2002; Perriton et al., 2002; Seifert et al., 2008; Yamada et al., 2006).

GT emergence from pericloacal mesenchyme is integrated in the trunk to tail transition program and is induced shortly after hindlimb bud initiation. Cell tracing experiments in mice indicate that cells contributing to the GT mesenchyme originate from ventral mesoderm and tail bud (Tschopp et al., 2014). Interestingly, hindlimbs and GT seem to have shared their developmental origin in the ancestral condition but diverged in the course of evolution (Tschopp et al., 2014). In mammals, the two appendages share many

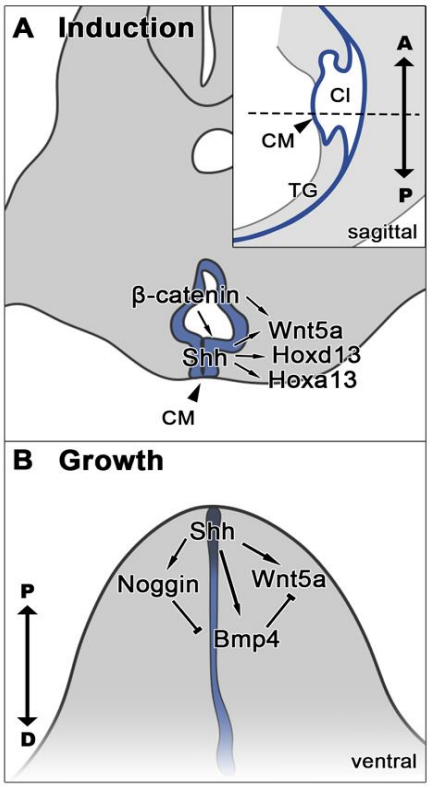

Figure 1-8. GT induction and growth. A. GT is induced as two PCM swellings on the either side of the cloacal membrane (CM black arrowhead on the inset) in response to endodermal Shh from cloaca (Cl). Inset shows sagittal view of cloaca. Dashed line shows approximate level of transversal view in (A). Endoderm is labelled in blue. TG – tail gut. **B.** Ventral view of growing GT. GT growth is positively regulated by Wnt5a. Bmp4 limits GT growth by inhibiting Wnt5a, while Noggin modulated Bmp4 activity. Endoderm is labelled in blue, dUE is marked by dark blue.

developmental programs and are often compared (Chiu et al., 2010; Lin et al., 2013; Yamada et al., 2006).

Shh signaling from the cloacal endoderm is crucial for GT initiation, and *Shh* KO embryos are characterized by complete GT agenesis (Haraguchi et al., 2007; Lin et al., 2009; Miyagawa et al., 2009; Perriton et al., 2002). Wnt/β-catenin signaling in the ventral mesoderm before GT onset is required for *Shh* expression in the cloacal endoderm and the UE, and for GT induction (Figure *1-8*A) (Miyagawa et al., 2009). Absence of β-catenin activity in the endoderm also leads to GT and cloaca agenesis (Lin et al., 2008). Furthermore, constitutive β-catenin activation under the *Shh* promoter rescues GT initiation in *Shh* mutants (Lin et al., 2009). Once *Shh* expression is initiated β-catenin is not required to maintain it (Miyagawa et al., 2009). This function is likely overtaken by other factors, for example endodermal *Foxa1* and *Foxa2* later in development (Gredler et al., 2020).

Cloacal *Shh* is the main regulator of GT induction. However, it is insufficient to induce GT growth in the absence of other factors. Particularly, mouse embryos with early conditional inactivation of Bmp4 in the axial tissues do not form GT, despite adequate *Shh* expression in cloaca (Kajioka et al., 2019).

Bmp4 is expressed in posterior gut endoderm before GT initiation, its expression domain is shifted towards the mesenchyme with GT initiation (Kajioka et al., 2019). Inactivation of *Bmp4* in Isl1-positive mesodermal cells led to development of a severely hypoplastic GT, rather than to complete GT agenesis (Suzuki et al., 2012). Inactivation of the Bmp receptor Bmpr1 in the Isl1-lineage cells does not seem to perturb early GT development either (Yang et al., 2006). This suggests that Bmp4 and Shh signaling from cloaca, are both required for GT induction.

Isl1 itself is a potential regulator of GT induction. First, premature expression of *Isl1* is sufficient to induce the GT at more anterior axial level, in complex with other terminal trunk structures, (Jurberg et al., 2013). Second, *Isl1* is one of earliest markers of pericloacal mesenchyme, expressed prior to GT initiation and descendance of the Isl1-positive cells majorly contribute to GT tissues (Suzuki et al., 2012; Yang et al., 2006). Finally, *Isl1* have been shown to be important for proper urogenital development (Kaku et al., 2013). Unfortunately, *Isl1* knock out is lethal prior to GT induction, and there are no clear evidence proving *Isl1* requirement for GT induction.

DUE – a signaling center for GT distal growth

The GT in mouse embryos is an unpaired appendage, which, as we shall discuss, shares many regulatory networks with the limbs. Researchers often parallel GT's endodermal dUE to limb's AER (Yamada et al., 2006). Indeed, the two structures share many marker genes, but more importantly, both serve as signaling centers for distal growth. Alike to mechanical removal of AER in the limb bud, GT growth is impeded by removal of the dUE (Haraguchi et al., 2000; Saunders, 1948). Similar to the AER, *Fgf8* is considered to be a canonical marker of dUE. The role of epithelial FGF signaling for GT distal growth is, however, difficult to establish. On the one hand, *Fgf8* and *Fgf4* expression in the dUE was shown to be dispensable for genital development (Miyagawa et al., 2009; Seifert et al., 2009b). On the other hand, FGF signaling response in the GT mesenchyme

via Fgfr1; Fgfr2 receptors is crucial for its growth (Lin et al., 2013). Mesenchymal receptors likely respond to redundant FGF ligands from dUE (in addition to *Fgf4* and *Fgf8,* the dUE expresses at least *Fgf9*), and to mesenchymal Fgf10, – deletion of either causes milder phenotype than compound knock out of the Fgfr1/Fgfr2 receptors (Harada et al., 2015; Lin et al., 2013; Satoh et al., 2004). Expression of *Fgf10* in early GT mesenchyme seems to be dispensable for GT growth up to E12.5, and *Fgf10*$^{-/-}$ display GT growth retardation only later in development (Haraguchi et al., 2000). Despite discrepancies regarding *Fgf8* importance in the regulation of GT growth, this factor was shown to be sufficient to activate expression of many mesodermal genes, including *Fgf10, Bmp4* and *Hoxd13* (Haraguchi et al., 2000).

After its initial requirement for GT initiation, Shh and β-catenin activity in the UE sustain mesenchymal growth and proliferation (Lin et al., 2009, 2008; Miyagawa et al., 2014, 2009). Similar to the limb bud AER, Wnt/β-catenin activates *Sp8* expression in the dUE which, for what it is worth, regulates *Fgf8* expression (Bell et al., 2003; Lin et al., 2013; Miyagawa et al., 2009). More importantly, the GT is absent in *Sp8* KO mice, along with other body appendages (Haro et al., 2014).

Network underlying GT growth

Endoderm-mesenchyme crosstalk underlies GT growth. Shh signaling from the UE is primary targeted towards the GT mesenchyme, evident by *Gli1* and *Ptch1* expression in this tissue (Haraguchi et al., 2007; Lin et al., 2009). Several factors essential for mesenchymal growth are expressed in respond to Shh, including *Wnt5a*, *Hoxa13* and *Hoxd13* (Kondo et al., 1997; Lin et al., 2009; Perriton et al., 2002; Suzuki et al., 2003; Warot et al., 1997; Yamaguchi et al., 1999). *Wnt5a* expression is additionally regulated by β-catenin from the UE (Lin et al., 2008). Mesenchymal RA modulates *Shh* expression, and consequently levels of downstream mesenchymal genes (Liu et al., 2011). Unlike in hindlimb buds, where it is expressed only transiently, in the GT *Isl1* is maintained and

positively regulates *Fgf10* and *Wnt5a* expression, while its loss past GT induction stage causes hypoplasia (Ching et al., 2018).

Similar to the limb bud, after its initial role for appendage bud induction, mesenchymal BMP signaling modulates GT growth. Many UE expressed factors, particularly *Shh* (Liu et al., 2011), *β-catenin* (Lin et al., 2008), and *Fgf8* (Haraguchi et al., 2000) positively regulate *Bmp4* expression. However, *Shh* conditional KO after the onset of GT development showed that HH signaling also positively regulates expression of the BMP inhibitor *Noggin* (Lin et al., 2009). Bmp4 limits GT growth by promoting apoptosis and inhibiting Wnt5a-dependent mesoderm proliferation, while Noggin, similarly to Gremlin1 in the limbs, modulates BMP activity by inhibiting it (Figure *1-8*B) (Suzuki et al., 2003). BMP response in the ectoderm limits GT growth as well, as conditional KO of the receptor *Bmpr1* in GT surface ectoderm causes GT and dUE hyperplasia (Suzuki et al., 2003).

Tgf-β signaling

As we have seen in the previous sections signaling pathways regulate multiple developmental processes. Among the mentioned signaling molecules many belong to the transforming grow factor beta (Tgf-β) superfamily. TGF-β signaling ligands include bone morphogenic proteins (BMPs), growth differentiation factors (GDFs), Nodal, Inhibins, Tgf-β and Nodal inhibitors Lefty (Hinck et al., 2016).

TGF-β signaling cascade

Tgf-β ligands are expressed as precursors with long N-terminal prodomain. Upon maturation ligands are cleaved by FURIN and Pace4 proteases (Hill, 2018). Many Tgf-β factors stay associated with the prodomain after cleavage, including Tgf-β, Myostatin, Gdf11, Bmp7, and Bmp9, while others (e.g., Bmp2) dissociate after secretion. Association with the prodomain keeps ligands

in a latent form and it has been proposed that this allows to concentrate them prior to signaling activation (Hinck et al., 2016). Tgf-β peptides work both as homo- or heterodimers, which modulates their potency and mode of activity. For example, activin is composed of inhibin β homodimers, while inhibin αβ heterodimers generate inhibin. Bmp2 heterodimers with Bmp4 or Bmp7 were shown to be more active than homodimers of either of them both *in vitro* and *in vivo* (Hinck et al., 2016). Nodal has the ability to heterodimerize with Gdf1, which potentiates its action (Hill, 2018).

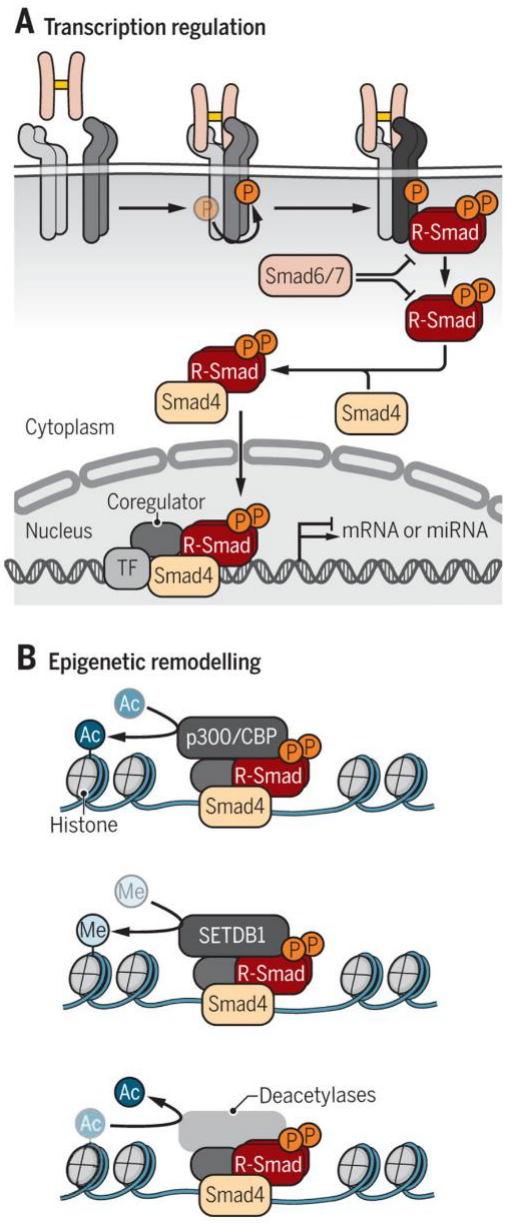

Figure 1-9. Tgf-β signaling cascade. A. Binding of the ligand results in activation of Smad transcription factor and their relocation to the nucleus, where they regulate target gene expression. B. Chromatin remodeling by Tgf-β signaling. From Derynck & Budi 2019.

Dimerized ligands bind to the ectodomain of the heterotetrameric complexes between type I and type II receptors (Moustakas and Heldin, 2009). Mammals have five type II and seven type I receptors. Type I and type II receptors share sequence and structure similarities: both have an ectodomain conferring ligand binding, a transmembrane region, a short juxtamembrane sequence and a cytoplasmic

kinase domain. Type II receptors are considered to be constitutively active kinases. The presence of ligands promotes the building of a complex between type II and type I receptors. Within this complex the kinase activity of the type II receptor phosphorylates conserved serine and threonine residues within a short glycine/serine-rich sequence in the juxtamembrane region of the type I receptor, called GS-domain, triggering the kinase activity of this receptor and activating the intracellular signaling cascade (Derynck and Budi, 2019). Interestingly, depending on affinity strength, ligands first bind to either type I or type II receptors to build the signaling complex. For example, Tgf-β, activins or GDFs first bind to the type II receptor, while BMPs first bind to the type I receptor (Martinez-Hackert et al., 2021).

According to canonical Tgf-β signaling pathway the activated type I receptor phosphorylates two C-terminal serines of the receptor regulated SMAD proteins (R-SMADs). This promotes R-SMAD binding to a co-SMAD. A complex consisting of two R-SMAD proteins with one co-SMAD protein are then actively transported to nucleus (Figure *1-9*A) (Massagué, 2012). There are eight SMAD proteins in mammals. Two of them are inhibitory (Smad6 and 7) and act to stabilize the receptors in the absence of ligand binding. The other six SMAD proteins participate in signal transduction. Typically, Smad2 and 3 are considered to be phosphorylated in response to Activin, Nodal, Tgf-β signaling and Gdf8/11, while Smad1, 5 and 8 respond to BMP and other GDFs. These rules, however, do not always hold true. For example, in the tooth primordium Tgfβ activity via Tgfbr1 initiates a Smad1/5/8 cascade (Yuan et al., 2015). Smad4 acts as a co-SMAD. SMAD proteins, with the likely exception of Smad2, are able to bind to the so-called SMAD binding elements (SBE) in the genomic DNA, regulating transcription of target genes (Derynck and Budi, 2019). Besides the canonical SMAD-dependent pathway Tgf-β ligands can also activate non-canonical pathways, including ERK/MAPK (Moustakas and Heldin, 2009). BMP, for example, acts non-canonically via p38 and ERK1/2 in tooth development (Yuan et al., 2015). Also, Bmp5 regulates interdigit apoptosis by acting both

canonically via Smad1/5/8 and non-canonically via MAPK p38 (Zuzarte-Luís et al., 2004).

Regulating specificity

Despite the large number of ligands, receptors, and their possible combinations, they still seem to converge into a limited number of intracellular cascades. In that case, how specificity in gene regulation by different ligands is conferred?

Co-factors.

SMAD protein complexes have weak DNA affinity and extensively interact with other DNA-binding transcription factors (TFs) to regulate target gene expression (Massagué, 2012). For example, Foxh1 is a known Smad2/3 DNA binding partner acting downstream of Nodal signaling and required for midline formation and mesoderm development in early mouse embryo (Chiu et al., 2014; Hoodless et al., 2001). BMP downstream effectors require Runx TFs to drive them to specific gene regulatory elements, particularly important in osteogenesis (Javed et al., 2008; Zaidi et al., 2002). In addition, the same ligand can trigger different effects in different cell contexts. Particularly, cell type specific activity of TGF-β signaling have been shown to be modulated by differential interaction R-SMADs with master TFs in different cell lines. For instance, in embryonic stem cells (ESC) Smad2/3 is recruited by Oct4 to specific regulatory elements in the genome (Mullen et al., 2011). Interestingly, R-SMADs can interact with group 13 Hox proteins *in vitro*, which may be relevant for development of multiple tissues where TGF-β ligands and *Hox13* genes are co-expressed, like limb buds or the tail bud (Williams, 2005).

Co-receptors.

In mammals the TGF-β superfamily comprises about 30 different ligands. Since most ligands preferentially bind to one of seven type II receptors, many

TGF-β pathways share one or both receptors types (Figure *1-10*) (David and Massagué, 2018; Heldin and Moustakas, 2016). The specificity of the signaling response is, at least in part, granted by co-receptors which potentiate ligand's affinity to receptors or are required for binding.

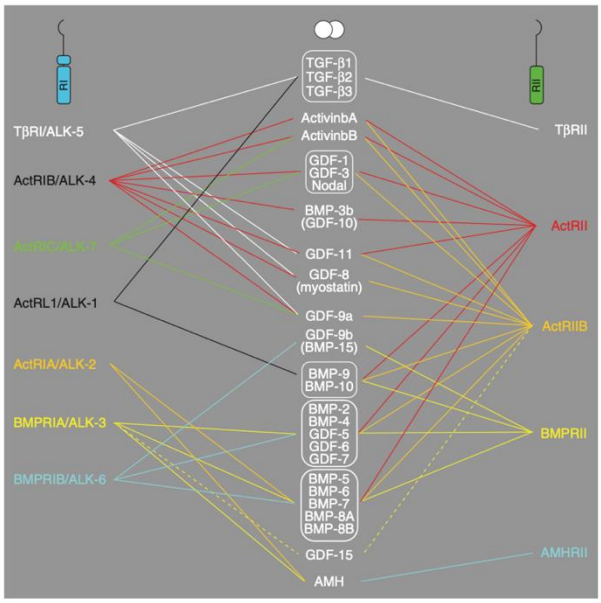

Figure 1-10. Selective binding of Tgf-β ligands to type I and type II receptors. From Heldin and Moustakas, 2016.

For example, both Nodal and Activin act through shared type I (Acvr1b and Acvr1c) and type II (Acvr2a and Acvr2b) receptors (Hill, 2018). Contrary to activin, Nodal requires co-receptor Crypto to confer its specificity to type I receptor. Crypto, therefore, acts as a switch between Nodal and Activin signaling. Another example is betaglycan, which interacts with Tgf-β2 and promotes its activity. Betaglycan mutant embryos die prenatally and share many phenotypic features with Tgf-β2 mutants (Stenvers et al., 2003).

BMP factors also have specific co-receptors. For instance, endoglin interacts with Bmp9 and Bmp10 and this interaction was shown to be involved in angiogenesis (Hinck et al., 2016). Another BMP co-receptor, neogenin, together with co-factor repulsive guidance molecule (RGM), facilitates BMP binding to its receptor complex particularly important in osteogenesis (Zhou et al., 2010).

Inhibitors.

Physiologically, many signaling molecules act as morphogens by forming signaling gradients. Inhibitor molecules are involved in creating these gradients.

Several examples of inhibitors' participation in tissue patterning have been already discussed in previous sections, including Lefty/Nodal antagonism in DVE migration, BMP/Gremlin interaction in the patterning of the limb bud, and BMP/Noggin antagonism in GT growth.

Many BMP inhibitors, like Noggin, Gremlin and Chordin, act by directly binding to the ligand dimers and blocking receptor binding epitopes. Interestingly, some BMP modulators, like Twisted Gastrulation (Tsg) or Crossveinless 2 (CV2) can either inhibit BMP signaling by binding the ligand or to enhance it by forming complexes with Chordin (Derynck and Budi, 2019; Hinck et al., 2016). Interaction between CV2, Tsg, Chordin and BMPs serve to form BMP signaling morphogenic gradients important in diverse developmental contexts, including the *Drosophila* wing, the *Xenopus* gastrula during dorsal-vental patterning, and in the developing mouse vertebral column (Zakin et al., 2008).

Nodal inhibitors Lefty1 and 2 interact either with the ligand or with co-receptor Crypto, to inhibit Nodal signaling (Robertson, 2014). Other mechanisms of specific inhibitory mechanisms include competing for type II receptor, used by Inhibins, to inhibit Activin/Nodal signaling (Martinez-Hackert et al., 2021). Also, follistatin inhibits Activin, BMPs, and Gdf8 and 11 by binding the ligand (Hinck et al., 2016).

Finally, competitive binding of one ligand to the receptor shared with another ligand can cause inhibition of the downstream signaling of the latter. For example, Activin, Gdf8 and Gdf11 outcompete BMP ligands by binding to type II receptor, inhibiting Smad1/5/8 and activating Smad2/3 *in vitro* (Martinez-Hackert et al., 2021). In a developmental context, Tgfbr1 inhibits Bmp9 signaling through its type I receptor Acvrl1, simply by sequestering a shared type II receptor (Wang et al., 2019).

Tgf-β dependent chromatin remodeling.

One of the possible outcomes of Tgf-β signaling is binding of the SMADs complex to particular *cis*-regulatory elements and regulation of target gene expression. Tgf-β signaling capacity to trigger coordinated processes, like EMT, implies the possibility of more integrative mode of action (Lin and Wu, 2020). Studies in cell lines have shown chromatin remodeling in response to treatment with Tgf-β ligands (Figure *1-9*B). Indeed, Smad TFs have been shown to bind to the closed chromatin regions and recruit chromatin remodeling complexes, histone acetyltransferases, demethylases etc. (Coda et al., 2017; Dahle et al., 2010; Ross et al., 2006; Xi et al., 2011, 2008). It have been shown that in early mouse embryo enhancers in *Eomes* genomic locus gain accessibility and Smad2/3 enrichment upon differentiation of definitive endoderm (Simon et al., 2017). Activin treatment in cells induced chromatin opening and histone acetylation in the vicinity of Smad2 binding sites (Coda et al., 2022, 2017). All of the above clearly show the capacity of Tgf-β signaling to regulate chromatin state.

THESIS AIMS

I – To investigate changes of gene expression in the axial growth zone after the trunk to tail transition and to define the role of Gdf11 in these changes.

II – To eliminate the redundancy between Gdf11 and other Tgf-β ligands by generation of the Tgfbr1 receptor knock out mouse line and to determine the role of Tgfbr1 in the process of trunk to tail transition.

III – To investigate Tgfbr1 functions in the development of the hindlimbs and external genitalia.

Chapter 2

TRUNK TO TAIL TRANSITION AND REGULATION OF GENE EXPRESSION IN THE AXIAL GROWTH ZONE

Authors contribution: Anastasiia Lozovska and Moisés Mallo designed experiments; Anastasiia Lozovska performed experiments; Anastasiia Lozovska analyzed data; Patrícia Duarte performed ATAC-seq analysis with GUAVA pipeline; Artemis Korovesi performed ATAC-seq footprinting analysis.

SUMMARY

An amniote body is laid down sequentially from head to tail. After the head primordium is specified from the anterior epiblast, the embryo starts extending by adding new tissue differentiated from the pool of axial progenitors located in the caudal growth zone. This continuous process can be subdivided in two stages corresponding to trunk and tail development. Transition between these stages requires reorganization of the caudal growth zone. At this time epiblast, serving as source of progenitors for trunk structures, regresses and a new growth zone is being established in the newly formed tail bud. Growth differentiation factor 11 (Gdf11), a member of Tgf-β signaling superfamily, is the main regulator of the trunk to tail transition. In the absence of Gdf11 trunk to tail transition is delayed and reorganization of the caudal growth zone is incomplete. However, the molecular mechanisms mediating Gdf11 activity are unclear. In this chapter we examined gene regulatory networks downstream of the Gdf11 in the context of the trunk to tail transition. We show that many genes associated with development of trunk structures are active already in the progenitors' region and that Gdf11 acts to downregulate those genes at the transition onset. Furthermore, Gdf11 activates the expression of the posterior *Hox* genes in the caudal growth zone. Our results suggest that Gdf11 confers efficient relocation of the axial progenitors from the epiblast to the tail bud by regulating expression of the cell adhesion molecules. Additionally, our differential gene expression analysis uncovers Gdf11 involvement in activity of multiple other signaling pathways. Finally, analysis of chromatin accessibility patterns suggests that changes in gene expression following the trunk to tail transition are mainly regulated by distal enhancers.

INTRODUCTION

Despite the great diversity of vertebrate's body shapes, they all contain four main regions along the anterior-posterior axis: head, neck, trunk, and tail.

The amniote body develops sequentially from head to tail. While the head primordium is formed in the early gastrulating embryo, the rest of the body is laid down during the process of axial extension by sequential production of new tissue from the progenitors located in the caudal growth zone that eventually differentiate to generate the different body components (Aires et al., 2018).

During trunk formation three main lineages are generated by epiblast-resident progenitors: the neural tube that will differentiate into the spinal cord; the lateral plate (LPM) and intermediate mesoderm (IM), which together with the embryonic endoderm will form the internal organs, the body wall, and limb skeleton; and the somitic mesoderm, which will differentiate into the axial skeleton, the body muscles, and the dermis (Tzouanacou et al., 2009; Wymeersch et al., 2016). Progenitors of these lineages have been mapped to specific locations in the epiblast. Precursors of the LPM are located in the most posterior part of the epiblast, while more anterior epiblast regions mainly contribute to the somitic mesoderm (Cambray and Wilson, 2007; Wymeersch et al., 2019, 2016). A region of the anterior epiblast proximal to the node (the node-streak border - NSB) contains a distinct population of cells routinely defined by simultaneous expression of the neural marker Sox2 and the mesodermal marker Tbxt and characterized by their potency to generate both neural and mesodermal tissue (Cambray and Wilson, 2002). Correspondingly, this cell population is termed neuro-mesodermal competent cells (NMCs) (Binagui-Casas et al., 2021).

In contrast to the trunk, LPM and IM derivatives are absent from the tail. The neural tube and the somites, on the other hand, are formed from the same NMC population as in the trunk (Cambray and Wilson, 2007, 2002; Tzouanacou et al., 2009) but at a different embryonic location resulting from a dramatic rearrangement of the caudal growth zone during the trunk to tail transition. At this stage the NMC cells delaminate from the NSB and relocate to the chordo-neural hinge (CNH) in the anterior-dorsal part of the tail bud (Cambray and Wilson, 2002; Dias et al., 2020; Wilson et al., 2009).

Transitions between body regions are important components of normal development and are coordinated by timely expression of specific regulatory genes (Aires et al., 2018). Loss and gain of function experiments identified the principal role of the *Gdf11* in initiating the trunk to tail transition. *Gdf11* mutants are characterized by posterior displacement of trunk to tail transition landmarks, namely the cloaca and the hindlimbs, and the elongation of the thoracic and lumbar axial skeletal regions, therefore indicating a delayed transition (Jurberg et al., 2013; Lee et al., 2010; Mcpherron et al., 1999). Complementarily, premature activation of the Gdf11 receptor in axial progenitors anteriorize the trunk to tail transition (Jurberg et al., 2013).

Gdf11 is a member of transforming growth factor beta (Tgf-β) superfamily. Its effects in axial tissues are mediated by binding to type I and type II serine/threonine kinase receptors (Tgfbr1 and ActRIIA, ActRIIB) and consequent phosphorylation of the Smad2 and Smad3 downstream effectors (Andersson et al., 2006; Gaunt et al., 2013; Ho et al., 2010; Oh and Li, 1997; Paul Oh et al., 2002). Phosphorylated Smad2/3 bind to Smad4 and as a complex enter the nucleus where they regulate target gene expression by binding to specific nucleotide sequence called Smad binding site (SBS). Besides promoting direct transcription factor (TF) activity, Tgf-β signaling pathways were also shown to act on chromatin conformation (Massagué, 2012).

The substantial differences between the trunk and tail in their tissue composition imply different regulatory activities in the corresponding caudal growth zone. In fact, even ever-present NMCs rely of different regulators to sustain their population and promote differentiation during trunk and tail formation (Aires et al., 2019, 2016; Robinton et al., 2019). Gdf11/Tgfbr1 signaling evidently launches profound molecular changes in the caudal growth zone during induction of the trunk to tail transition. Identifying these changes will shed light on the molecular events underlying the trunk to tail transition. In this chapter we describe changes in the transcriptome of axial progenitors during the trunk to tail transition and correlate them with changes in chromatin

conformation. Furthermore, we identify a subset of genes whose dynamic expression depends on Gdf11 activity in the context of the trunk to tail transition.

MATERIALS AND METHODS

Ethics statement

All animal procedures were performed in accordance with Portuguese (Portaria 1005/92) and European (directive 2010/63/EU) legislations and guidance on animal use in bioscience research. The project was reviewed and approved by the Ethics Committee of "Instituto Gulbenkian de Ciência" and by the Portuguese National Entity "Direcção Geral de Alimentação Veterinária" (license reference: 014308).

Mouse lines and embryos.

Gdf11 mutant embryos were obtained from crosses between the *Gdf11*$^{+/-}$ animals (McPherron et al., 1999). Pregnancy was verified by the presence of plug (E0.5). Mouse embryos were collected from pregnant females by caesarean section. Embryos were dissected in ice cold PBS, and the relevant tissue pooled in the RNase-free tubes on dry ice and stored at -80˚C. Tail buds from *Gdf11* mutant embryos were collected individually in RNase-free tubes and stored at -80˚C until their genotype was verified by PCR with the primers: Fw GCATCCTTTCATGGAGCTTCG, WT-Rv CTGGCCGGAGCAGTAGTTGG, Mut-Rv AGTAGAAGGTGGCGCGAAGG. Embryos were genotyped from their yolk sacs. Yolk sacs were collected to 50 μL of lysis buffer (50 mM KCl, 10 mM Tris-HCl, pH 8.3, 2 mM $MgCl_2$, 0.45% Tween-20, 0.45% NP40) supplemented with 100 μg/mL of proteinase K and incubated at 55˚C overnight. Samples were heat-inactivated for 15 minutes at 95˚C and 1 μL of each sample used in PCR reaction.

RNA extraction and RNA-Seq data analysis

For each sample 15-20 tails were pooled together before RNA extraction. Total RNA was extracted with TRI reagent (T9424, Sigma) according to the manufacturer's instructions. The quality of the samples was assessed with the Fragment Analyser (Advanced Analytical Technologies, Inc) and samples with RNA quality number (RQN)>9 were used for library preparation. Two biological replicates were used for each condition.

cDNA libraries were prepared with Smart-Seq2 protocol and sequencing was done with the Illumina NextSeq. Initial bioinformatic analysis was performed using the IGC Galaxy server. Single-end reads were trimmed to remove adaptors and aligned to the mouse reference genome GRCm38/mm10 with HiSat2. Gene expression was assessed by using FeatureCounts (Liao et al., 2014). Further analysis was performed in R (R Development Core Team https://www.r-project.org/). Differential gene expression between the samples (E9.5 vs E8.5 and E9.5 *Gdf11* mutant vs E9.5 wild type) was calculated using DeSeq2 (Love et al., 2014). Gene Ontology (GO) analysis was applied to the differentially expressed genes (DEG) with the log2 fold change greater that 2, (adjusted *P*-value<0,05) using GOrilla (Eden et al., 2009). KEGG pathways enrichment analysis was made on all DEGs with p<0.05 using the pathfindR package in R (Ulgen et al., 2019). Volcano plots were generated on the DESeq2 results output with EnhancedVolcano, heatmaps were generated with the Pheatmat package in R and barcharts with gglot2. Variance stabilising transformation (VST) was performed on DESeq2 data with the vsd function and principal component analysis (PCA) was made with the plotPCA function from DESeq2. Sample distance matrix was generated on the top 2500 most variable genes.

E8.5 wild type, E9.5 wild type and E9.5 *Gdf11*$^{-/-}$ samples were analysed with the EdgeR package (Robinson et al., 2009). For statistical analysis ANOVA-like test was applied to the genes with more than 10 counts per million (CPM) in

at least two samples. Pairwise analysis was done by evaluating individual contrasts.

ATAC-seq

ATAC-seq was performed as in (Buenrostro et al., 2016) with minor modifications. E11.25 mouse embryos were dissected on ice in DMEM High Glucose medium (Biowest #L0102-500) containing 10% FBS (this will be referred to as medium in the rest of the protocol). Epiblasts and tail buds were dissected out and collected on ice-cold media. Single cell suspension was prepared by treating the tissue with 500 μL of Accutase (Sigma #A6964-500ML) for 30 minutes at 37˚C with shaking at 600 rpm. Single cells were pelleted at 6000 rcf for 5 minutes at 4˚C, resuspended in 200 μL of media and counted. 50000 viable cells from each sample were used for nuclei extraction. Cells were incubated with 50 μL of ATAC resuspension buffer (10 mM Tris HCl pH 7.4, 10 mM NaCl, 3 mM $MgCl_2$, 0.1% NP-40, 0.1% Tween-20 (Sigma-Aldrich, P7949), 0.01% Digitonin (Target Mol #282T2721-1ml/10mM in DMSO) for 3 minutes on ice. Lysis was quenched by adding 1 mL of ATAC resuspension buffer without NP-40 and Digitonin. Nuclei were pelleted by centrifugation at 500 rcf for 10 minutes at 4˚C. The pellet was then resuspended in 50 μL of transposition buffer [for 50 μL: 25 μL 2x TD buffer, 2.5 μL Tn5 transposition enzyme (100 nM final) (Illumina #15028212), 16.5 μL PBS, 0.5 μL 1% digitonin, 0.5 μL 10% Tween-20, 5 μL H_2O] and incubated at 37˚C for 30 minutes with shaking at 1000 rpm. The DNA was purified with the Qiagen MinElute PCR purification kit (Qiagen #50928004) and eluted in 20 μL of the kit's elution buffer. Libraries were amplified by PCR with NEBNext High-Fidelity 2X PCR Master Mix (New England Biolabs #174M0541S) for 9 cycles in 96-well Thermal cycler (Biorad) and purified with the Qiagen MinElute PCR purification kit. Tagmentation efficiency was assessed on TapeStation 4200 (Agilent). Double size selection to remove primer dimers and fragments exceeding 1 kb was performed using SPRIselect beads (Beckman Coulter). Another quality control was performed with High

Sensitivity DNA assay using the Fragment Analyzer (Agilent). The 4 nM libraries pool was sequenced with Illumina NextSeq 2000 (100 cycles, Pair-end 50 bp). Two biological replicates were performed per tissue.

Differential analysis was done with GUAVA pipeline (Divate and Cheung, 2018). Peak annotation was done using the ChIPseeker package in R (Q. Wang et al., 2022). TF footprinting was done with program RGT HINT-ATAC (Li et al., 2019).

RESULTS

The trunk to tail transition is followed by significant changes of gene expression profiles in the axial progenitors region.

To identify changes in gene expression in the axial progenitor region during the trunk to tail transition, we performed RNA-seq before and after the transition. We recovered epiblasts, including the NSB, from embryos containing

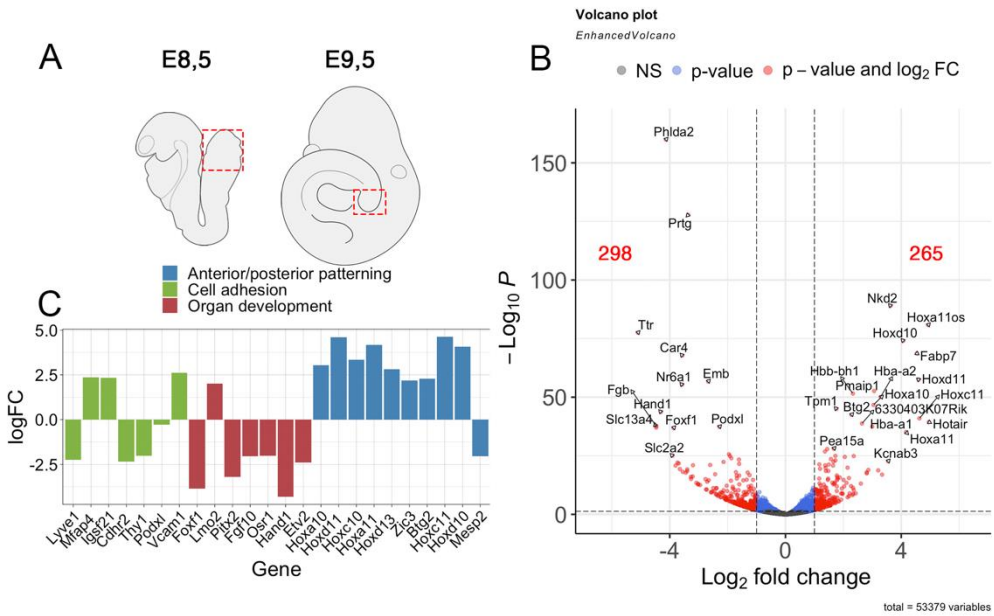

Figure 2-1. Gene expression changes during trunk to tail transition. A. Posterior epiblast at E8.5 and tail bud at E9.5 dissected for RNA extraction are shown in red rectangles. **B.** Volcano plot showing DEG between E9.5 and E8.5 in wild type embryos. Blue: p<0.05, red: p<0.05 and log2FC>1. **C.** Log2FC of the genes assigned to GO terms.

6 to 12 somite pairs (E8.5, trunk stages) and tail buds, including the CNH and the mesodermal compartment, from embryos at the 25 to 30 somites stage (E9.5, tail stages) (red rectangles in Figure *2-1*A).

We identified a total of 563 differentially expressed genes (DEGs) [p<0.05, Log2FC>1], among which 265 genes were upregulated, and 298 downregulated after the transition (Figure *2-1*B, Table *2-1*). Gene ontology (GO) analysis revealed significant enrichment of genes associated with anterior-posterior patterning [GO:0009952, p-values 1,41E-11], most of which belonged to posterior *Hox* genes (Figure *2-1*C). We also identified enrichment in GO terms corresponding to organ development [GO:0048513, p-value = 1,92E-5] and cell adhesion [GO:0007155, p-value = 1,12E-6] (Figure *2-1*C). Among genes included under the GO term "organ development" we found downregulation of genes related to the lateral and intermediate compartments of the mesoderm,

Table 2-1. Top 20 DEGs at the trunk to tail transition sorted by log2FC.

Upregulated after transition			Downregulated after transition		
Gene	log2FoldChange	pvalue	Gene	log2FoldChange	pvalue
Hotair	4,95332433	3,87E-40	Ttr	-5,100068187	3,24E-78
Hoxa11os	4,931941775	1,72E-81	Slc13a4	-4,469626822	9,30E-38
Hoxc11	4,626695927	1,15E-41	Fgb	-4,463646625	2,45E-38
Hoxd11	4,59990306	2,76E-58	Hand1	-4,305245022	2,23E-44
Fabp7	4,538539778	1,99E-69	Phlda2	-4,133919384	1,23E-160
Hoxa11	4,166753431	7,51E-36	Slc2a2	-3,906458418	1,00E-25
Hoxd10	4,068796296	9,15E-75	Foxf1	-3,868938416	1,49E-37
Nkd2	3,630953269	1,09E-89	Cer1	-3,799367189	1,53E-21
Kcnab3	3,544973919	2,24E-23	Amn	-3,733161197	8,77E-23
Hoxc10	3,337129012	1,12E-17	Apoa4	-3,689471131	1,90E-22
Hba-a2	3,287907122	7,90E-51	Soat2	-3,651103548	4,66E-20
Ebf2	3,205048252	1,68E-19	Nr6a1	-3,575641954	4,82E-56
Pmaip1	3,062134426	2,31E-53	Car4	-3,567288414	1,70E-68
Hoxa10	3,042017608	2,00E-47	Apom	-3,54972243	7,13E-19
Hba-a1	2,999473675	3,59E-38	Apoa1	-3,445881934	1,67E-18
Cd83	2,862286758	1,07E-19	Spp2	-3,399089913	3,38E-19
Hoxd13	2,809502824	3,36E-18	Rbp4	-3,39612869	6,24E-20
Ndrg2	2,807670837	1,17E-18	Prtg	-3,361215286	1,42E-128
6330403K07I	2,640968974	1,70E-39	Fgg	-3,270186044	1,06E-16
Vcam1	2,604700432	7,41E-14	Apob	-3,2612736	7,78E-16

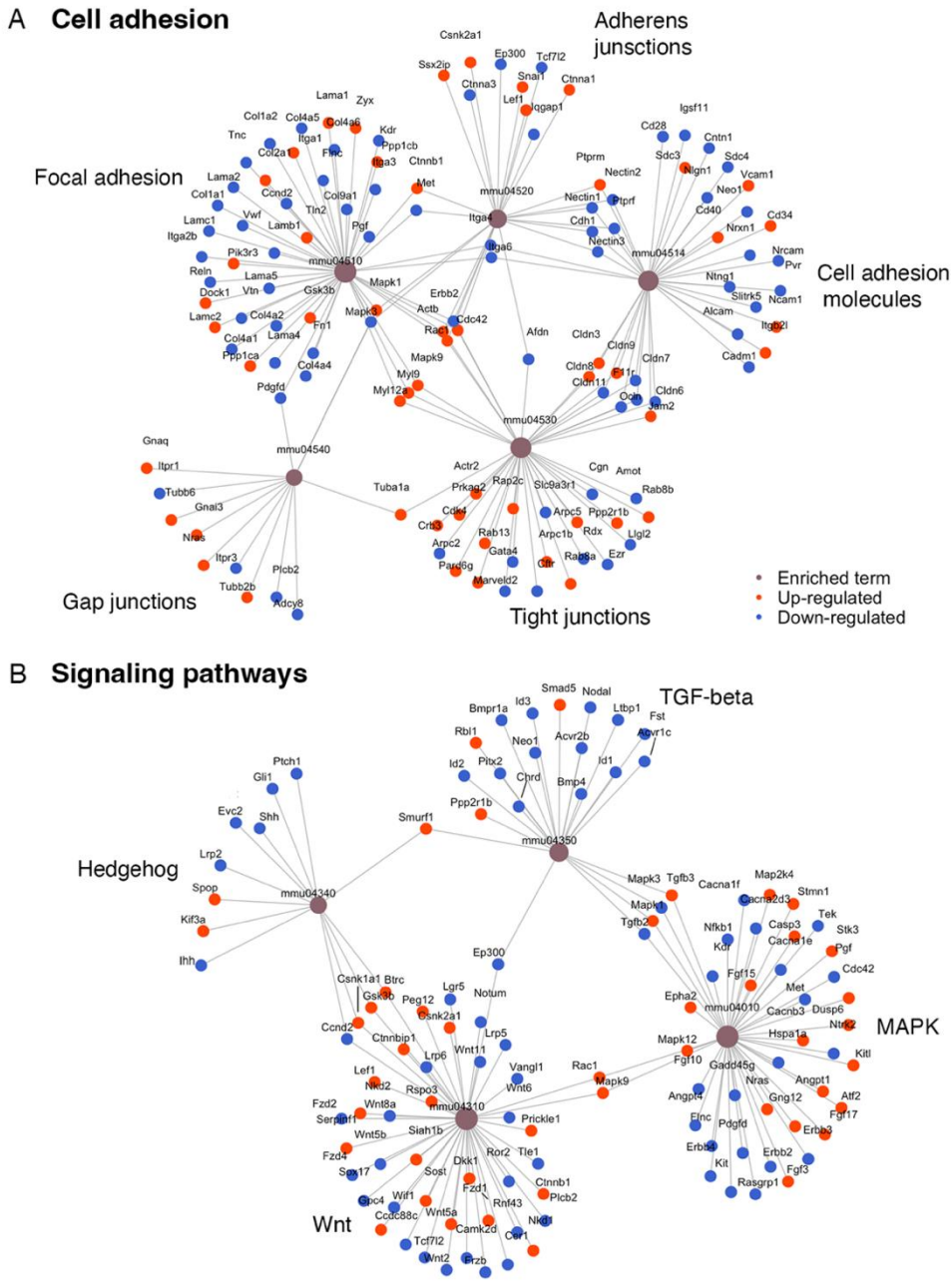

Figure 2-2. KEGG pathways enrichment in DEGs E9.5 vs E8.5 in wild type embryos [p<0.05] A. Terms associated to cell adhesion **B.** Terms associated to signaling pathways.

including *Foxf1, Hand1,* and *Osr1* (Mahlapuu et al., 2001; Maska et al., 2010; So and Danielian, 1999), consistent with the completion of LMP/IM differentiation from the epiblast after the trunk to tail transition (Figure *2-1*C). Among the NMC

markers, the neural marker *Sox2* [p=0,7] did not show significant difference after the transition, but we observed upregulation of *Tbxt* [logFC = 1,3; p=1e-21], which likely reflects the Tbxt-positive tail bud mesoderm population present in the E9.5 sample.

We then performed KEGG pathway enrichment analysis on the set of DEGs [p<0.05], and once again we identified significant changes in the composition of cell adhesion molecules associated with the trunk to tail transition (Figure *2-2*A). Interestingly, we found many enriched KEGG terms belonging to signaling pathways, including TGF-β, Hedgehog, Wnt and MAPK (Figure *2-2*B). We particularly noticed downregulation of the members of BMP and Activin/Nodal subfamilies of the TGF-β signaling and members of Hedgehog signaling, including *Shh, Ihh, Gli1* and *Ptch1* after the transition (Figure *2-2*B). Consistent

Table 2-2. Top 20 DEGs between E9.5 wild type and Gdf11$^{-/-}$ embryos, sorted by log2FC

Genes downgerulated in *Gdf11* KO			Genes upregulated in *Gdf11* KO		
Gene	log2FoldChange	pvalue	Gene	log2FoldChange	pvalue
Hotair	-5,531397834	4,34E-65	Gm26461	7,390999193	3,45E-140
Hoxd12	-5,387280042	2,23E-80	Hand1	3,516846397	1,44E-27
Gdf11	-5,054391004	8,54E-154	Gm14226	3,28637068	1,88E-92
Hoxc12	-4,524352044	1,58E-24	Foxf1	3,157398603	1,41E-26
Lzts1	-4,353745055	4,73E-54	Nynrin	2,920727581	6,31E-17
Hoxc13	-3,980015601	3,01E-21	Nr6a1	2,827405329	1,27E-41
Gm7125	-3,975530296	6,20E-21	Gm37233	2,814294903	1,72E-09
Vcam1	-3,971907904	4,25E-49	Barx1	2,789780028	1,85E-09
Ebf2	-3,733149307	9,05E-53	mt-Nd3	2,782583616	2,45E-16
Hoxc11	-3,686967953	5,18E-54	Alx4	2,78086943	3,94E-20
Hoxd11	-3,612060215	2,96E-69	Npbwr1	2,689623508	2,68E-17
Hoxa11os	-3,470499917	4,46E-73	Gfra1	2,679382535	1,65E-11
Tg	-3,453860096	1,40E-34	Pax6	2,67931431	1,07E-15
Lefty2	-3,333295649	1,05E-13	Carmn	2,660123264	9,91E-09
BC002163	-3,320656517	7,38E-15	AV026068	2,653178624	2,48E-17
Gm6667	-3,298487643	1,13E-24	Pitx2	2,636196147	4,20E-10
Eno1b	-3,180789745	8,03E-44	CT009480,2	2,586108995	5,07E-12
Cd40	-3,129292075	8,15E-44	Fgf10	2,526151451	1,29E-14
Apoa1	-3,055331845	1,29E-13	AC158987,1	2,52451061	8,44E-08
Gm6594	-3,023823135	9,10E-11	Ndnf	2,494420453	2,31E-34

with its role as a trigger of the trunk to tail transition, *Gdf11* was upregulated after the transition [logFC = 1,5; p = 1e-21].

Gdf11 regulates a subset of genes changed at the trunk to tail transition.

Due to the known role of *Gdf11* in the trunk to tail transition, we compared the gene expression profile at E9.5, right after the transition, between *Gdf11* KO and wild type tail buds. We found 1588 gene differentially expressed, 876 upregulated and 712 downregulated, in *Gdf11* mutants compared to wild type controls [p<0.05, log2FC>1] (Figure *2-3*A, Table *2-2*). As in the analysis involving E8.5 and E9.5 embryos, many of the posterior *Hox* genes were among the most significant DEGs. However, they now represented downregulated genes, consistent with previously reported role of Gdf11 in the activation of the posterior *Hox* genes at the trunk to tail transition (Aires et al., 2019; Gaunt et al., 2013; Jurberg et al., 2013; Matsubara et al., 2017; McPherron et al., 1999).

KEGG pathway enrichment analyses revealed that many of the pathways affected by the absence of *Gdf11* were common with those identified in the wild type embryos undergoing the transition (Figure *2-4*). Particularly, many enriched KEGG terms were associated with cell adhesion molecules (Figure *2-4*B). Significantly enriched KEGG terms also included many of the signaling pathways also identified in the previous analysis of wild type embryos undergoing trunk to tail transition (Figure *2-4*A). Interestingly, many genes belonging to these pathways changed in the *Gdf11* mutants with the reverse orientation than in the transition.

Particularly we noted that many of the Hedgehog pathway members were upregulated in the *Gdf11* mutants relative to wild type controls at E9.5 (Figure *2-4*A). This suggests that Gdf11 acts to downregulate the Hedgehog signaling pathway at the trunk to tail transition. Many genes downregulated in the *Gdf11* mutants at E9.5 were among those upregulated at E9.5 as compared to E8.5 in the wilt type condition (and vice versa), therefore following a pattern of expression characteristic of E8.5 wild type embryos. This is consistent with the

delayed trunk to tail transition in the *Gdf11* KO embryos. To identify the cohort of genes under the regulation of *Gdf11* within those changing expression during the trunk to tail transition, we integrated the data of E8.5 and E9.5 wild type embryos with data from E9.5 *Gdf11* KO embryos. This analysis showed that wild type samples (E8.5 and E9.5) clustered closer together on the sample distance map and along the principal component 1 (PC1) of the principal component

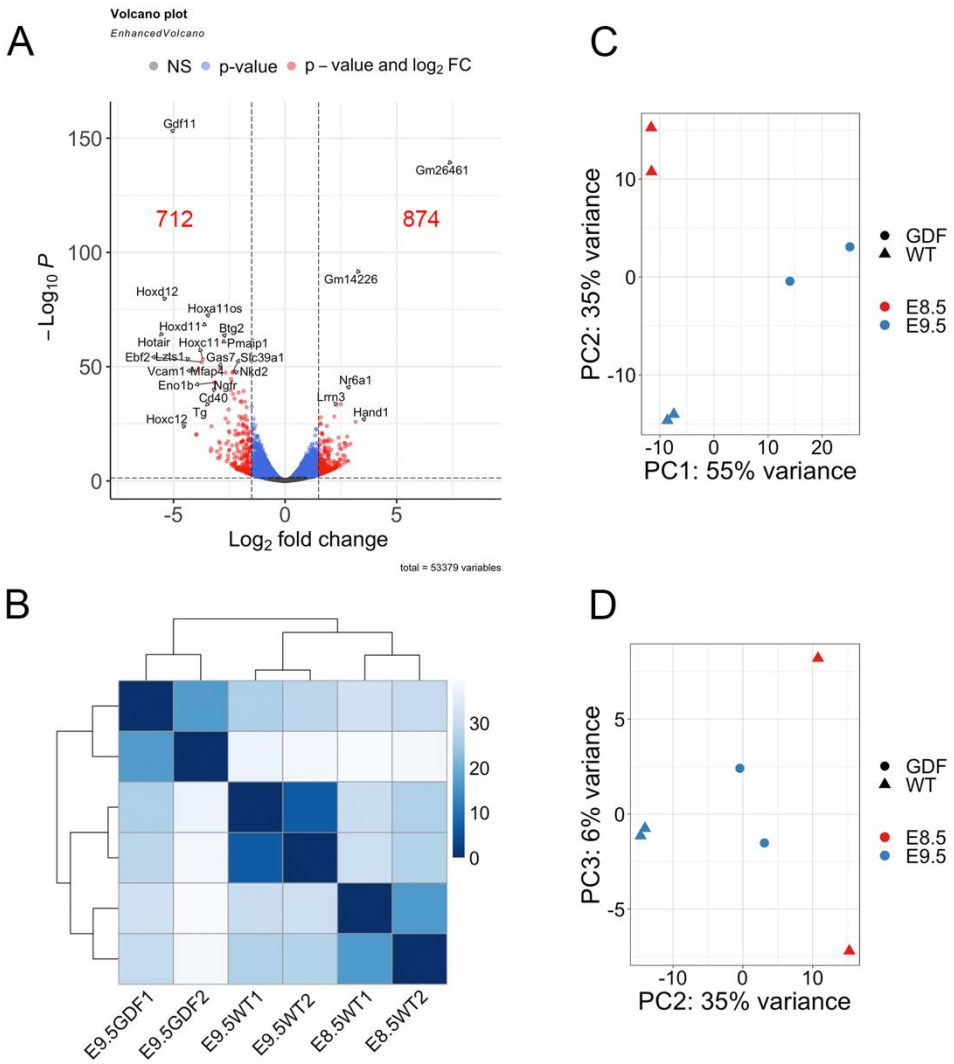

Figure 2-3. Gdf11 regulates expression of multiple genes in the context of trunk to tail transition. A. Volcano plot showing DEGs between E9,5 GDf11$^{-/-}$ and wild type tail buds. Blue: p<0.05, red: p<0.05 and log2FC>1 **B.** Samples distance heatmap showing clustering of the samples. **C.** PCA plot showing samples distribution along the PC1 and PC2. **D.** PCA plot showing samples distribution along the PC2 and PC3.

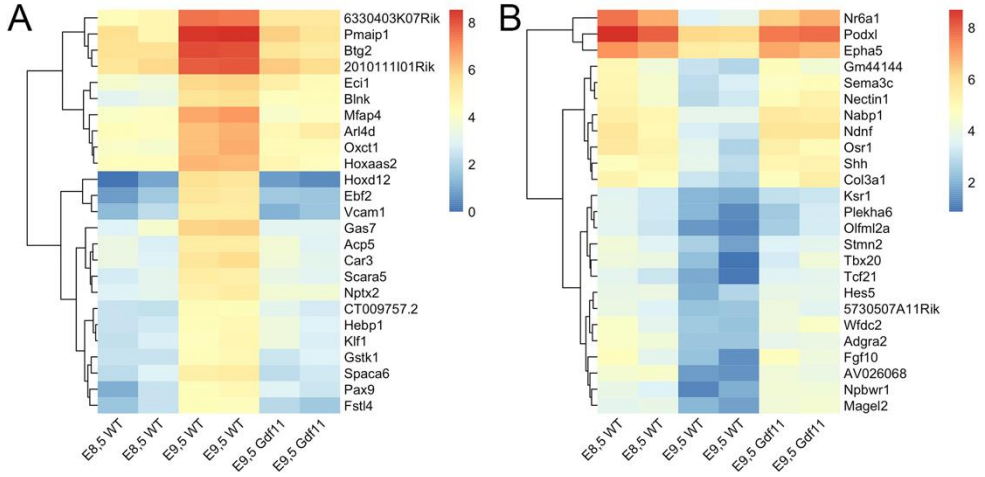

Figure 2-4. Genes differentially expressed after the trunk to tail transition in the wild type, but not in Gdf11$^{-/-}$ embryos. Heatmaps showing log2 normalized counts. **A.** Top 25 genes upregulated at E9.5 comparing to E8.5 **B.** Top 25 genes downregulated at E9.5 comparing to E8.5.

analysis (PCA) graph, reflecting significant gene expression perturbation by loss of *Gdf11* beyond that explained by the delayed transition (Figure *2-3*B, C). When PC2 and PC3 were analyzed, however, E9.5 *Gdf11* samples were placed between the E8.5 and E9.5 wild type samples, possibly reflecting the "delayed" status of some genes (Figure *2-3*D). To identify these "delayed" trunk to tail transition genes, we selected genes differentially expressed between E9.5 wild type and *Gdf11* mutant samples, that were not found differentially expressed between E8.5 wild type and E9.5 *Gdf11* mutant genes. We identified 108 genes following this pattern [$p<0.05$, log2FC>1], 95 upregulated and 87 downregulated at the trunk to tail transition in wild type embryos, but not in *Gdf11* mutants. Our analysis showed *Gdf11* involvement in downregulation of the LPM/IM-related genes *Foxf1* and *Osr1*, and in upregulation of posterior *Hox* genes (e.g., *Hoxd8, Hoxd12, Hoxd13*) (Figure *2-5*A, B).

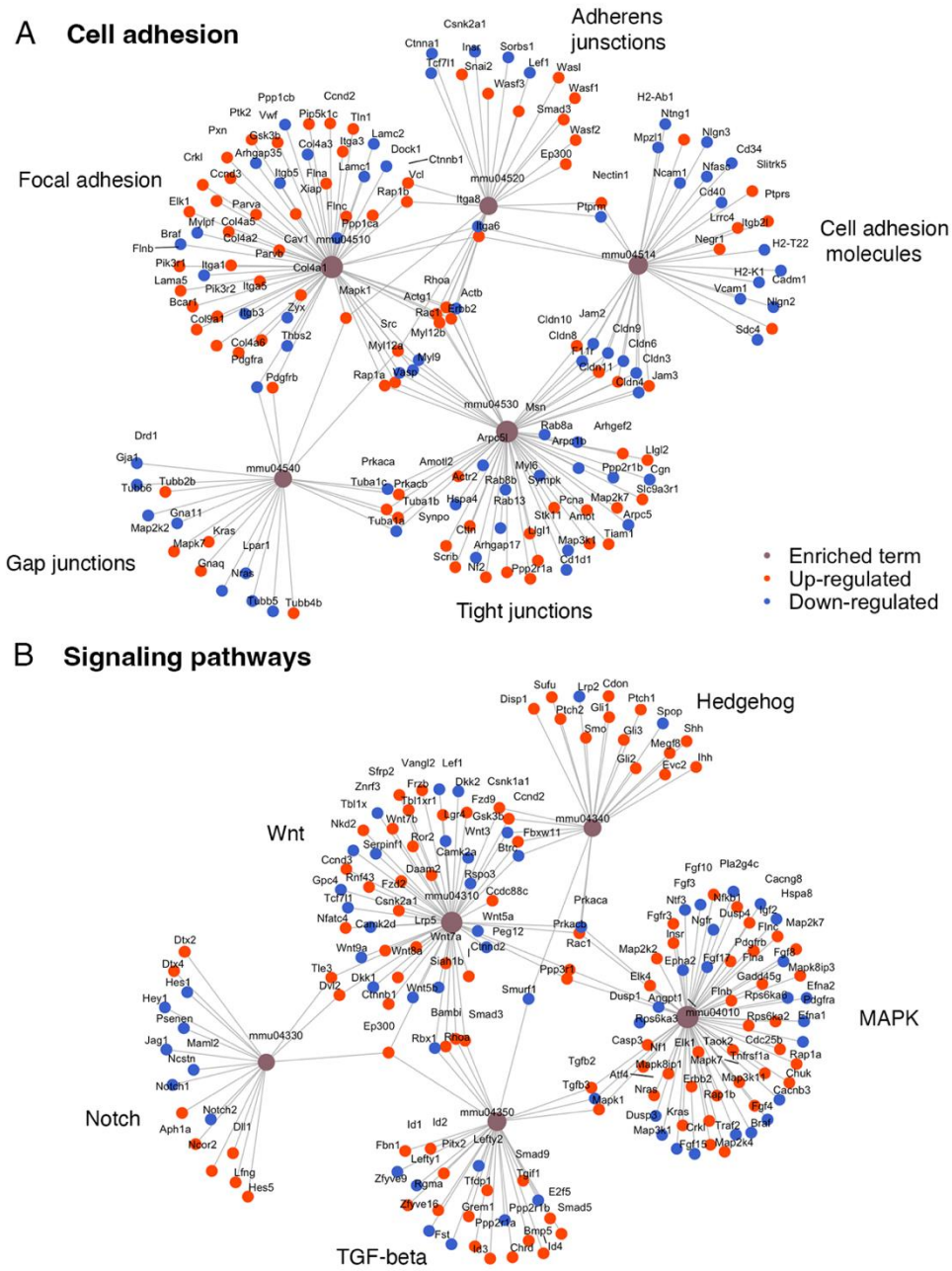

Figure 2-5. KEGG pathways enrichment in DEGs E9.5 Gdf11$^{-/-}$ vs wild type [p<0.05]. A. Terms associated to cell adhesion **B.** Terms associated to signaling pathways.

The trunk to tail transition is accompanied by changes in chromatin accessibility.

To see how the gene regulatory landscape is changed upon the trunk to tail transition, we compared the chromatin accessibility patterns between the epiblast of E8.5 and tail bud of the E9.5 wild type embryos. We found 286 and 602 regions that respectively gained or lost accessibility at E9.5 compared to E8.5 [$p<0.05$, $log2FC>2$] (Figure *2-6*A). We then annotated differentially accessible peaks (a peak was assigned to a gene if it was located within 5 kb upstream of its TSS or within the gene region) and correlated them with genes differentially expressed during the trunk to tail transition in wild type embryos [$p<0.05$]. We identified 25 peaks assigned to the DEGs (Figure *2-6*B). Notably, for the majority of these genes upregulation correlated with gained accessibility of the associated peaks, and downregulation with lost accessibility of the peak (Figure *2-6*B). Seven of the annotated peaks were located within the loci of the "delayed" trunk to tail transition genes (labelled with blue triangle in Figure *2-6*B), and 6 peaks were found in the presumed promoter region of the corresponding genes (withing 5 kb from TSS, labelled with red circles in Figure *2-6*B). Interestingly, while the majority of the accessible peaks were located in the promoter regions in the E8.5 and E9.5 samples, the same was not the case for the differentially accessible peaks (Figure *2-6*C). More than half of the peaks which changed their chromatin accessibility upon the trunk to tail transition were located in intergenic regions (Figure *2-6*C). This implies that changes in gene regulation (at least at the chromatin conformation level) in this developmental context is mainly mediated through the rearrangement of the distal cis-regulatory elements. Curiously, when we performed differential TF footpriting analysis on our ATAC-seq datasets we did not identify differential enrichment of Gdf11 canonical downstream effectors Smad2 and Smad3 (Figure *2-6*F, G). However, we did observe higher signals of Hoxd13 [$p = 0.02$] (Figure *2-6*D) and Cdx2 [$p = 0.02$] at E9.5 (Figure *2-6*), hinting to the gain of regulatory activity for these TFs in the tail bud.

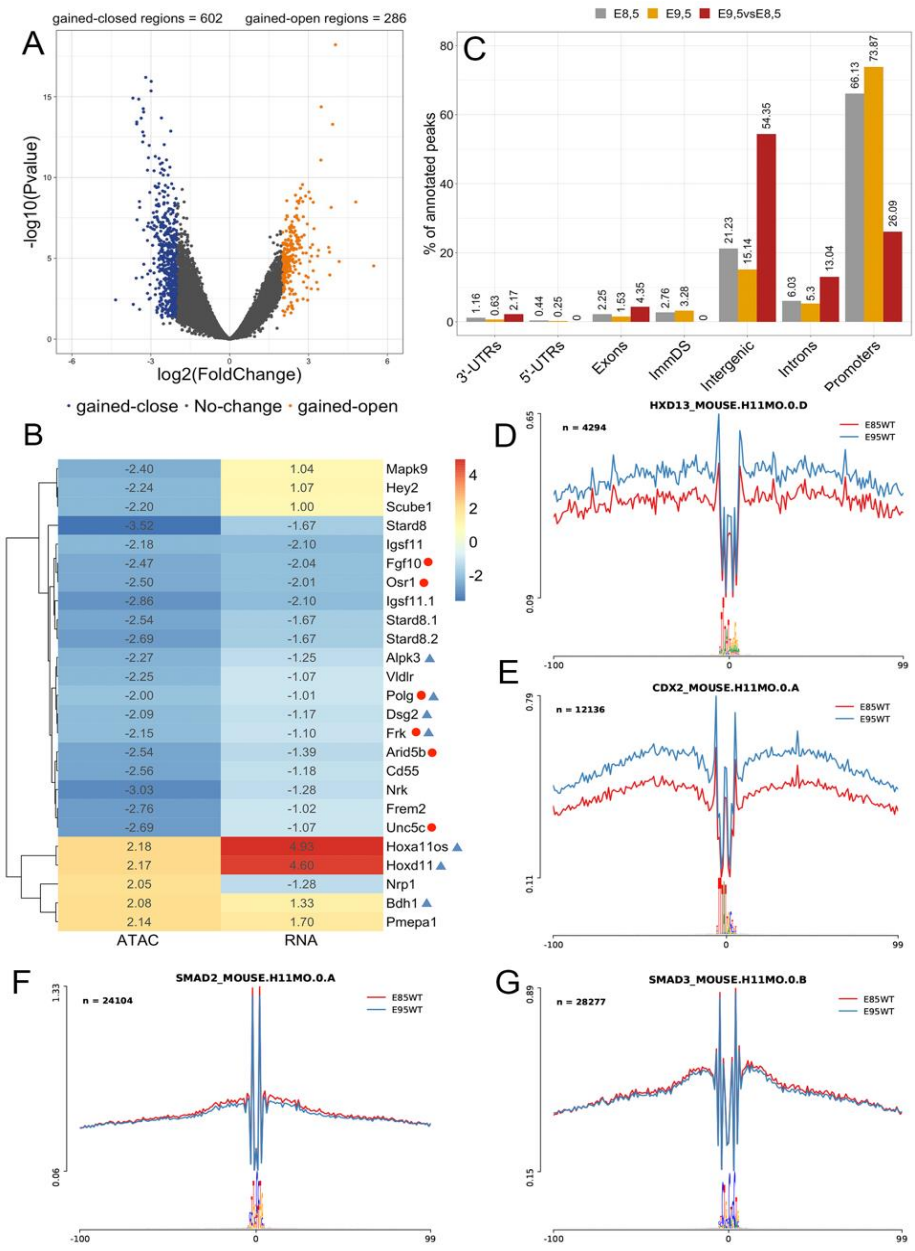

Figure 2-6. Trunk to tail transition is accompanied by changes in chromatin accessibility. A. Volcano plot showing differentially accessible peaks in E9.5 comparing to E8.5 wild type embryos. Yellow: gained-open, blue: gained-closed p<0.05, log2FC>2. **B.** Heatmap showing log2FC of annotated differentially accessible peaks and DEGs in E9.5 comparing to E8.5 wild type embryos. **C.** Peaks marked by blue triangles are located in promoter regions (< +5kb from TSS), genes marked by the red circles belonged to genes "delayed" in Gdf11$^{-/-}$ embryos. **D-G.** TF foootprinting profiles of Hoxd13 (D), Cdx2 (E), Smad2 (F) and Smad3 (G) motifs. Red: E8.5; blue: E9.5.

DISCUSSION

Our comparative analyses of the axial progenitor region before and after the trunk to tail transition reveals interesting tendencies in the progenitors' behavior. Of note, at the trunk to tail transition cells in the axial progenitor region undergo a switch in their profile of cell adhesion molecules. At trunk forming stages mesodermal tissues differentiate by delaminating from the epiblast through an epithelial to mesenchymal transition (EMT). Consistently, the canonical epithelial marker *Cdh1* is downregulated after the transition. Moreover, we found that the mesenchymal associated EMT factor *Snai1* (Fazilaty et al., 2019) is upregulated after the transition. Transition is concurrent with the axial progenitors' relocation from the NSB to the CNH in the tail bud (Jurberg et al., 2013; Wilson et al., 2009). The molecular signature of progenitor-like CNH cells indicates that they retain some epithelial properties. Interestingly, *Gdf11* does not seem to impact neither *Cdh1* nor *Snai1* expression, because these genes were unchanged in the tail bud of the *Gdf11* KO when compared with wild type controls.

On the other hand, many features of the trunk to tail transition proved to require *Gdf11*. For example, our analysis associates *Gdf11* with downregulation of the LPM/IM markers *Foxf1* and *Osr1* during the transition. *Foxf1* will be discussed in greater details in the next chapter. *Osr1*, expressed in the IM, was recently linked to the Tbx6-positive paraxial mesodermal cells, where it is activated by BMP signaling, and represses somitic fate to activate the nephric mesenchyme lineage (Hayashi et al., 2021). In wild type embryos several members of BMP pathways, including *Bmp4* and its receptor *Bmpr1b*, are downregulated after the transition (Figure *2-2*B). In *Gdf11* KO, however, these genes remained unchanged, suggesting that *Osr1* expression is maintained in the *Gdf11* mutant tailbud independently of BMP. Curiously, despite of the upregulation of the nephric mesenchymal marker *Osr1, Gdf11* mutants often lack one or both kidneys (Mcpherron et al., 1999).

While there no is clear pattern showing *Gdf11* regulating the BMP pathway, our results reveal that *Gdf11* is required to downregulate members of the Hedgehog signaling pathway after the trunk to tail transition. Indeed, Hedgehog signaling has been shown to be active in the posterior embryo before the transition (Daane and Downs, 2011), while being mainly represented by *Shh* expression in the notochord during tail growth (data not shown). Interestingly, a recent study revealed Shh signaling requirement to activate transcription of the retinoic acid degrading enzyme *Cyp26a1* in different developmental contexts, including in the tail (El Shahawy et al., 2019). Our RNA-seq experiment, however, shows downregulation of *Cyp26a1* in the tail bud, consistent with previously reported data (Jurberg et al., 2013; Lee et al., 2010). Therefore, the functional relevance of upregulated Hedgehog signaling in the *Gdf11* mutant tail bud remains unclear.

High retinoic acid signaling is known to promote neural fates in the axial progenitors (Gouti et al., 2017). Downregulation of *Cyp26a1* possibly leads to the observed downregulation of *Tbxt* in *Gdf11 KO* tail bud as a result of progenitors favoring neural fate due to excessive exposure to retinoic acid (Aires et al., 2019).

Our ATAC-seq analysis of chromatin accessibility before and after the trunk to tail transition shows that the majority of differentially accessible peaks are located in intergenic regions and likely represent distal enhancers. Surprisingly, Gdf11 intracellular effectors Smad2 and Smad3 were neither upregulated after the transition, nor their footprints were differentially enriched at the ATAC-seq peaks. While *Smad2/3* expression is not necessarily a read out of the Gdf11 activity, we had expected to find enhanced Smad2/3 binding to genomic regions following the activation of Gdf11 signaling.

The TF footprinting analysis revealed increased binding of Hoxd13 and Cdx2 at E9.5. *Cdx* genes positively regulate *Wnt3a* and *Cyp26a1* expression in the axial progenitor zone, required for the axial extension in both trunk and tail (Young et al., 2009). Axial progenitors in the tail, however, seem to be more

sensitive to the *Cdx* deficiency, as *Cdx2*$^{+/-}$/*Cdx4*$^{-/-}$ embryos exhibit axial truncation at the sacral level (Young et al., 2009). *Hox13* genes are activated in the axial progenitor region after the trunk to tail transition in response to *Gdf11* and are involved in cessation of axial extension (Aires et al., 2019; Deschamps and Duboule, 2017; Economides et al., 2003). Considering the importance of both *Cdx* and *Hox13* genes to balance axial growth of the tail region, their enhanced footprints enrichment after the trunk to tail transition, and the lack of an increase in Smads footprint enrichment after the transition, it is tempting to speculate whether Gdf11 activity might be in part mediated via these genes. Interestingly, while *Hoxd13* is upregulated at the transition and is dependent on *Gdf11*, *Cdx2* is expressed at the same level before and after the transition and its expression level is unchanged in *Gdf11* mutants. This might illustrate two different modes of TFs activity regulation: one, like in case of Hoxd13, is based on TF availability, and the other on the accessibility of the chromatin to allow their access to their target elements.

Acknowledgements

We would like to thank the members of the Mallo lab, especially Ana Casaca for continuous support at different stages of this project, the IGC mouse facility for their help with animal housing and genomics facility for helping with the RNA-seq and ATAC-seq procedures. This project was funded by Fundação para a Ciência e a Tecnologia (FCT) grants PTDC/BIA-BID/30254/2017 to MM, and PhD fellowships PD/BD/128437/2017 to AL, and Congento LISBOA-01-0145-FEDER-022170 to the animal facility, financed by Lisboa Lisboa 2020/FEDER and FCT (Portugal).

Chapter 3

TGFBR1 AS THE MAIN REGULATOR OF THE TRUNK TO TAIL TRANSITION.

Authors contribution: Anastasiia Lozovska and Moisés Mallo designed experiments. Anastasiia Lozovska performed experiments; André Dias performed immunofluorescence analysis of the EMT molecular markers and in situ hybridization for several markers; Ana Nóvoa performed pronuclear microinjection of DNA constructs; Anastasiia Lozovska and Moisés Mallo analyzed data.

Part of this chapter is included in André Dias, **Anastasiia Lozovska**, Filip J Wymeersch, Ana Nóvoa, Anahi Binagui-Casas, Daniel Sobral, Gabriel G Martins, Valerie Wilson, Moises Mallo (2020) A Tgfbr1/Snai1-dependent developmental module at the core of vertebrate axial elongation *eLife* 9:e56615.

This chapter is adapted from **Anastasiia Lozovska**, Ana Nóvoa, Ying-Yi Kuo, Arnon Jurberg, Anna-Katerina Hadjantonakis & Moises Mallo (2023) Tgfbr1 regulates lateral plate mesoderm and endoderm reorganization during the trunk to tail transition. *In preparation.*

SUMMARY

The major compartments of the vertebrate body – neck, head, trunk, and tail - are sequentially laid down during embryonic development. The transition between these compartments requires strict genetic control and results in drastic tissue remodeling. Particularly, the trunk to tail transition is associated with significant reorganization of the embryo's caudal end. Regression of the epiblast, the main source of new tissues during extension through the trunk, is followed by formation of the tail bud – a new growth zone for axial extension. Trunk termination is marked by the merge of the lateral plate mesoderm (LPM) layers limiting the coelomic cavity, and the induction of the posterior appendages – hindlimbs and external genitalia. Precursors of these structures are laid down during the trunk to tail transition in the form of the hindlimb buds and pericloacal mesenchyme. Premature activation of the Tgf-β signaling family receptor Tgfbr1 in axial tissues is sufficient to anteriorize the transition, and therefore all corresponding structures. In this chapter we analyze the phenotype of *Tgfbr1* mutant embryos and showed the requirement of this receptor to initiate the trunk to tail transition. Our results indicate that Tgfbr1 activity is necessary for tail bud formation and continuation of tail extension. Additionally, we show that Tgfbr1, acting upstream of *Isl1*, regulate the reorganization of the caudal trunk concurrent with the trunk to tail transition.

INTRODUCTION

The transition from trunk to tail development is a complex process resulting in major changes in the general structure of the embryo and involving a switch in the mechanisms regulating axial extension. Extension through the trunk is driven by axial progenitors located within the epiblast that generate the spinal cord, the embryonic gut, and the different mesodermal compartments (Cambray and Wilson, 2007; Tzouanacou et al., 2009; Wymeersch et al., 2019). At this stage, the caudal end of the mouse embryo is occupied by the allantois

that will play an essential role in the connection between embryonic and extraembryonic structures (Rodriguez et al., 2017). The transition to tail development is associated with changes in the global anatomy of the caudal embryonic end, involving the progressive relocation of the allantois in an anterior direction along the ventral side of the embryo. During this process, the embryo forms the tail bud at the posterior end of the embryo, which replaces the epiblast as the main driver of axial extension (Cambray and Wilson, 2002). Formation of the tail bud results from changes in the progenitors generating the neural and paraxial mesodermal structures, the so called neural-mesodermal competent (NMC) population, that relocates from the epiblast to the chordo-neural hinge in the dorsal tail bud (Binagui-Casas et al., 2021; Cambray and Wilson, 2002; Tzouanacou et al., 2009).

At this stage, the LPM also undergoes a major reorganization. This mesodermal compartment, generated by progenitors at the caudal region of the epiblast (Wymeersch et al., 2019), is composed of two layers, a ventral splanchnopleure that contributes to the formation of the various body organs, as well as their vascularization, and a lateral somatopleure involved in the formation of the body wall (Prummel et al., 2020). These two layers delimit the celomic cavity, which will hold the animal's internal organs. During allantois relocation, the two layers converge towards the midline ending the celomic cavity and marking the posterior border of the trunk. This remodeling of the caudal part of the embryo is associated with the induction of the hindlimbs from the somatopleure (Prummel et al., 2020; Tanaka, 2013), and the generation of the pericloacal mesenchyme, the genital tubercle (GT) primordium, from the ventral tail bud mesoderm (Tschopp et al., 2014).

Concomitant with the reorganization of the embryonic mesoderm, the transition from trunk to tail development also involves major changes in the embryonic endoderm and in the patterns of vascularization that will functionally connect embryonic and extraembryonic structures. When the allantois relocates, the embryonic endoderm, whose posterior end reaches the

base of the allantois, bends ventrally and posteriorly forming a cavity that will originate the cloaca - an endodermal expansion that becomes the common end of the excretory, intestinal, and genital tracts (Huang et al., 2016; Matsumaru et al., 2015). In the mouse, the embryonic endoderm expands further caudally to generate the tail gut, a transient structure with unknown functional role. It has been shown that the region of the posterior visceral endoderm abutting the allantois provides the progenitors that facilitate the bending and growth of the embryonic endoderm, eventually generating a considerable part of the hindgut epithelium (Kwon et al., 2008; Rodriguez et al., 2017).

The major blood vessels also become reorganized with the anterior relocation of the allantois. The caudal end of the paired dorsal aortas (DA) merge and connect with the umbilical artery generated within the allantois (Rodriguez and Downs, 2017). As the allantois move forward, the caudal end of the DA bends to form the recurved dorsal aorta (rDA) (Walls et al., 2008). It is thought that this process requires the generation of a vessel of confluence from the caudal end of the primitive streak abutting the allantois, which will constitute a major part of the rDA (Rodriguez et al., 2017). Reorganization of the DA/umbilical artery connection will generate the blood vessels connecting the embryo with the placenta (Inman and Downs, 2007).

Not much is known about the regulation of the different processes associated with the trunk to tail transition. Premature expression of a constitutively active form of the Tgfbr1 receptor promotes early activation of the trunk to tail transition (Jurberg et al., 2013). Therefore, we analyzed possible involvement of this signaling in the global reorganization of the caudal embryonic end during this transition. Our findings indicate that *Tgfbr1* null mutant embryos fail to undergo trunk to tail transition. *Tgfbr1* is required specifically in the caudal most part of the trunk to regulate reorganization of the LPM layers and for initiation and development of their terminal derivatives - the hindlimbs and the genital tubercle. Although *Tgfbr1* KO embryos can complete

the process of turning, the associated cloaca/hindgut development and vascular reorganization are compromised in the mutants.

MATERIALS AND METHODS

Mouse lines and embryos

The *Tgfbr1* KO line was generated using the CRISPR-Cas9 system [Jinek, 2012]. The gRNA was designed to target the sequence TTGACCTAATTCCTCGAGAC in the second exon of the gene. The donor DNA consisted of a single stranded oligonucleotide (Replacing oligo, Table *3-1*) containing three stop codons in the frame of the gene, followed by a BamHI site, flanked by 60 nucleotide-long homology arms. The gRNA was produced by *in vitro* transcription from a vector containing the target sequence linked to the tracRNA scaffold. *In vitro* transcription was performed with the MEGAshortscript T7 kit (Life Technologies) and purified with the MEGAclear kit (Life Technologies). The purified gRNA (10 ng/μL) was microinjected into fertilized mouse oocytes together with 10 ng/μL of Cas9 mRNA and 10 ng/μL of the replacement ssDNA.

Founder pups were genotyped from tail biopsies. Samples were incubated overnight at 55˚C in 100 μL Laird's lysis buffer (100 mM Tris- HCl, pH 8.5, 5 mM EDTA, 0.2% SDS, 200 mM NaCl) supplemented with 100 μg/mL of proteinase K.

Table 3-1. List of oligonucleotides.

Replacing oligo			
ACCACAGACAAAGTTATACACAATAGTATGTGTATAGCTGAAATTGACCTAATTCCTCGATGATGATAGGATCCGACAGGCCAT TTGTATGTGCACCATCTTCAAAAACAGGGGCAGTTACTACAACATATTGC			
Genotyping primers			
Name	Forward	Name	Reverse
Tgfbr1-F1	TGTGAGACAGATGGTCTTTGC	Tgfbr1-R	TATTGCAGTGGTCCTGATTGC
Tgfbr1-F2	CTACTGTGTTTCAAATGGGAGGGC	Mut-R	GGCCTGTCGGATCCTATCATC
Common-F	CTACTGTGTTTCAAATGGGAGGGC	WT-R	ACATACAAATGGCCTGTCTCG
Cre-F	CGAGTGATGAGGTTCGCAAG	Cre-R	CCTGATCCTGGCAATTTCGGCT
Isl1-F	GCCACTATTTGCCACCTAGC	Isl1-wtR	CAAATCCAAAGAGCCCTGTC
		Isl1-mutR	AGGCAAATTTTGGTGTACGG
In situ probes			
Foxf1	GAATTCCTTCCGAAGGAAATGCCAGG		TCTAGAGAGGCCCCGCTGTTGAGAG
Irx3	GAATTCCCTCCAGAAGCCCAAGATCTG		TCTAGAGAGGCCCCGCTGTTGAGAG
Apela	CGGAATTCTTTCCTTGGCTCTACCAGAAG		GTGGATCCATAAAAGAGACCTGCAGGAGG

DNA was then precipitated with an equal volume of isopropanol and dissolved on 50 μL of TE buffer (1 mM EDTA, 10 mM Tris-HCl, pH 8.0). PCR was performed using 1 μL of genomic DNA with following primers Tgfbr1-F and Tgfbr1-R (Table *3-1*). The PCR product was run in a 15% polyacrylamide gel, the band with the expected size of the mutant product excised from the gel and crushed into 30 μL of TE buffer followed by incubation at 37˚C overnight. The DNA extract was then used as a template for a PCR reaction using the same primers and the product sequenced to verify the insertion.

Once the mutant line was established by crossing positive founders with wild type females, pups were genotyped from ear of digit biopsies. Samples were incubated in 50 μL of the PBND buffer (50 mM KCl, 10 mM Tris-HCl, pH 8.3, 2.5 mM $MgCl_2$, 0.1 mg/mL gelatin, 0.45% NP40, 0.45% Tween 20) supplemented with 100 μg/mL of proteinase K at 55˚C overnight. Samples were incubated at 95˚C for 15 minutes to heat-inactivate proteinase K. 1 μL of genomic DNA was used in the PCR reaction with primers Tgfbr1-F2 and Mut-R amplifying the mutant allele.

Embryos obtained from heterozygous crossings were genotyped from their yolk sacs. Yolk sacs were collected to 50 μL of lysis buffer (50 mM KCl, 10 mM Tris-HCl, pH 8.3, 2 mM $MgCl_2$, 0.45% Tween-20, 0.45% NP40) supplemented with 100 μg/mL of proteinase K and incubated at 55˚C overnight. Samples were heat-inactivated as described above. PCR was performed using 1μL of genomic DNA with two sets of primers: Common-F and Mut-F to amplify mutant allele and Common-F and WT-R to amplify wild type allele.

The *Isl1-Cre* mouse line was previously described (Srinivas et al., 2001). Homozygous *Isl1* KO embryos were obtained by crossing *Isl1-Cre* heterozygous mice. Pups were genotyped with primers Cre-F and Cre-R and embryos were genotyped with primers Isl1-F and Isl1-R listed in Table *3-1* as previously described.

Whole mount in situ hybridization and sectioning

Embryos were fixed in 4% paraformaldehyde in PBS (PFA) overnight, then dehydrated through 25%, 50% and 75% series of methanol in PBT (PBS, 0,1% Tween 20), and incubated in 100% methanol. Embryos were then rehydrated through a reverse methanol/PBT series and washed three times in PBT for at least 5 min each at room temperature. Embryos were then bleached for 1 hour in 6% hydrogen peroxide in PBT and permeabilized in 10 μg/mL of proteinase K in PBT for a time period that depended on the embryo size. The reaction was then quenched with a 2 mg/mL solution of glycine in PBT, washed twice in PBT and postfixed in a 4% PFA and 0,2% glutaraldehyde mix for 20 minutes, followed by two washes in PBT. Hybridization was performed at 65˚C overnight in hybridization solution (50% formamide, 1.3 x SSC pH 5.5 [20 x SSC is 3M NaCl, 300 mM sodium citrate], 5 mM EDTA, 0.2 % Tween 20, 50 μg/mL yeast tRNA, 100 μg/mL heparin) containing the relevant digoxigenin-labelled antisense RNA probes. RNA probes were transcribed from the vector in an *in vitro* reaction for 3 hours at 37˚C with the relevant RNA polymerase and DIG RNA Labeling Mix (Roche 11277073910). Primers used to clone new probes are listed in Table *3-1*. The reaction product was verified in 0.8% agarose gel and diluted in hybridization solution for further use.

After two 30 min washes at 65˚C with hybridization solution without tRNA, heparin, and the RNA probe, embryos were washed in a 1:1 mix of hybridization solution and TBST (25 mM Tris.HCl, pH 8.0, 140 mM NaCl, 2.7 mM KCl, 0.1% Tween 20) for 30 min at 65˚C, then washed three times with TBST at room temperature, equilibrated in MABT (100 mM Maleic acid, 150 mM NaCl, 0.1 % Tween-20, pH 7.5) and blocked in MABT blocking buffer [MABT containing 1% blocking reagent (Roche #11096176001)] with 10% sheep serum for 2.5 hours at room temperature. Embryos were then incubated overnight at 4˚C with a 1:2000 dilution of alkaline phosphatase-conjugated anti-digoxigenin antibody (Roche # 11093274910) in MABT blocking buffer with 1% sheep serum. After extensive washes with MABT at room temperature, embryos

were equilibrated in NTMT buffer (100 mM Tris HCl, pH 9.5, 50 mM $MgCl_2$, 100 mM NaCl, 0.1% Tween-20) and developed with a 1:50 dilution of a NBT/BCIP solution (Roche # 11681451001) in NTMT at room temperature in the dark. Stained embryos were mounted in a 0,45% gelatin, 27% bovine serum albumin (BSA), 18% sucrose mix, jellified with 1,75% glutaraldehyde and sectioned at 35 μm on a Leica Vibratome VT 1000 S.

Whole mount immunofluorescence and image processing

Embryos were fixed in 4% PFA on ice for 2 hours and then dehydrated through a 25%, 50%, 75% methanol/PBST (PBS, 0,1% Triton-X 100) series followed by 100% methanol. Embryos were then rehydrated through a reverse methanol PBST series, washed with PBST and permeabilized in 0,5% Triton-X 100 in PBS for 1 hour and incubated in 1M Glycine in PBST for 30 minutes to reduce unspecific binding. After several washes in PBST embryos were blocked in 1% BSA, 3% donkey serum in PBST at 4˚C overnight. Embryos were then incubated for 72 hours with the following dilutions of the primary antibodies in blocking buffer: α–Pecam1 1:50 (ab28364, abcam), α–Keratin8 1:100 (troma-i-c, developmental studies hybridoma bank) Secondary antibodies were diluted 1:1000 in blocking buffer and embryos incubated for 48 hours at 4˚C. After extensive washes in PBST embryos were stained with a 1:10000 DAPI dilution in PSBT at 4˚C overnight. Embryos were then mounted on a depression slide with RariClear 1.49 clearing reagent (sunjin lab). Embryos were imaged on a Prairie Multiphoton microscope using an Olympus 20X 1.0 NA W objective. Stacks were then digitally stitched in Fiji using the Grid/Collection stitching plugin. After removing the outliers, tissues were segmented using Amira Software.

Proliferation and apoptosis assay on frozen sections

Embryos were fixed in 4% PFA for 2 hours on ice, rinsed in PBS and equilibrated in 15% sucrose in PBS at 4˚C overnight. Sucrose was then replaced

with prewarmed 15% sucrose, 7% gelatin mix in PBS, and embryos incubated for 4 hours at 37˚C. Embryos were then mounted in the same mixture and molds frozen in liquid nitrogen. Gelatin blocks were sectioned at 10 μm thickness on a Leica Cryostat CM 3050 S. Degelatinized sections were then permeabilized with PBST for 15 minutes at room temperature and blocked in blocking solution (3% donkey serum 1% BSA in PBST) for 1 hour. Primary α-pH3 antibody (06-570 Millipore) was diluted 1:100 in blocking solution and samples incubated overnight at 4˚C. Slides were then washed in PBS and incubated with 0,1% sodium citrate in PBST for 2 minutes on ice. A positive control was prepared by treatment of the samples with 3 U/mL of DNase I in 50 mM Tris-HCL, pH 7.5, 1 mg/mL BSA for 10 min to induce double-strand breaks. TUNEL reaction was prepared according to manufacturer instructions and applied to the samples. Samples were incubated for 1 hour at 37˚C. Slides were then incubated with the secondary antibody diluted 1:1000 in blocking solution for 3 hours and with DAPI 1:10000 dilution for 5 minutes. After that, samples were mounted with Vectashield mounting medium and images acquired on a Leica Sp5 confocal microscope.

RESULTS

Generation of a Tgfbr1 knock out mouse line.

To generate a *Tgfbr1* null allele we used CRISPR/Cas9 (Jinek et al., 2012) to target the exon 2 coding for the extracellular domain of the receptor and introduced three stop codons in frame with the *Tgfbr1* coding sequence and a BamHI restriction site, which would itself produce a shift in the open reading frame (Figure *3-1*A). By introducing premature translation-termination codons we expect that in addition to block protein production, the mRNA will also be degraded by the nonsense mediated RNA decay mechanism (Brogna and Wen, 2009). Founders were screened by PCR with the primers designed to include genomic loci outside of the length of homology arms. The presence of a second

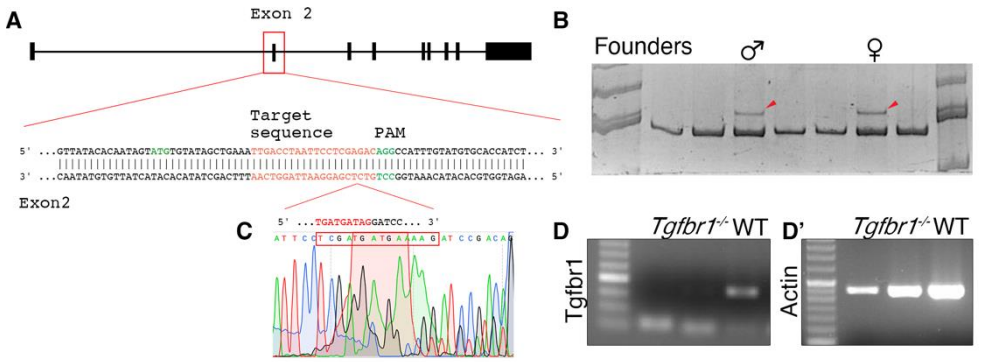

Figure 3-1 Generation of the Tgfbr1 KO mouse line A. Schematic representation of the design for CRISPR-Cas9 targeting. **B.** PCR screening of the founders. Red arrowheads indicate larger amplicon representing mutant allele. **C.** Sequencing chromatogram at the site of insertion. **D.** RT-PCR of the region within Tgfbt1 cDNA.

amplicon with bigger size signified successful targeting (red arrowheads in Figure *3-1*B). Out of fifteen pups two carried the mutant allele. Insertion was verified by sequencing (Figure *3-1*C). A male founder was crossed with wild type (C57BL/6) females. A line for this mutant strain was then started from one F1 male by crossing it with wild type (C57BL/6) females. Homozygous *Tgfbr1* null embryos obtained from heterozygous crosses produced an embryonic lethal phenotype equivalent to the one previously described (Larsson et al., 2001). Particularly, *Tgfbr1* null embryos became developmentally arrested around E10.0 and were resorbed by E11.5. Mutant embryos were characterized by an enlarged heart and defective hematopoiesis, as evident by their pale color comparing to their littermates. We confirmed the absence of *Tgfbr1* mRNA in *Tgfbr1* homozygous null mutant embryos by RT-PCR (Figure *3-1*D, D'). These features are consistent with an essential role of *Tgfbr1* in heart and vascular development, as well as in hematopoiesis (Larsson et al., 2001; Sridurongrit et al., 2008).

Tgfbr1 mutant embryos fail to undergo trunk to tail transition and cease axial extension.

Previous work from our lab showed that Gdf11 signaling through Tgfbr1 is sufficient to activate the trunk terminal module, including the hindlimb buds, the GT, and the cloaca (Jurberg et al., 2013). Analysis of *Tgfbr1* mutant embryos at E10.5 revealed that this signaling is also necessary to activate the transition. Mutant embryos failed to induce hindlimb buds and GT, as estimated by the absence of expression of specific molecular markers, like *Tbx4* and *Ptx1* (white arrows in Figure *3-2*A-B'). Also, expression of *Isl1*, a gene required for induction of both the hindlimbs and, possibly, the GT (Jurberg et al., 2013; Kawakami et al., 2011), was not activated in the posterior part of the mutant embryos at E9.5, consistent with the lack of the primordia for these structures (Figure *3-2*C, C').

E10.5 *Tgfbr1* KO embryos lacked a defined tail, displaying a rather abrupt truncation at the posterior trunk level. At this embryonic stage the tail bud of

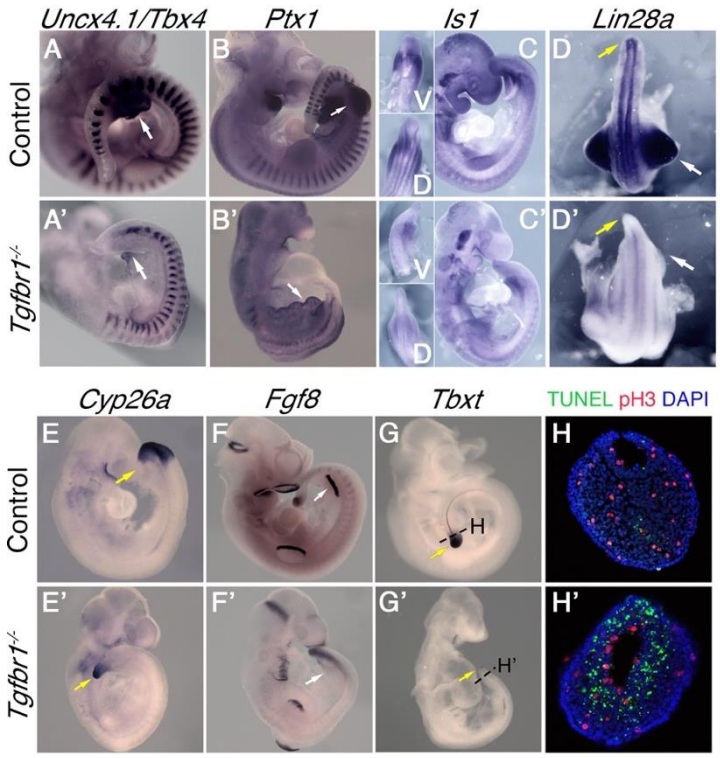

Figure 3-2. Tgfbr1$^{-/-}$ embryos do not undergo trunk to tail transition. A – G'. Whole mount in situ hybridization in control (A - G) and *Tgfbr1*$^{-/-}$ (A' – G') embryos. **A – B'.** Expression of the hindlimbs markers *Tbx4* (A, A') and *Ptx1* (B, B') in E10.5 embryos. **C – C'.** Expression of the *Isl1* in E9.5 embryos. **D – D'.** Expression of the hindlimb and tail bud marker *Lin28a* in E10.5 embryos. **E – G'.** Expression of the tail bud markers *Cyp26a* (E – E') in E9.5 embryos, *Fgf8* (F – F', also marks limb buds) and *Tbxt* (G – G') in E10.5 embryos. **H – H'.** Analysis of cell proliferation (pH3) and apoptosis (TUNEL) in the transversal section through the tail region. White arrows indicate hindlimb bud, yellow arrows – tail bud. V – ventral, D - dorsal.

mutant embryos seemed to mainly consist of an enlarged neural tube with very little tissue corresponding to the mesodermal compartment. Indeed, expression patterns of several tail bud markers, including *Tbxt, Fgf8* and *Cyp26a1*, were consistent with tail bud mesoderm deficiency in *Tgfbr1* KO embryos (yellow arrows in Figure *3-2*E-G'). The tail bud is formed as a result of axial progenitor relocation from the epiblast to the chordo neural hinge (CNH) through the process of epidermal to mesenchymal transition (EMT) (Dias et al., 2020; Wymeersch et al., 2019). We, therefore, examined the main EMT markers in the mutant embryos to evaluate EMT efficiency in their tail bud. The switch from E-cadherin to N-cadherin characteristic of EMT was compromised in *Tgfbr1* KO embryos (Figure *3-3*A-b). In addition, mutant embryos also failed to accumulate the mesenchymal marker Vimentin, typically observed in the tail bud of wild type embryos, retaining instead high levels of the epithelial marker Epcam (Figure *3-3*C-d).

During tail development axial progenitor activity is regulated by *Lin28* (Aires et al., 2019; Robinton et al., 2019). E10.5 *Tbfr1* KO embryos lacked tail bud *Lin28a* expression, an observation in agreement with the lack of transition

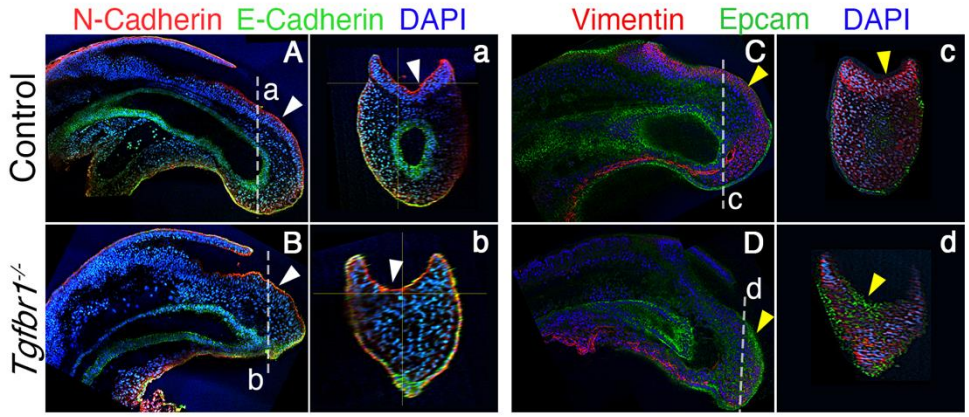

Figure 3-3. EMT markers in Tgfbr1 KO tail region. A-b. Wholemount immunostaining for E-Cadherin (green) and N-cadherin (red) in the posterior region of control (A, a) and Tgfbr1$^{-/-}$ (B, b) E9.5 embryos. Incomplete switch from E-cadherin to N- cadherin in the mutant is shown by white arrowhead. a and b show transversal section through the region marked by the dashed line in A and B. **C-d.** Immunostaining for Vimentin (red) and Epcam (green) in the posterior region of control (C, c) and Tgfbr1$^{-/-}$ (D, d) E9.5 embryos. Yellow arrowheads show deficient Vimentin and persistent Epcam in the mutant embryo. c and d show transversal section through the region marked by the dashed line in C and D.

to a tail developmental mode (Figure 3-2D, D'). In addition, we observed high levels of apoptosis in the mutant tail region, which might also contribute to progenitor depletion and cessation of axial extension (Figure *3-2*H, H').

Tgfbr1 is, therefore, the main activator of the trunk to tail transition, required for the formation of the tail bud and switch to the tail growth program.

Tgfbr1 is a crucial modulator of the caudal trunk mesoderm differentiation.

Analysis of E9.5 *Tgfbr*1 KO embryos indicated abnormal behavior of the LPM at the caudal embryonic end (Figure *3-4*A-d'). The somatic and splanchnic layers of LPM failed to converge, keeping their separation that resulted in a persistent coelomic cavity that extends until the posterior end of the embryo (Figure *3-4*a'-d'). Interestingly, while in *Tgfbr1* null mutant embryos *Irx3* and *Foxf1*, markers of the somatic and splanchnic LPM, respectively, were expressed following normal patterns at trunk levels, at the posterior end of the embryo they lost normal regulation (Figure *3-4*a-d'). In this region, they were both upregulated and their expression not restricted to their respective layers, expanding to the whole tissue surrounding the celomic cavity (arrowheads in Figure *3-4*a'-d'). The intermediate mesoderm (IM) of the *Tgfbr1* KO embryos also did not follow normal developmental patterns. For instance, we observed strong *Pax2* upregulation and branching of the expression signal in the caudal part of the mutant embryos at E10.5 (Figure *3-4*E-f'). Apparently, LPM differentiation into somatic and splanchnic layers is independent of *Tgfbr1* throughout the trunk. At the caudal end of the trunk, however, *Tgfbr1* is required to induce LPM differentiation and produce their caudal-most derivatives.

Proper endoderm patterning and angiogenesis require Tgfbr1.

Analysis of sagittal sections of the *Tgfbr1* mutant embryos suggested that the endodermal tube followed abnormal morphologies. At E9.5 the caudal tip of the gut tube was wrinkly with strong expression of endoderm markers at the ventral side (Figure 3-5A-b). Notably, at E10.5 *Tgfbr1* KO embryos seemed to

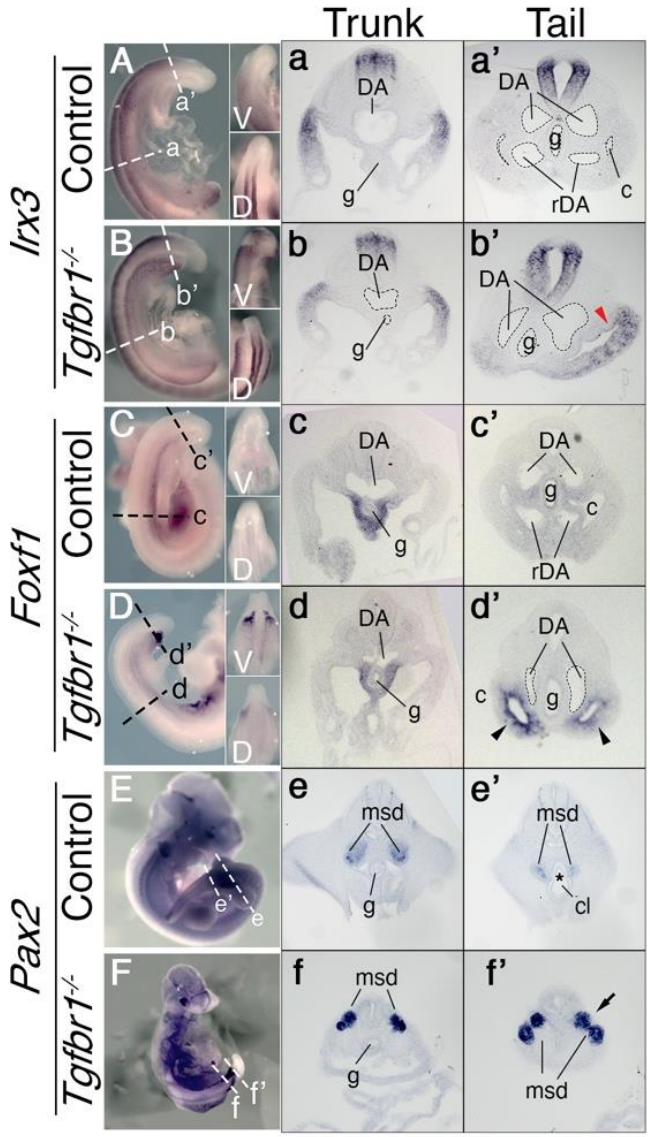

Figure 3-4. In situ hybridization showing expression patterns of the main mesodermal markers. A – d'. Expression of Somatic LPM marker *Irx3* (A, B) and splanchnic LPM marker *Foxf1* (C, D) in control (A, C) and *Tgfbr1*$^{-/-}$ (B, D) E9.5 embryos. Next to the images of the whole mount embryos shown transversal sections through trunk (a – d) and tail (a' – d') regions. Red arrowhead indicates ectopic expression of *Irx3* in splanchnic LPM, black arrowhead – ectopic expression of *Foxf1* in somatic LPM. V – ventral, D – dorsal. **E - f'.** Expression of the IM marker *Pax2* in E10.5 control (E) and *Tgfbr1*$^{-/-}$ (F) embryos. Next to the images of the whole mount embryos shown transversal sections through trunk (e, f) and tail (e', f') regions. Black arrow indicates duplication of the mesonephric duct. Asterisk – place of mesonephric duct fusion with cloaca. c – coelomic cavity, cl – cloaca, DA – dorsal aorta, g – gut, msd - mesonephric duct, g – gut, rDA – recurved dorsal aorta.

form the cloacal membrane, as identified by the contact between the gut endoderm and the ventral ectoderm (Figure 3-5C, D). However, these mutant embryos failed to form a structure resembling the cloaca, were never able to initiate the cloacal widening nor to extend the endodermal tube caudal to the cloacal membrane to form the tail gut (Figure 3-5C, D). Consequently, the embryonic gut ended as a simple tube contacting the ventral surface of the embryo. Remarkably, expression of the early definitive endoderm marker *Apela*

(Hassan et al., 2010) followed abnormal patterns in *Tgfbr1* mutants (Figure 3-5E-f'). Contrary to wild type embryos, most of the endodermal tube was negative for this marker, its expression being observed only in a few cells in the dorsal part of the gut tube (black arrows in Figure 3-5e, e', f, f'). Instead, *Apela* positive cells were found within the ventral part of the expanded LPM (black arrowheads in Figure 3-5e', f'). These results might indicate that the absence of cloaca and tail gut in *Tgfbr1* mutant embryos could derive from the inability of

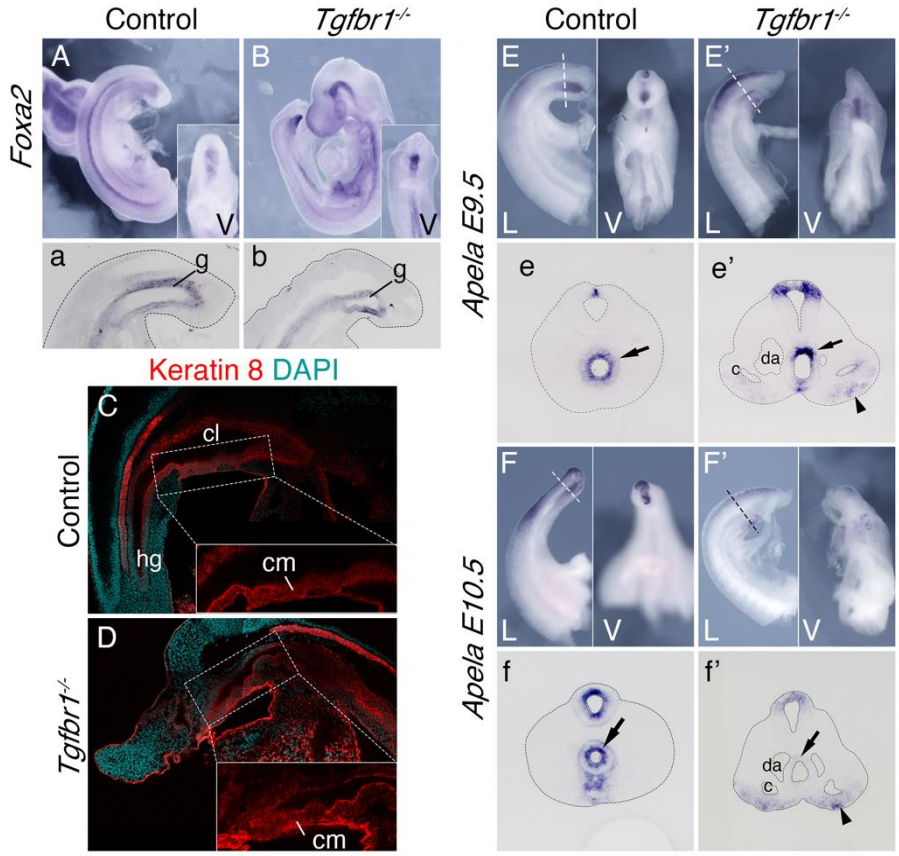

Figure 3-5 Endoderm of the *Tgfbr1* KO. A – b. Expression of *Foxa2* in E9.5 control (A, a) and Tgfbr1 KO (B, b) embryos. (a, b) show sagittal sections though tail region. **C, D.** Keratin 8 staining of the cloaca region in the control (C) and *Tgfbr1*$^{-/-}$ (D) E10.5 embryos. **E – e'.** *Apela* expression in the posterior region of the E9.5 control (E, e) and mutant (E', e') embryos. e and e' show transversal sections of regions marked by the dashed line in E and E'. **F – f'.** *Apela* expression in the posterior region of the E10.5 control (F, f) and mutant (F', f') embryos. f and f' show transversal sections of regions marked by the dashed line in F and F'. Black arrow – gut endoderm, arrowhead – Apela-expressing cells in LPM. V – ventral, L – lateral, cl – cloaca, c – coelomic cavity, cm – cloacal membrane, da – dorsal aorta, g – gut, hg – hindgut.

the endodermal cells to become incorporated into the gut tube, becoming mixed with the otherwise mis-patterned LPM cells.

The initial analysis of transverse sections of *Tgfbr1* mutant embryos also suggested faulty reorganization of the main vascular tree. The four orifices surrounding the hindgut, diagnostic of the recurved dorsal aorta (rDA) at E9.5 were not observed in *Tgfbr1* mutants, in which only a single expanded vessel was visible on each side of the embryo (Figure *3-4*a'-d'). These data suggest the absence of rDA in these embryos. The allantois relocation, related to establishment of embryonic-extraembryonic bloodstream connection, however, still occurred in these embryos. To further study DA morphology of the *Tgfbr1*

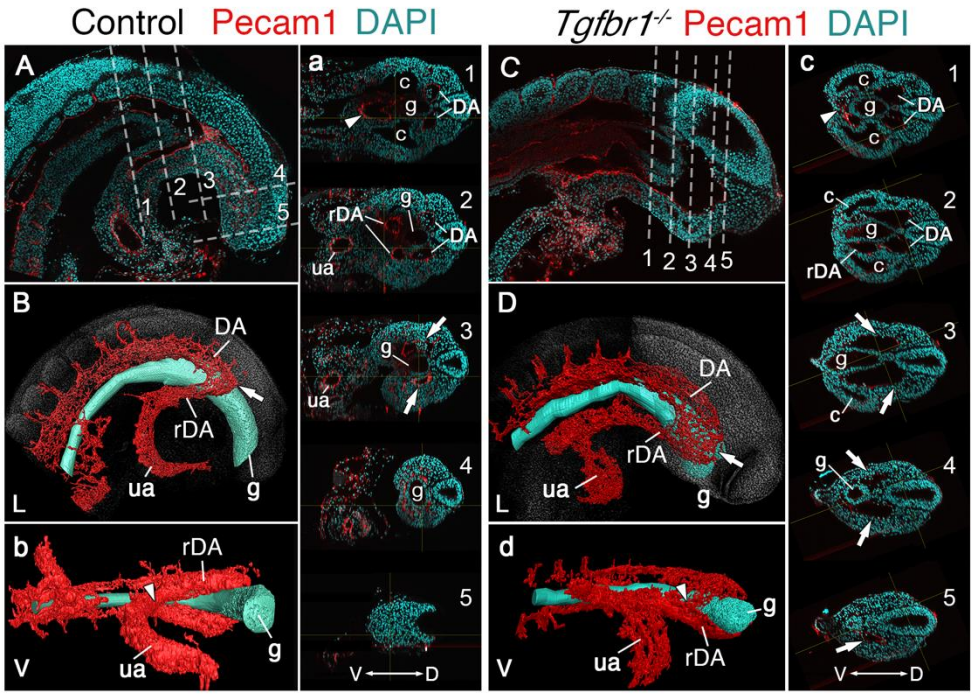

Figure 3-6. Main vascular tree of the *Tgfr1*$^{-/-}$ embryos. A, a, C, c. Wholemount immunostaining for Pecam1 (red) labelling endothelial cells in E9.5 control (A, a) and mutant (C, c) embryos. Transversal sections through regions marked by the dashed lines in A and C are shown in (a1-5) and (c1-5). **B, b, D, d.** 3D reconstruction of the main vascular tree (red) and the gut (cyan) of the immunostaining shown in (A, a, C, c). Connection between the umbilical artery (ua) and recurved dorsal aortae (rDA) is marked by the arrowhead. Turn of dorsal aortae (DA) where it is connected to rDA is labelled by the arrow. In the mutant this region is enlarged while rDA is short (compare A, a3 and B to C, c2-5, and D). D – dorsal, L – lateral, V – ventral, c – coelomic cavity, g – gut.

mutants, we performed segmentation of embryos stained with the endothelial marker Pecam1. Reconstruction of their main blood vessels with Pecam1 staining showed enlarged diameter of the posterior portion of DA in the mutant, thus fitting with the observations in the histological sections (Figure *3-6*). In addition, the DA was elongated posteriorly in relation to the base of allantois (Figure *3-6*B, D). Morphological features resembling the rDA could be observed, although it seems significantly shorter and less developed in the mutant embryos (Figure *3-6*b, d). This feature, together with widened DA elongation, produces the phenotype observed in transversal sections. The absence of *Tgfbr1*, therefore, leads to a disruption of the tissue reorganization associated with the trunk to tail transition that integrates the extraembryonic lineages within the embryo proper leading to the formation of the rDA.

Tgfbr1 activity in the LPM and function in angiogenesis is mediated by the Isl1.

Tgfbr1 has previously been proposed to act upstream of *Isl1* gene in the caudal region of the trunk (Jurberg et al., 2013). Consistently, we show that *Isl1* is not activated in the hindlimb field and pericloacal mesenchyme of *Tgfbr1* mutants (Figure *3-2*C, C'). *Isl1* role for the induction of the hindlimbs has been previously shown (Itou et al., 2012; Kawakami et al., 2011). Whether this gene regulates other processes occurring in the LPM during the trunk to tail transition was unclear.

Direct analysis of the *Isl1* mutant ought to clarify this gene's contribution to the phenotype observed in the *Tgfbr1* KO. To evaluate the phenotype of *Isl1* mutants we crossed heterozygous mice carrying the Cre recombinase in the *Isl1* genomic locus. Homozygous Cre-positive embryos obtained from these crosses do not carry a functional *Isl1* allele. *Isl1* mutants were viable until E9.5-E10.0. While showing multiple phenotypic abnormalities, they were still able to turn and relocate their allantois, suggesting that they reached the trunk to tail transition stage. Due to *Isl1* expression in the hindlimb field and pericloacal

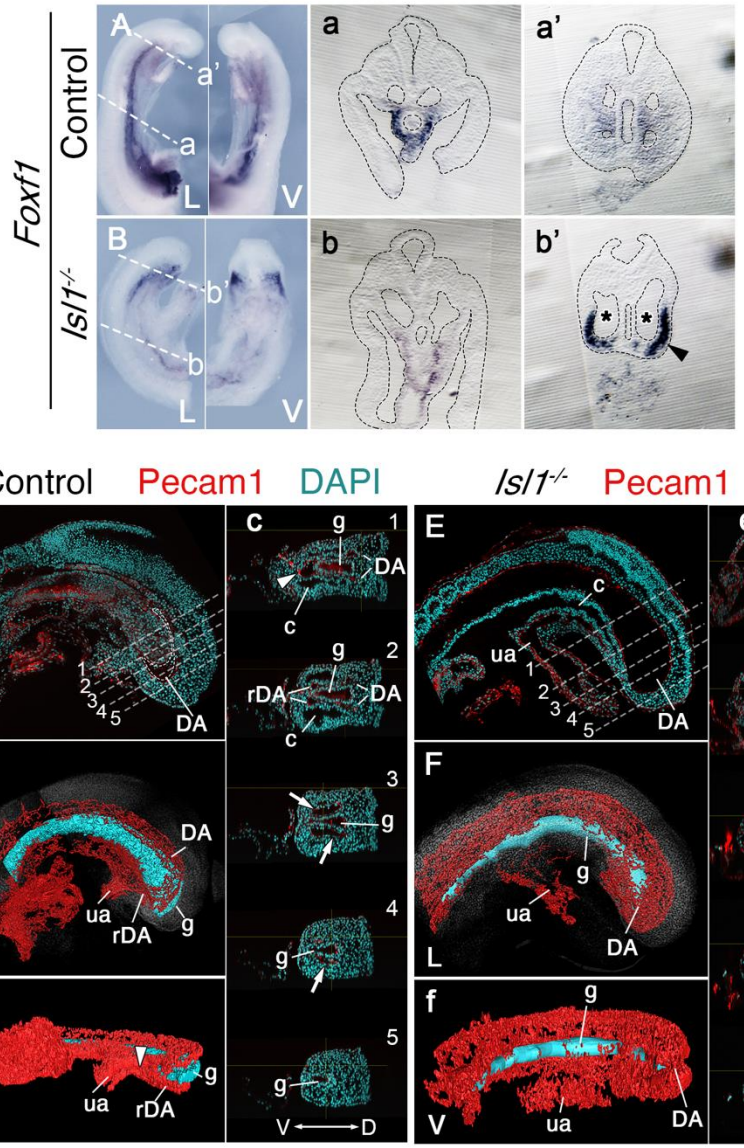

Figure 3-7. Effects of Tgfbr1 in the LPM and DA are mediated by Isl1. A-b'. Whole mount *in situ* hybridization showing expression of *Foxf1* in the E9.5 control (A-a') and *Isl1*$^{-/-}$ (B, b') embryos. a and b show transversal sections through the trunk region marked by the dashed line in A and B. a' and b' show transversal sections through the tail region marked by the dashed line in A and B. In *Isl1*$^{-/-}$ tail *Foxf1* is ectopically expressed in the splanchnopleure (black arrowhead in b'). Black asterisks in b' show dorsal aortae in the mutant. **C, c, E, e.** Wholemount immunostaining for Pecam1 (red) labelling endothelial cells in E9.5 control (C, c) and mutant (E, e) embryos. Transversal sections through regions marked by the dashed lines in C and E are shown in (c1-5) and (e1-5). **D, d, F, f.** 3D reconstruction of the main vascular tree (red) and the gut (cyan) of the immunostaining shown in (C, c, E, e). In the mutant recurved dorsal aorta (rDA) is absent and connection between dorsal aortae (DA) and the umbilical artery (ua) is established by a small vessel (white arrowhead in e 1 and 2). Branches of DA are enlarged in the Isl1-/- and merge together posteriorly and ventrally to the gut (e3-5, f). Turn of dorsal aortae (DA) where it is connected to rDA is labelled by the arrow in the control embryo. D – dorsal, L – lateral, V – ventral, c – coelomic cavity, g – gut.

mesenchyme, we first looked at the LPM of the *Isl1* mutant. Similar to the *Tgfbr1 KO* embryos, we noted strong *Foxf1* expression in the caudal end of the embryo, posterior to the connection with the allantois (Figure *3-7*A, B). Analysis of transversal sections revealed reduced expression in the trunk region confined to the splanchnic LPM (Figure *3-7*a, b). In the caudal region, on the other hand, *Foxf1* signal was upregulated and ectopically expressed in the outer LPM (Figure *3-7*a', b').

Analysis of transversal sections revealed another feature common for *Tgfbr1* and *Isl1* KO embryos: *Isl1* mutants did not show presence of the rDA, having significantly enlarged paired vessel next to the gut (black asterisks in Figure *3-7*b'). To better understand the morphology of the main vascular tree in the *Isl1* mutant embryos, we performed immunostaining with the endothelial marker Pecam1 and made 3D reconstruction of the obtained staining (Figure *3-7*C-f). This analysis confirmed the presence of a single massive blood vessel on the either side of the gut. The two branches of the DA then merged together at their most posterior end enveloping the caudal tip of the gut (Figure *3-7* e3-4, f). Markedly, unlike in the *Tgfbr1* KO, the rDA could not be identified in the *Isl1* mutant embryos, only showing a single narrow vessel branching from the DA, and potentially connecting DA with the umbilical artery (white arrowhead in Figure *3-7*e1, 2). However, it was difficult to confirm the connection between the embryonic and extraembryonic vasculature in the mutant embryos due to intermittent staining in this region. Common phenotypical features of the *Isl1* and *Tgfbr1* mutants support the idea that *Isl1* acts downstream of *Tgfbr1* in the LPM, and likely causes DA enlargement observed in *Tgfbr1* KO embryos.

DISCUSSION

The transition from trunk to tail development involves major tissue reorganization. While the NMC cells are maintained by switching them from the epiblast into a new niche in the tailbud, the LPM terminates through the induction of the hindlimb buds and pericloacal mesenchyme in the terminal part

of the trunk (Aires et al., 2016; Cambray and Wilson, 2002; Tzouanacou et al., 2009). It has been shown that constitutive activation of Tgfbr1 is sufficient to prematurely initiate the trunk to tail transition and to induce formation of its morphological landmarks, namely the hindlimb buds, the cloaca, and the GT (Jurberg et al., 2013). Here, using a complementary genetic approach by generation of a null mutant allele of this gene we demonstrated that *Tgfbr1* is necessary to organize all major processes occurring during the trunk to tail transition.

We show that *Tgfbr1* KO embryos fail to form a functional tail bud due to defective EMT, impacting most particularly the tail bud mesodermal compartment. The apparent absence of *Lin28a* expression in the mutant's tail bud indicates that failure to activate the regulatory network driving NMC cell activity in the tailbud (Aires et al., 2019; Robinton et al., 2019) might also play a relevant role in the *Tgfbr1* mutant phenotype. The enlarged neural tube observed in the *Tgfbr1* mutants resembles the phenotype observed in *Gdf11* mutants, where progenitor cells favor neural over mesodermal fates (Aires et al., 2019), indicating that Gdf11 might be the physiological ligand of Tgfbr1 for this activity. It is also consistent with loss of *Lin28a*, which functions as a pro-mesodermal gene in the tail bud (Robinton et al., 2019).

Tgfbr1 mutant's inability to form hindlimb, but not forelimb, buds further emphasize the difference between the mechanisms of induction of these two otherwise equivalent structures (McQueen and Towers, 2020). Our results also indicate that hindlimb and GT induction are closely coordinated processes that share many of their key regulators. *Isl1* is one of the earliest genes expressed in the limb field and pericloacal mesenchyme (Yang et al., 2006). Genetic data indicates that *Isl1* is one of the earliest genes involved in the induction of the hindlimb buds (Itou et al., 2012; Kawakami et al., 2011). It has been previously proposed that *Gdf11* acts upstream of *Isl1* in the context of the trunk to tail transition (Jurberg et al., 2013). In line with this observation, *Isl1* expression was lost from the prospective hindlimb field and pericloacal mesenchyme of the

Tgfbr1 mutant embryos (Figure *3-2*C, C'). Furthermore, the phenotype of *Isl1* KO embryos recapitulates some features of the *Tgfbr1* KO phenotype, particularly in the caudal LPM and the main vascular tree.

Alterations in endodermal development are among the most conspicuous phenotypes observed in *Tgfbr1* mutant embryos. The observation that the gut endoderm finishes at the ventral surface of the embryo, where it seems to form a cloacal membrane, but is unable to expand to form a recognizable endodermal cloaca or to extend posteriorly, could be explained by a physical constraint due to the absence of tail growth. Several features of E10.5 *Tgfbr1* KO embryos, however, suggest a more complex origin of the gut phenotype of these mutants. *Apela* expression in the *Tgfbr1* mutants suggest that many of the prospective endodermal cells normally contributing to the posterior gut are still generated but fail to enter the endodermal tube, becoming instead mis-located within the caudally extended LPM. It is likely that this plays a significant role in the mutant's inability to form the cloaca or to extend into the tail gut.

Interestingly, other aspects of the *Tgfbr1* mutant phenotype might be also associated with the activity of this receptor to coordinate tissue rearrangements at the caudal end of the trunk. While the hindlimbs are likely to derive from the somatic layer of the LPM (Gros and Tabin, 2014), the origin of the pericloacal mesoderm is not so clear. Cell labeling experiments in mouse embryos showed that the GT (and thus most likely the pericloacal mesenchyme) derives from the ventral posterior mesoderm (Tschopp et al., 2014), whose origin has been mapped to the posterior primitive streak (Wymeersch et al., 2016). Before and during the trunk to tail transition, this region expresses high levels of *Foxf1* (Astorga and Carlsson, 2007; Tsiairis and McMahon, 2009). It is then possible that the absence of pericloacal mesoderm in the *Tgfbr1* mutants could result from compromised development of the tissue originating from the posterior primitive streak during the trunk to tail transition. In this regard, the strong *Foxf1* expression observed in the posterior end of the extended lateral mesoderm of the *Tgfbr1* mutants might derive from the posterior primitive

streak cells that instead of generating ventral posterior mesoderm, invaded the trunk LPM. The persistent *Foxf1* expression could be an additional sign of the failure of these cells to enter their normal developmental program. According to cell tracing data, the ventral mesoderm and the hindgut have significant contribution from adjacent tissues within the posterior PS/allantois/posterior visceral endoderm. The rather similar distribution of *Foxf1* and *Apela* expressing cells in the extended LPM of *Tgfbr1* mutant embryos might thus represent two aspects of a global deregulated development of this region in the absence of *Tgfbr1*.

The rDA has also been shown to derive from the posterior primitive streak/allantois junction, playing an important role in establishing proper connection between the embryonic and extraembryonic circulation. Indeed, *Foxf1* seems to play a relevant role in this process (Astorga and Carlsson, 2007). It is then possible that, similarly to what we discussed for the pericloacal mesoderm and the endoderm, the primitive streak/allantois fail to provide the cells that would form the rDA, which could allow the trunk dorsal aorta to keep extending further caudally following the extension of the trunk LPM. The reorganization of the major blood vessels would therefore be another example of the incorrect integration of the extraembryonic-derived tissues.

The phenotype of the *Isl1* mutant embryos supports this idea. Before the trunk to tail transition *Isl1* is expressed in the base of allantois/primitive streak junction (Cai et al., 2003). The underdeveloped of rDA in the *Isl1* mutant, therefore, likely results from requirement of *Isl1* for proper differentiation of the vessel of confluence in the allantois. The similarity between the phenotypes of the *Tgfbr1* and *Isl1* KO embryos further support their mutual role in the organization of the trunk caudal end. Expression of *Isl1* in the extraembryonic tissues, however, could be partially independent of *Tgfbr1*. This would explain the aggravated rDA phenotype of the *Isl1* mutant compared to the *Tgfbr1* KO.

Together, the mesodermal, endodermal, and vascular phenotypes of *Tgfbr1* mutant embryos suggest a central role for this signaling in the control of

the tissue interactions and fates of the tissues within the posterior primitive streak/allantois/posterior visceral endoderm, to properly integrate embryonic and extraembryonic lineages during the trunk to tail transition.

Acknowledgements

We would like to thank the members of the Mallo lab, especially Ana Casaca for continuous support at different stages of this project, the IGC mouse facility for their help with animal housing and advanced imaging facility, especially Gabriel Martins, for help with image acquisition and analysis. This project was funded by Fundação para a Ciência e a Tecnologia (FCT) grants PTDC/BIA-BID/30254/2017 to MM, and PhD fellowships PD/BD/128437/2017 to AL, and the research infrastructures PPBI-POCI-01-0145-FEDER-022122 to the Advanced Imaging Facility, and Congento LISBOA-01-0145-FEDER-022170 to the animal facility, both co-financed by Lisboa Lisboa 2020/FEDER and FCT (Portugal).

Chapter 4

TGFBR1 CONTROLS DEVELOPMENTAL PLASTICITY BETWEEN THE HINDLIMB AND EXTERNAL GENITALIA BY REMODELING THEIR REGULATORY LANDSCAPE.

Authors contribution: Anastasiia Lozovska and Moisés Mallo designed experiments; Anastasiia Lozovska performed experiments; André Dias performed OPT experimental procedures; Alexandre Lopes acquired OPT images; Donald Fowler did skeleton segmentation; Artemis Korovesi and Moisés Mallo performed β-galactosidase reporter assays; Artemis Korovesi performed Tgfbr1^{3ex3} cDNA and protein analysis, size selection for ATAC-seq libraries and bioinformatic analysis; Anastasiia Lozovska and Moisés Mallo analyzed the data.

This chapter is adapted from Anastasiia Lozovska, Artemis G. Korovesi, André Dias, Alexandre Lopes, Donald Fowler, Gabriel G. Martins, Ana Nóvoa, and Moisés Mallo (2023) Tgfbr1 controls developmental plasticity between the hindlimb and external genitalia by remodeling their regulatory landscape. *In review.*

SUMMARY

The hindlimb and external genitalia of present-day tetrapods are thought to derive from an ancestral common primordium that evolved to generate a wide diversity of structures adapted for efficient locomotion and mating in the ecological niche conquered by the species. We show that despite long evolutionary distance from the ancestral condition, the early primordium of the mouse external genitalia preserved the capacity to take hindlimb fates. In the absence of *Tgfbr1*, the pericloacal mesoderm generates an extra pair of hindlimbs at the expense of the external genitalia. It has been shown that the hindlimb and the genital primordia share many of their key regulatory factors. *Tgfbr1* controls the response to those factors acting in a pioneer-like mode to modulate the accessibility status of regulatory elements that control the gene regulatory networks leading to the formation of genital or hindlimb structures. Our work uncovers a remarkable tissue plasticity with potential implications in the evolution of the hindlimb/genital area of tetrapods and identifies a novel mechanism for *Tgfbr1* activity that might also contribute to the control of other physiological or pathological processes.

INTRODUCTION

The same signaling pathways are frequently adopted to regulate a large variety of different developmental processes. Nonetheless, a context-dependent response assures tissue specific outcomes. The development of tetrapod's appendages is a vivid example of such specificity. Limb buds and the genital tubercle (GT), the precursor of the external genitalia, utilize practically the same set of regulatory pathways in their development, including members of Bmp, Fgf, Wnt and Shh signaling (Cohn, 2011).

Both structures rely on epithelial signaling centers to ensure their distal growth: the apical ectodermal ridge (AER) in the limb bud and the cloaca-derived distal urethral epithelium (dUE) in the GT (Yamada et al., 2006). During

the early stages of development, limb bud growth is regulated by the so-called Shh/FGF positive feedback loop (Niswander et al., 1994). Limb bud's AER expresses many FGF ligands inhibited by the mesenchymal BMP. BMP activity in the central AER is counteracted by Gremlin (Grem1), a BMP signaling inhibitor expressed in response to Shh (Zúñiga et al., 2004). Fgf4 expressed in the AER, in turn, positively regulates Shh expression (Niswander et al., 1994). *Grem1* is excluded from the posterior limb bud by Tbx2 and high levels of Shh (Farin et al., 2013; Nissim et al., 2006). This allows BMP activity to limit the AER and, therefore, limb field dimensions posteriorly. In the GT, *Shh* expression in the dUE is the main driver of the distal growth (Haraguchi et al., 2007; Perriton et al., 2002). It is required for the expression of the essential GT growth regulators: *Wnt5a*, *Hoxa13* and *Hoxd13* (Lin et al., 2009; Suzuki et al., 2003; Warot et al., 1997; Yamaguchi et al., 1999).

Despite being analogous structures, the forelimb and hindlimb buds are induced from the lateral plate mesoderm (LMP) by different mechanisms. The forelimb is induced at the anterior border of the trunk by the activity of *Tbx5* (Agarwal et al., 2003). Hindlimb buds, on the other hand, are initiated from the caudal-most part on the LPM as embryo undergoes the trunk to tail transition.

Interestingly, hindlimb bud induction occurs in close coordination with that of the GT, sharing some of their induction mechanisms (Jurberg et al., 2013). Hindlimb and GT induction involves a major reorganization of the LPM. In the trunk, this mesodermal compartment is divided into two layers, a lateral somatic layer and medial splanchnic layer surrounding the gut, that enclose the celomic cavity. At the level of trunk to tail transition the LPM layers converge towards the midline ending the celomic cavity and marking the posterior border of the trunk. In mouse embryos, limbs are induced from the somatic LPM, whereas the GT is formed from the pericloacal mesenchyme, a tissue originating from ventral posterior mesoderm close to the tail bud (Haraguchi et al., 2007; Tschopp et al., 2014). The origin of the hindlimb and GT primordia seems to vary among tetrapods. Studies in chicken show that both structures originate from the

neighboring regions in the somatic LPM (Herrera and Cohn, 2014), while in squamates paired external genitalia arise from the prospective hindlimb buds (Tschopp et al., 2014). Despite the differences in their primordia, hindlimbs and external genitalia of all tetrapod species are formed at the caudal end of the trunk in response to the signals inducing the trunk to tail transition (Matsubara et al., 2017).

Gdf11, a Tgf-β/BMP superfamily ligand, is the main regulator of the trunk to tail transition, conserved among the tetrapods (Matsubara et al., 2017). *Gdf11* mutant mice are characterized by delayed trunk to tail transition and the subsequent extension of trunk length (Jurberg et al., 2013; Mcpherron et al., 1999). The Tgf-β/BMP signaling cascade is mediated by ligand binding to a hetero-tetrameric complex formed by two type I and two type II receptors. Initiation of the trunk to tail transition is effected through Tgfbr1 and either Acvr2a or Acvr2b receptors (Paul Oh et al., 2002). Gdf11/Tgfbr1 acts upstream of the *Isl1*, a gene required for induction of hindlimb buds and possibly GT, but that seems to play no role in the forelimb buds (Itou et al., 2012; Jurberg et al., 2013). Redundancy between Tgf-β ligands in the context of the trunk to tail transition is clearly illustrated by the aggravated phenotype of the *Gdf8/Gdf11* double mutant comparing to single *Gdf11* KO fetuses. Indeed, the trunk to tail transition landmarks in the *Gdf8*/*Gdf11* compound mutants are more posteriorized than in the single *Gdf11* KO fetuses (McPherron et al., 2009). An even more severe phenotype was observed in *Tgfbr1* KO embryos, unable to initiate the trunk to tail transition as indicated by the absent of the primordia for hindlimbs, GT and cloaca (see Chapter 3 and (Dias et al., 2020)). In accordance with the Tgfbr1 specific role for hindlimb induction, the hindlimbs of the *Gdf8*/*Gdf11* compound mutants were practically absent. Strikingly, these mutants formed ectopic protrusions next to the forelimbs or, in most severe cases, an entire ectopic limb (McPherron et al., 2009).

In order to overcome the early *Tgfbr1* requirement for hindlimb and GT induction, and to elucidate the role of Tgf-β/BMP signaling in the development

of these structures, we used a conditional inactivation approach. We show that the pericloacal mesenchyme is a plastic tissue which has potential to generate either GT or limbs. *Tgfbr1* regulates this plasticity by acting on the regulatory landscape of the pericloacal mesenchyme and, therefore, modulating the cellular response to the common signals controlling hindlimb bud and GT development.

MATERIALS AND METHODS

Tgfbr1-flox mouse line and embryos

To introduce LoxP sites to the *Tgfbr1* locus we used the CRISPR/Cas9 system (Jinek et al., 2012). Two gRNAs were designed targeting: CCAATGGTGAACTATAAGAT 194 bp upstream of the Exon 3 with PAM AGG and CTATATAACTTGAGCCTGGG 244 bp downstream of the Exon 3 with PAM AGG. crRNA:tracrRNA duplexes were purchased from Integrated DNA Technologies. Cas9 mRNA and gRNAs were delivered by pronuclear injection into fertilized mouse oocytes together with single stranded replacing sequence. Replacing construct was cloned using primer extension mutagenesis method and inserted into the pBluescript II KS (+) backbone between XhoI and EcoRI restriction sites. Single stranded replacing DNA was then generated as follows. First, a PCR product was amplified from the targeting plasmid template with the biotinylated forward primer ssDNA-F and a non-biotinylated primer ssDNA-R (Table *4-1*). Next, the PCR product was incubated with 100 μl of Streptavidin Dynabeads (Thermo Fisher Cat. No. 65001) in 300 μL of buffer A (10mM Tris HCl pH 7.5, 30mM NaCl, 1mM EDTA) overnight at room temperature with rotation. The non-biotinylated DNA strand was then released by incubation in 300 μL of denaturing buffer B (0.15N NaOH, 1mM EDTA) for 4 hours with rotation at room temperature, then neutralized with 1M Tris-HCl pH 7.5 and ethanol-precipitated with 3M sodium acetate pH 5.3.

Founders were genotyped from tail biopsies as described in chapter 3 using primers surrounding LoxP sites and reaching beyond the length of the

donor DNA (LoxP-3' and LoxP-5' in Table *4-1*). Amplified bands were sequenced. Two founders were crossed with wild type females to start *Tgfbr1^{flox}* lines. Pups from the two lines were genotyped from tail, ear or digit biopsies as described in Chapter 3 using primers LoxP-5' (Table *4-1*).

The *Cdx2-creERT* mice were previously reported (Jurberg et al., 2013). *Tgfbr1-cKO* (*Cdx2-creERT$^{+/0}$::Tgfbr1$^{flox/-}$* or *Cdx2-creERT$^{+/0}$::Tgfbr1$^{3ex3\text{-}flox/-}$*)

Table 4-1. List of oligonucleotides

Genotyping primers		
LoxP-5'-F	Forward	GACTCGAGCTTCTGCTATAATCCTGCAGTAAACTTGG
	Reverse	CATTTAGTCACACAGGGCTTCCC
LoxP-3'-F	Forward	TTGAGCTTGCTGTCTGACTGGATAG
	Reverse	CTGTGGTTGGCAGGCATGTG
Cre	Forward	CGAGTGATGAGGTTCGCAAG
	Reverse	CCTGATCCTGGCAATTTCGGCT
Tgfbr1-null	Forward	CTACTGTGTTTCAAATGGGAGGGC
	Reverse	GGCCTGTCGGATCCTATCATC
b-galactosidase	Forward	AGCAGTTTTTCCAGTTCCGTTTATC
	Reverse	AGCGGCGTCAGCAGTTGTTTTTTAT
Cloning of regulatory elements		
CR-Isl1	Forward	GACTCGAGTCTGTGATACAAAACAATATATC
	Reverse	GAGGATCCAATCTTTCAAAGACATGGAGGG
CR-Tbx5	Forward	GACTCGAGCTTTATGTATCTGAGCACACTG
	Reverse	GAAGATCTTCCTTCAACAAACCAT CCAC
CR-Fgf10	Forward	CAGCTCGAGACTAGTAATCTGAGGTGGTTGCTCACTC
	Reverse	CATCCATGGCTATGGAAGGCTTATGTATCAC
Grem1-Enh	Forward	GACGTCGACACTAGTGTCATGTGTTCCTGTGATTCTG
	Reverse	GAGCCTGTATAAGAAGTTCAGGGCCA TGGCAG
Other primers		
ssDNA-F	Forward	GAAGAAAAGACCAAAGTGCTTTATAAAAAAATGAG
	Reverse	CATGTTAAAGAGGCTAATCAGCTTCC
qPCR-Tgfbr1	Forward	ACCGTGTGCCAAATGAAGAGG
	Reverse	CATCTAGATCTTGTAACACAATGGTCCTGGC
qPCR-Actin	Forward	ATGAAGATCCTGACCGAGCG
	Reverse	TACTTGCGCTCAGGAGGAGC
Tgfbr1-CDS	Forward	GAGAATTCCGGGCCACAAACAGTGGC
	Reverse	GAGTCGACCATTTTGATGCCTTCCTGT TGGC
Oligonucleotides for generating in situ probes		
Lmx1b	Forward	CTGCTGTGCAAGGGTGACTATGAG
	Reverse	GAGGCAAAGTAGGAGCTCTGCATG
Fgf10	Forward	TTCCTAGAAGTTATGGATGTTG
	Reverse	GTACTGCATCCACCAACAGTG
Grem1	Forward	AATGAATCGCACCGCATACAC
	Reverse	GACTAATACGACTCACTATAGGGAAGCAACTGCTGGTTCTTCTG

embryos were obtained by crossing *Tgfbr1*$^{flox/flox}$ or *Tgfbr1*$^{3ex3\text{-}flox/+}$ females with *Tgfbr1*$^{+/-}$*:Cdx2-creERT*$^{+/0}$ males. Noon of the day of the plug was considered E0.5. To induce recombination pregnant females were treated with tamoxifen (Sigma, T5648) dissolved in corn oil. Tamoxifen was administered at 0.1 mg per gram of body weight by oral gavage either once at E6.75 when *Tgfbr1*$^{3ex3\text{-}flox}$ females were involved, or twice, at E6.75 and E7.25 when *Tgfbr1*^{flox} females were involved.

Embryos were obtained by cesarean section and processed for further analyses (see below). They were genotyped from their yolk sacs for *Cre, Tgfbr1*$^{-}$ and *Tgfbr1*^{flox} when analyzing *Tgfbr1*-cKO embryos or for *β-galactosidase* when analyzing the reporter transgenic embryos (primers listed in Table *4-1*). Yolk sacs were collected in 50 μL of yolk sac lysis buffer (50 mM KCl, 10 mM Tris-HCl, pH8.3, 2 mM $MgCl_2$, 0.45% Tween-20, 0.45% NP40) supplemented with 100 μg/mL of proteinase K and incubated at 55˚C overnight. Samples were heat-deactivated as previously described and used for PCR.

Transgenic embryos

To generate transgenic constructs, the relevant enhancers (genomic coordinates shown Table *4-2*) were amplified by PCR (primers in Table *4-1*) from genomic DNA and cloned into a vector containing the adenovirus major late promoter, the coding region of the *β-galactosidase* gene and the SV40 polyadenylation signal (Jurberg et al., 2013) . The enhancers were confirmed by direct sequencing. The constructs were isolated from the plasmid backbone, gel-purified using the NZYGelpure (NZYTech #MB01102) and eluted from the columns with 50 μL of the kit's elution buffer. The purified constructs were diluted in microinjection buffer (10 mM Tris.HCl, 0.25 mM EDTA, pH 7.5) at 2

Table 4-2. Coordinates of the genomic elements used in the reporter assays

Name	Coordinates from from the GRCm38/mm10 reference genome
CR-Isl1	chr13:116,284,024-116,286,017
CR-Tbx5	chr5:119,700,950-119,703,188
CR-Fgf10	chr14:28,412,202-28,414,123
Grem1 enhancer	chr2:113,580,726-113,582,264

ng/μL and microinjected into the pronucleus of fertilized FVB/N oocytes according to standard protocols 45. Microinjected oocytes were transferred into the uteri of pseudopregnant NMRI females and embryos were recovered at E10.5 or E11.5 and stained for β-galactosidase activity.

RT-qPCR

To assess recombination efficiency, the posterior parts of the E10.5 *Tgfbr1-cKO* embryos, including their hindlimbs, were dissected in PBS (137 mM NaCl, 2.7 mM KCl, 10 mM Na_2HPO_4, and 1.8 mM KH_2PO_4) on ice. Whole E10.5 *Tgfbr1*$^{-/-}$ embryos were used as controls. RNA was extracted from fresh tissue using TRI reagent (Sigma, #T9424) according to manufacturer's protocol. 200 ng of RNA from each sample was used to prepare complementary DNA using a random hexamer mix (NZYTech #MB12901) and following the protocol of the NZY Reverse Transcriptase enzyme (NZYTech #MB12401). All cDNA samples were diluted 1:5 and 1 μL was used in quantitative PCR (qPCR) reactions with iTaq Universal SYBR Green Supermix (Bio-Rad, #1725124), according to manufacturer's instruction and using the Applied Biosystems QuantStudio 7 flex qPCR System. Primers were localized in exon 3 and exon 4 of *Tgfbr1* mRNA (listed in Table *4-1*), so that in case of successful recombination the product is not amplified.

PCR product concentration in each sample was calculated using the standard curve with following formula Quantity = 10^(mean Ct-b/m) (where "m" is slope and "b" is an intercept of the standard curve), and *Tgfbr1* expression level was normalized to *β-Actin* expression. Linear model was fitted (*Tgfbr1* normalized expression ~ Genotype) with R built-in function (lm). Analysis of variance (ANOVA) was performed on the linear model with the built-in function in R (anova). Significance levels between groups of samples were assessed by Tukey method using the "glht" function from "multicomp" package in R. Differences were considered significant at *p<0.05, **p<0.01 and ***p<0.001. Boxplot was generated with "ggplot2" and "ggdignif" packages in R.

Cell culture and transfection

HEK 293T cells (ATCC #CRL-3216) were cultured in Dulbecco's modified Eagle's medium (DMEM, Life Technologies) supplemented with 10% fetal bovine serum (FBS, Life Technologies) and 1% penicillin/streptomycin at 37 °C in a 5% CO_2 atmosphere. Cells were seeded in 35 mm plates and when they reached 70% confluency, the medium was changed to transfection medium (DMEM supplemented with 10% FBS). Expression vectors were constructed by amplifying the coding region of the *Tgfbr1* transcript isolated from wild type or *Tgfbr1*$^{3ex33\text{-}flox}$ homozygous embryos by RT-PCR (primers in Table *4-1*) and cloned into the pRK5 expression vector. Constructs were verified by sequencing. 3 μg of each plasmid was transfected into the 393T cells using Lipofectamine 2000 (Thermo Fisher Scientific #11668027) according to the manufacturer's instructions. After 24 hours incubation, cells were processed for western blot analysis.

Protein extraction and western blot

The transfected cells were washed twice with ice-cold PBS and then 150 μL of lysis buffer (50 mM Tris-HCl, 150 mM NaCl and 1% Triton X-100, pH 8.0) was added to each plate and incubated on ice for 10 minutes. Lysates were scraped into microcentrifuge tubes on ice and centrifuged at 20000 rcf for 10 minutes at 4˚C. The supernatant was collected, frozen on dry ice and stored at -80˚C. Protein lysates were mixed (2:1) with 3X loading buffer (150 mM Tris.HCl, pH 6.8, 6% SDS, 30% glycerol, 7.5% β-mercaptoethanol, 0.03% bromophenol blue). Samples were incubated for 15 minutes at 65˚C and resolved by SDS-PAGE in a 10% polyacrylamide gel. Proteins were transferred to PVDF membranes in 20% methanol, 25 mM Tris, 200 mM glycine at 200 mA for 1 hour. The membranes were blocked in blocking solution [5% dry milk dissolved in PBS containing 0.1% Tween-20 (PBT)] for 1 hour at room temperature and then incubated with primary antibodies overnight at 4˚C. Primary antibodies were anti-Tgfbr1 (Sigma-Aldrich #HPA056473, 1:1000 in blocking solution) and anti-

actin (Abcam #ab179467, 1:1000 in blocking solution). Membranes were then washed in PBT and incubated with HRP conjugated-anti-rabbit IgG (GE Healthcare # NA9340, 1:5000 in blocking solution) at room temperature for 1 hour and washed twice in PBT. Signals were developed by chemiluminescence using Amersham ECL Prime Western Blotting Detection Reagent (GE Healthcare #RPN2232) and images were captured using the GE Amersham Imager 600.

Skeletal preparation

E17.5 fetuses were recovered from pregnant females by cesarean section and dissected from the extraembryonic membranes, eviscerated, the skin removed and then fixed in 100% ethanol for 2 days. Cartilages were then stained by incubation with 450 mg/L of alcian blue (Sigma, #A5268) in 80% ethanol/20% acetic acid for one day. Fetuses were then postfixed in 100% ethanol overnight. Tissue was cleared by incubation in 2% KOH for 6 hours, followed by staining of ossified bones with a 50 mg/L of alizarin red S (Sigma, #130-22-3) solution in 2% KOH for 3 hours. Specimens were then further incubated in 2% KOH until tissues were fully cleared. Skeletons were stored in 25% glycerol in water. All incubations were performed at room temperature with rolling. Genotyping was performed on gut tissue by incubating in Laird's buffer (100 mM Tris-HCl pH 8.5, 5 mM EDTA, 0.2% SDS, 200 mM NaCl) containing 10 μg/mL proteinase K at 55ºC overnight. Genomic DNA was then recovered by precipitation with isopropanol (1:1, vol:vol) and transferred to TE pH 8.0. Genotyping was then performed by PCR using oligos specified in Table *4-1*.

Optical projection tomography

Optical projection tomography (OPT) was used to image E16.5 fetuses as previously described (Dias et al., 2021) with minor modifications. Briefly, fetuses were recovered by cesarean section in ice cold PBS, washed several times in PBS and fixed in 4% paraformaldehyde (PFA) in PBS at 4ºC for several

days. After several washes with demineralized water fetuses were dehydrated by sequential incubation in demineralized water with increasing concentrations of methanol (10% increases) and then twice in 100% methanol. Fetuses were then bleached in a three-day process with a sequence of 2.5%, 5% and 10% hydrogen peroxide in methanol at room temperature. Fetuses were then rehydrated through a reverse methanol/demineralized water series and embedded in a 0,7% low-melting agarose. Clearing was done with a 1:2 solution of Benzoic Alcohol:Benzyl Benzoate (BABB) using a BABB/methanol series (25% BABB increases). 100% BABB was introduced on day 3 and replaced every day for the next 4 days, until the fetuses became completely transparent. Anatomical datasets were then obtained using a custom built OPT scanner and procedures. Briefly, green auto-fluorescence was acquired on 1600 sequential angles for a full revolution, the raw dataset was pre-processed with a custom-built ImageJ macro, and then back-projection reconstructed using SkyScan's nrecon as in (Martins et al., 2021), and then post-processed to reduce noise and enhance contrast in ImageJ. 3D reconstruction and visualization and manual segmentation of the limb skeleton and internal organs was performed using the Amira software (Thermo Fisher).

Whole mount in situ hybridization and sectioning

Whole mount in situ hybridization and sectioning was done as described in Chapter 3. The probes used in this work are listed in Table *4-3*. Additional probes were amplified from the relevant mouse cDNA using primers listed in Table *4-1*, cloned into transcription vector and transcribes as described in chapter 3.

Table 4-3. In situ probes

In situ probes	
Bmp4	(Jones et al., 1991)
En1	(Davis and Joyner, 1988)

Fgf10	Whole coding region cloned into TOPO. Oligonucleotides listed in Table 4-1.
Fgf8	(Crossley and Martin, 1995)
Grem1	PCR fragment with the whole coding region and T7 promoter at the 3' end. Oligonucleotides listed in Table 4-1.
Hand2	(Srivastava et al., 1997)
Isl1	(Jurberg et al., 2013)
Lin28a	(Aires et al., 2019)
Lmx1b	PCR fragment encompassing nucleotides 504 to 1202 of the mRNA cloned into pKS bluescript. Oligonucleotides listed in Table 4-1.
Pitx1	(Szeto et al., 1999)
Shh	(Echelard et al., 1993)
Tbx5	(Chapman et al., 1996)
Wnt5a	(Yamaguchi et al., 1999)

β-galactosidase staining

Embryos were dissected out in ice cold PBS and fixed in 4% PFA at 4ºC for 30 minutes. They were then washed three times in β-gal wash buffer (PBS plus 0.02% Tween 20) for 10 minutes at room temperature and β-galactosidase activity developed in PBS containing 5 mM $K_3Fe(CN)_6$, 5 mM $K_4Fe(CN)_6$, 2 mM $MgCl_2$, 0.02% Tween 20, 0.4 mg/ml X-gal (Promega #V3941) overnight in the dark at 37ºC. The reaction was stopped with β -gal wash buffer, embryos postfixed in 4% PFA overnight at room temperature and stored in PBS.

ATAC-Seq, bioinformatic and statistical analysis

The experimental procedure was done as described in Chapter 2. Bioinformatic data analysis was performed on the Galaxy server (Afgan et al., 2016). Raw sequencing fastq files for each library were assessed for quality, adapter content and duplication rates with FastQC (v0.11.9) (Andrews, 2010). Adapters were trimmed and reads with length < 20 bp were removed using Cutadapt (v1.16.5) (Martin, 2011) (3´ adapter sequence: CTGTCTCTTATACACATCT). The trimmed reads were aligned to the mouse

reference genome (GRCm38/mm10 Dec. 2011) using Bowtie2 (v2.4.2) (Langmead and Salzberg, 2012) [parameters paired-end options (-X/–maxins 1000, --fr, --dovetail), --very-sensitive]. The aligned reads were filtered using BamTools Filter (v2.4.1) (Barnett et al., 2011) (parameters --isProperPair true, --mapQuality ≥ 30, and --reference!=chrM) and the duplicate reads were removed using Picard MarkDuplicates (v2.18.2.2) (http://broadinstitute.github.io/picard). The resulting BAM files were converted to BED and the reads that overlap to the blacklisted regions listed in were removed using Bedtools (v2.30.0) (Quinlan and Hall, 2010). The filtered BED files were used as inputs for peak calling. Peaks were called from individual replicates using MACS2 callpeak (v2.1.1) (Feng et al., 2012) (parameters --format single-end BED, --nomodel, --extsize 200, --shift -100, --qvalue 0.05).

BAM files were then converted to BigWig with "deeptools" (Ramírez et al., 2014) normalizing to 1x effective genome size (2652783500 for GRCm38/mm10). BigWig files were used for data visualization in IGV with the addition of the conservation scoring by phyloP (phylogenetic p-values) (Pollard et al., 2010) for 60 vertebrate genomes from the UCSC genome browser (mm10.60way.phyloP60way.bw file downloaded from) and ChIP-seq data for Hoxa13 (GSE81356) (Sheth et al., 2016) and Gli3 (GSE133710) (Lex et al., 2020).

The raw count matrix was created by merging peaks across samples as in the following pipeline (git clone https://github.com/tobiasrausch/ATACseq.git). DESeq2 object was built from the raw count matrix and blind dispersion estimated with the "vst" function from the "DESeq2" package in R (Love et al., 2014). Top 2500 most variable peaks estimated with the "rowVars" function in R were selected for the principal component analysis (PCA) and sample distance matrix. PCA was performed using the built-in "prcomp" function in R. Sample distance matrix was made using the built-in "dist" function in R. For statistical analysis raw reads were analyzed using EdgeR (Robinson et al., 2009). ANOVA-like test was performed on all samples and pairwise comparisons between the samples were made by

analyzing individual contrasts. Venn diagrams were created from the lists of selected differentially accessible peaks with "eulerr" package in R (Larsson, 2022). Heat Maps were made from dataframes containing log2 normalized counts across samples with the "pheatmap" package (https://CRAN.R-project.org/package=pheatmap).

Footprinting analysis of ATAC-Seq data

We further used the program RGT HINT-ATAC (Li et al., 2019) and motif matching to identify, plot and compare transcription factors (TF) footprints in the different samples. In detail, the BAM files containing the filtered aligned reads for each biological replicate were merged and used as a matrix for the footprinting analysis for the regions corresponding to the peaks called by MACS2 (described above). The resulting footprints were used for motif matching to the Hocomoco database (Kulakovskiy et al., 2018) for finding the motif-predicted binding sites (mpbs). Motif enrichment analysis was performed on the footprinting results for the peaks of pattern 1 and pattern 2, using as a background the footprinting results from all the peaks called in GT and limb, respectively.

RESULTS

Generation of the Tgfbr1 conditional KO

First, we generated mouse lines with the *Tgfbr1*^{flox} allele, that contains *LoxP* sites flanking Exon 3, which codes for parts of transmembrane and GS domains of the receptor (Agrotis et al., 2000). CRISPR/Cas9 (Jinek et al., 2012) targeting strategy was designed to produce a double strand break on either side of the exon 3. Single stranded donor construct containing exon 3 surrounded by LoxP sites and 140 bp homology arms was then introduced by homologous recombination. Founders were screened by PCR for two loci to amplify the sequences containing each of the LoxP sites. In each design one of the primers

annealed to the genomic sequence outside of the homology arms, so we evaluated the existence of recombination within the endogenous loci. We obtained two founders carrying LoxP sites insertions, as verified by sequencing. Both founders were crossed with FVB/N mice to start the mouse lines. DNA obtained from one F1 male from each litter was sequence verified and crossed

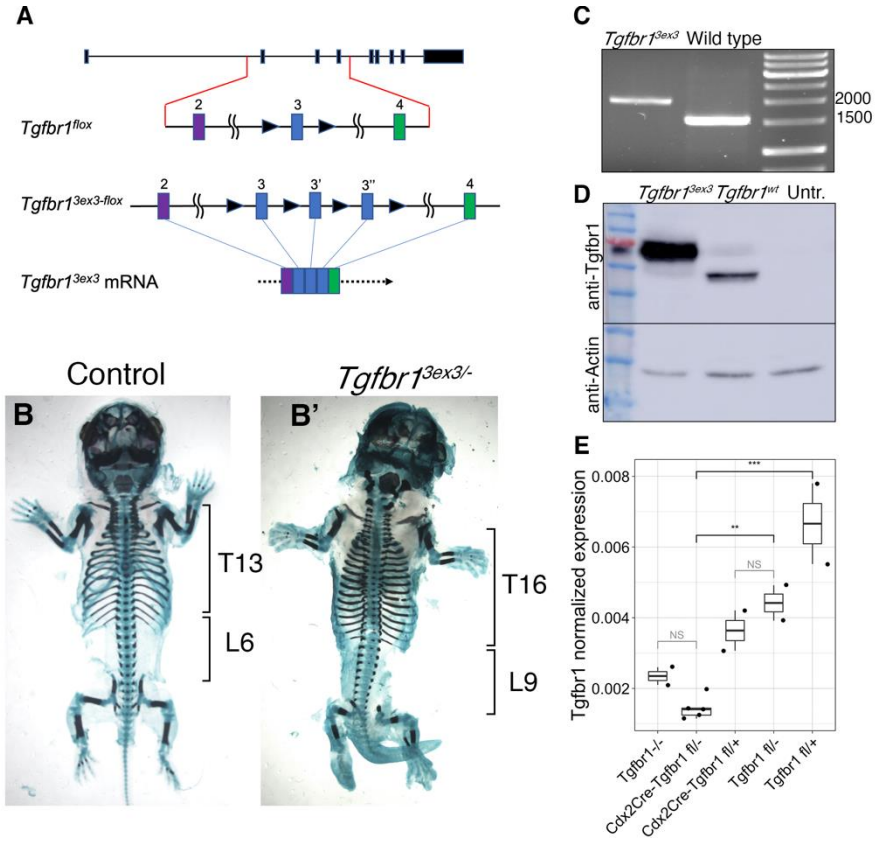

Figure 4-1 Generation on the *Tgfbr1-cKO*. A. Scheme showing *Tgfbr1*^{flox} and *Tgfbr1*$^{3ex3\text{-}flox}$ alleles. Highlighted is the region of exons 2, 3 and 4 (colored boxes) and the LoxP sites (black triangles). Also represented is the generation of a mRNA with a triplicated exon 3 after splicing of the transcript from the *Tgfbr1*$^{3ex3\text{-}flox}$ allele. **B, B'.** Skeletal staining of a E17.5 wild type (B) and *Tgfbr1*$^{3ex3\text{-}flox/-}$ fetus (B'), showing the presence of additional thoracic (T) and lumbar (L) vertebrae, resembling a *Gdf11* mutant phenotype. **C.** RT-PCR of the Tgfbr1 coding region from wild type (1.5 kb) and *Tgfbr1*$^{3ex3\text{-}flox/3ex3\text{-}flox}$ (2 kb) embryos. **D**. Western blot analysis of protein extracts from 293T cells transfected with mammalian expression vectors carrying either the *Tgfbr1*^{3ex3} or the Tgfbr1 coding regions, showing that the Tgfbr1^{3ex3} transcript produces a protein with a higher molecular mass than its wild type counterpart. **E.** RT-qPCR showing recombination efficiency in the *Tgfbr1*$^{flox/-}$*:Cdx2Cre*$^{ERT+/0}$ embryos. Normalized *Tgfbr1* expression level in *Tgfbr1*$^{flox/-}$*:Cdx2Cre*$^{ERT+/0}$ is not different from *Tgfbr1*$^{-/-}$. Level of normalized expression in *Tgfbr1*$^{+/flox}$*:Cdx2Cre*$^{ERT+/0}$ equals that of *Tgfbr1*$^{flox/-}$ and half of *Tgfbr1*$^{flox/+}$ control, consistent with it carrying only one functioning allele. NS: nonsignificant, **p<0.01, ***p<0.001

with FVB/N female. Heterozygous F2 animals were crossed to obtain homozygous lines.

In one of our lines, from now on referred to as *Tgfbr1*^{flox} an expected Mendelian ratio of 1:2:1 was met and homozygous "floxed" animal did not show any deficiencies. Surprisingly, in crosses from another line homozygous animals did not survive (1:2,23:0 in 84 animals). Further analysis showed that the "floxed" *Tgfbr1* allele of this line contained a triplication of Exon 3 interspaced by LoxP sites (Figure *4-1*A). We will refer to this line as *Tgfbr1*$^{3ex3\text{-}flox}$. Analysis of the mRNA generated from this allele indicated that the three Exon3 were correctly spliced between themselves and to the adjacent exons 2 and 4, and that the resulting transcript kept the normal *Tgfbr1* open reading frame (Figure *4-1*C). Western blot analysis from 293T cells transfected with a mammalian expression vector carrying the *Tgfbr1* cDNA produced from *Tgfbr1*$^{3ex3\text{-}flox}$ homozygous embryos confirmed the production of a *Tgbfr1* protein with increased size resulting from the triplication of the sequence coded by Exon 3 (Figure *4-1*D). We will refer to this protein as Tgfbr1^{3ex3}.

Unviability of the *Tgfbr1*$^{3ex3\text{-}flox/3ex3\text{-}flox}$ mice indicated that the Tgfbr1^{3ex3} protein was not fully functional. However, embryos homozygous for this allele were able to activate the trunk to tail transition and develop into late-stage fetuses. Notably, *Tgfbr1*$^{3ex3\text{-}flox/3ex3\text{-}flox}$ fetuses developed an extended trunk resembling that of *Gdf11* mutants, indicating that Tgfbr1^{3ex3} is not inactive but rather a hypomorphic receptor (Figure *4-1*B, B'). The *Tgfbr1*$^{3ex3\text{-}flox}$ allele turned out to facilitate the analysis of the conditional *Tgfbr1* mutants, as *Tgfbr1*$^{3ex3\text{-}flox/-}$ embryos required half of the dose of tamoxifen than the *Tgfbr1*$^{flox/-}$ embryos to obtain the same mutant phenotype, thus reducing the chance of tamoxifen-derived embryo miscarriage.

We inactivated *Tgfbr1* in the progenitor zone using the *Cdx2-CreERT2* transgenic driver (Jurberg et al., 2013) and triggering recombination by administering tamoxifen to pregnant females at E6.75 in case of *Tgfbr1*$^{3ex3\text{-}flox/-}$ and at E6.75 and E7.25 for *Tgfbr1*$^{flox/-}$. This treatment resulted in inactivation of

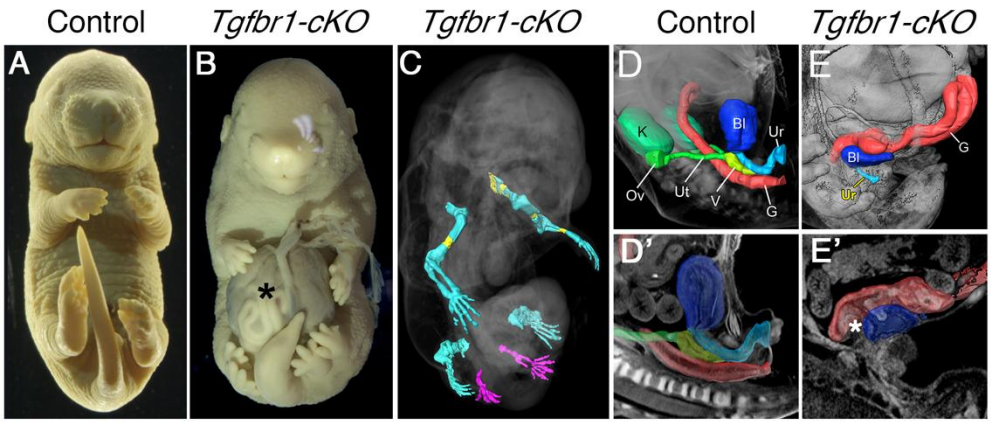

Figure 4-2. Malformations in the E16,5 *Tgfbr1-cKO* fetuses. A, B. Images of the fixed WT (A) and *Tgfbr1-cKO* (B) fetuses. The mutant fetus shows the presence of an omphalocele (asterisk) and hindlimb duplication. **C.** 3D reconstruction of the limb skeleton of a *Tgfbr1-cKO* fetus obtained by OPT and after segmentation of the limb skeleton. Extra hindlimbs are in magenta. Ossification shown in yellow. **D–E'.** 3D reconstruction of organs and the excretory outlets of the control (D, D') and *Tgfbr1-cKO* (E, E') fetuses. Images were obtained by OPT, followed by segmentation of the relevant structures. D' E' show virtual sections of the segmented 3D specimen. Asterisk in E' shows the gut-bladder connection in the mutant. K: kidney; G: gut; Bl: bladder; Ov: ovary Ut: uterus; V: vagina; Ur: urethra.

the *Tgfbr1* in the tissues caudal from the forelimb bud. High recombination efficiency was confirmed by RT-qPCR performed on total RNA extracted from the posterior part of the embryo, including the hindlimbs, of E10.5 *Tgfbr1$^{flox/-}$::Cdx2-CreERT2$^{+/0}$* embryos (Figure *4-1*E). The amount of *Tgfbr1* transcripts in tamoxifen-treated *Tgfbr1$^{flox/-}$::Cdx2-CreERT2$^{+/0}$* embryos was equivalent to that in *Tgfbr1$^{-/-}$*, and tamoxifen-treated *Tgfbr1$^{flox/+}$:Cdx2-CreERT2$^{+/0}$* contained equivalent *Tgfbr1* transcript levels as *Tgfbr1$^{-/+}$*. Tamoxifen-treated embryos and fetuses with the *Tgfbr1$^{-/flox}$:Cdx2CreERT2$^{+/0}$ or Tgfbr1 $^{-/3ex3\text{-}flox}$:: Cdx2-CreERT2$^{+/0}$* genotype will be referred to as *Tgfbr1-cKO*.

Conditional inactivation of Tgfbr1 in axial progenitors descendants leads to multiple malformations.

The most prominent feature of *Tgfbr1-cKO* mutants was a duplication of their hindlimbs [4/5 at embryonic age (E)16.5] (Figure *4-2*A, B). The fifth fetus analyzed at this stage lacked overt hindlimb duplication but still contained small protrusions posterior to the hindlimbs, a phenotype likely derived from less

efficient recombination. The limb identity of the duplicated structures was confirmed by the presence of skeletal structures that, although variable in morphology, were clearly identified as belonging to limbs, like the presence of digits (Figure *4-2*A-C). All four mutant hindlimbs, however, lacked distinct hindlimb morphological features, like longer metatarsal bones or a clearly distinguished calcaneus. This characteristic possibly derives from delayed development of the mutant hindlimbs. Analysis of E16.5 skeletons revealed that mutant hindlimbs remained mostly cartilaginous, while at this stage the limbs of control littermates already underwent a significant level of ossification (Figure *4-2*C). *Tgfbr1*$^{3ex3\text{-}flox/-}$ fetuses displayed additional morphological alterations in their skeleton, including an elongated trunk [T16, L8] (Figure *4-2*B, B').

Tgfbr1-cKO fetuses failed to close the ventral midline thus having internal organs exposed to the outside (a phenotype called omphalocele, Figure *4-2*B). Visceral organs of mutant fetuses suffered significant perturbations as well, including absence of both kidneys (Figure *4-2*D-E'). Furthermore, the outlets of the excretory and intestinal systems were severely disorganized in the mutant fetuses. While they formed a small bladder connected to a hypomorphic urethra, the hindgut was never properly organized in these mutants (Figure *4-2*D, E). Instead of forming a rectal channel, the posterior intestine merged with the bladder generating a structure resembling a persistent cloaca (Figure *4-2*E'). Additionally, *Tgfbr1-cKO* fetuses developed a severely hypoplastic GT. The malformations in the bladder and rectum were already observed at midgestational stages when these structures are initially formed through the morphological reorganization of cloaca. These included a significant enlargement of the cloacal cavity, and multiple protrusions entering the intra-cloacal lumen instead of the organized septation observed in control embryos (Figure *4-2*d, d', Figure *4-2*a, a').

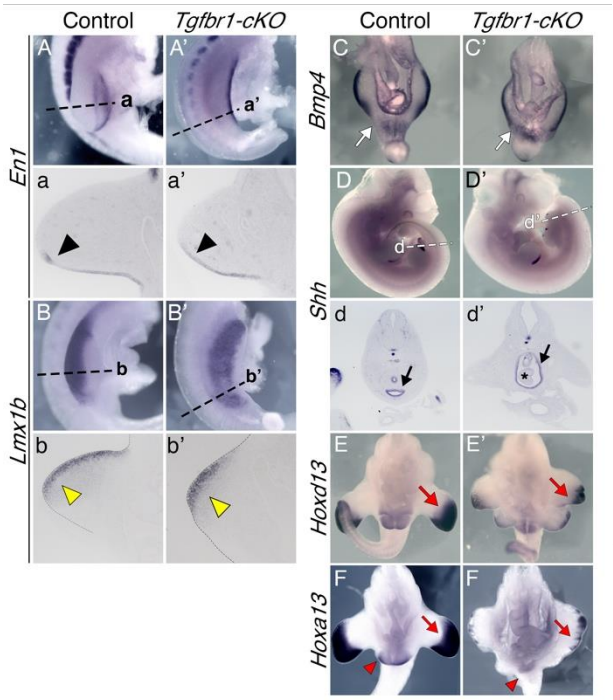

Figure 4-3. Molecular characterization of the *Tgfbr1-cKO* embryos. A-b'. Dorsal-ventral polarity of the *Tgfbr1-cKO* mutant's hindlimb. Expression of the ventral limb marker *En1* in E10.5 control (A, a) and *Tgfbr1-cKO* (A', a') embryos. (A, A') show lateral views of the hindlimb region in whole mounted embryos; (a, a') show transversal sections through the region indicated in A, A'. Black arrowheads show *En1* expression in the ventral ectoderm of the limb bud. Expression of the dorsal mesodermal limb marker *Lmx1b* in E10.5 control (B, b) and *Tgfbr1-cKO* (B', b') embryos. (B, B') show lateral views of the hindlimb region in whole mounted embryos; (b, b') show transversal sections through the region indicated in B, B'. Yellow arrowheads show *Lmx1b* expression in the dorsal mesenchyme of the limb bud. **C, C'.** Ventral views of E10.5 wild type (C) and *Tgfbr1-cKO* (C') embryos stained for *Bmp4* showing the extension of the signal into the pericloacal region in the mutant embryos (white arrow). **D-d'**. Expression of *Shh* in E11.5 control (D, d) and *Tgfbr1-cKO* (D', d') embryos. (D, D') show lateral views of whole mounted embryos; (d, d') show transversal section through the region indicated in D, D' to show the enlarged cloaca (black arrows) with presence of the intralumenal protrusions in the mutant embryo (asterisk), still keeping endodermal Shh expression. **E-F'** Expression of *Hoxd13* (E, E') and *Hoxa13* (F, F') in E11.5 control (E, F) and *Tgfbr1-cKO* (E', F') embryos. Red arrows show expression in distal limb mesenchyme, red arrowhead – GT.

Extra hindlimbs originate from pericloacal mesenchyme recruited to the hindlimb field.

To understand the origin of the duplicated hindlimbs we analyzed *Tgfbr1-cKO* embryos at mid-gestation. Morphological alterations in the hindlimb area of these embryos were already visible at E10.0. The hindlimb field was expanded posteriorly and the proximo-distal axis of the expanded bud was shorter than in wild type embryos. While at E10.25-E10.75, the hindlimb area of *Tgfbr1-cKO* embryos looked like a continuous structure, at E11.0 the presence of two independent buds became clearly distinguished (Figure *4-3*).

Native and extra hindlimbs of the *Tgfbr1-cKO* embryos maintained normal expression of the dorsal-ventral markers, including *En1* (Figure *4-3*A, A') and *Lmx1b* (Figure *4-3*B, B'), although the separation between the domains was not as sharp as in controls (Figure *4-3*a, a', b, b'). Antero-posterior patterning was perturbed more significantly. Expression of *Shh,* normally restricted to the posterior mesenchyme, was expanded to the anterior region of the limb bud (Figure *4-3*A, A'). Expression levels of *Shh* and distal *Hoxd13* and *Hoxa13* were reduced to uneven, spotty loci of expression in close proximity to the AER (Figure *4-3*D, D', E-F').

In the mutant embryos *Fgf8* expression was observed throughout the whole distal border of the extended limb buds almost reaching the ventral midline of the embryo (Figure *4-4*A, A'), although in some cases this expression was not as continuous and homogeneous as in control embryos. Conversely, *Fgf8* expression in the cloacal endoderm was absent in the mutant embryos (Figure *4-4*A'). This pattern suggested that pericloacal mesenchyme becomes recruited by AER and contributes to the extra hindlimb.

Indeed, the expression domain of the exclusive limb bud markers *Lin28a, Ptx1* and *Fgf10* (Figure *4-4*B-D') was extended into the pericloacal region, while the GT-specific *Tbx5* was significantly downregulated or totally absent from the pericloacal region of the *Tgfbr1-cKO* embryos (Figure *4-4*G, G'). *Isl1* showed residual expression next to the expanded endodermal cloaca (note that *Isl1* is also expressed in the cloacal endoderm) but became downregulated in the adjacent mesoderm in the area likely to generate the extra hindlimb bud (Figure *4-4*H, H').

Markers common to the hindlimb and the pericloacal/GT region, including *Wnt5a*, *Hand2* (Figure *4-4*E-F') and *Bmp4* (Figure *4-3*C, C'), were continuously expressed in the *Tgfbr1-cKO* embryos with the extended hindlimb bud invading the pericloacal tissue, instead of forming the distinct hindlimb and GT domains observed in wild type embryos. Notably, expression of the *Wnt5a* and *Hoxa13* –

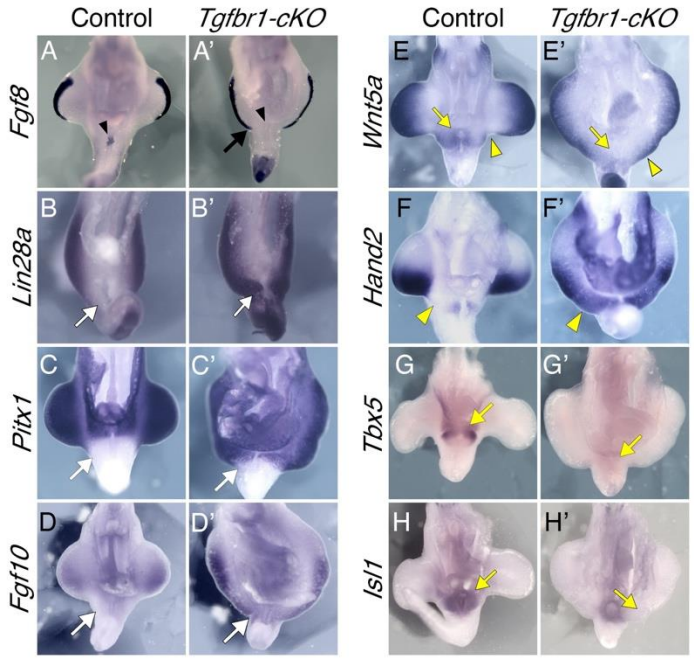

Figure 4-4. The pericloacal mesenchyme of the *Tgfbr1-cKO* embryos adopts hindlimb fate. Ventral views of the hindlimb/cloacal region of wild type (A-H) or *Tgfbr1-cKO* embryos (A'-H') stained for *Fgf8* (A, A'), *Lin28a* (B, B'), *Pitx1* (, C'), *Fgf10* (D, D'), *Wnt5a* (E, E'), *Hand2* (F, F'), *Tbx5* (G, G') or *Isl1* (H, H'). *Fgf8* expression show posterior and medial elongation of the AER (black arrow) and the absence of expression in the cloacal endoderm (black arrowhead). Hindlimb markers *Lin28a*, *Pitx1* and *Fgf10* extend into the pericloacal region in E10.5 *Tgfbr1-cKO* embryos (white arrows). *Wnt5a* and *Hand2* switch their expression profiles in the pericloacal mesoderm (yellow arrowheads), now following a limb-like pattern. In addition, pericloacal expression of *Wnt5a*, *Tbx5* and *Isl1* is lost in the mutant embryos (yellow arrows).

some of the main factors associated with GT growth - seemed reduced in vicinity of the dUE (Figure *4-3*F, F', Figure *4-4*E, E').

Together, these results indicate that in the absence of *Tgfbr1* the pericloacal mesoderm fails to enter its normal GT fate, but becomes incorporated into the hindlimb field, thus suggesting developmental plasticity of the pericloacal mesoderm, regulated by Tgfbr1 signaling.

Tgfbr1 regulates a subset of pericloacal mesenchyme enhancers to confer GT fate.

Shh signaling from cloaca drives GT outgrowth by activating *Wnt5a*, *Hoxa13* and *Hoxd13* (Kondo et al., 1997; Lin et al., 2009; Perriton et al., 2002), all found downregulated in the *Tgfbr1-cKO* mutants. Although the morphology of the mutant's endodermal cloaca was altered, it retained strong expression of *Shh* (Figure *4-3*d', Figure *4-5*A-a'). Expression of *Shh* downstream effector *Gli1* in the pericloacal mesenchyme (Figure *4-5*B, B') argues against the possibility that

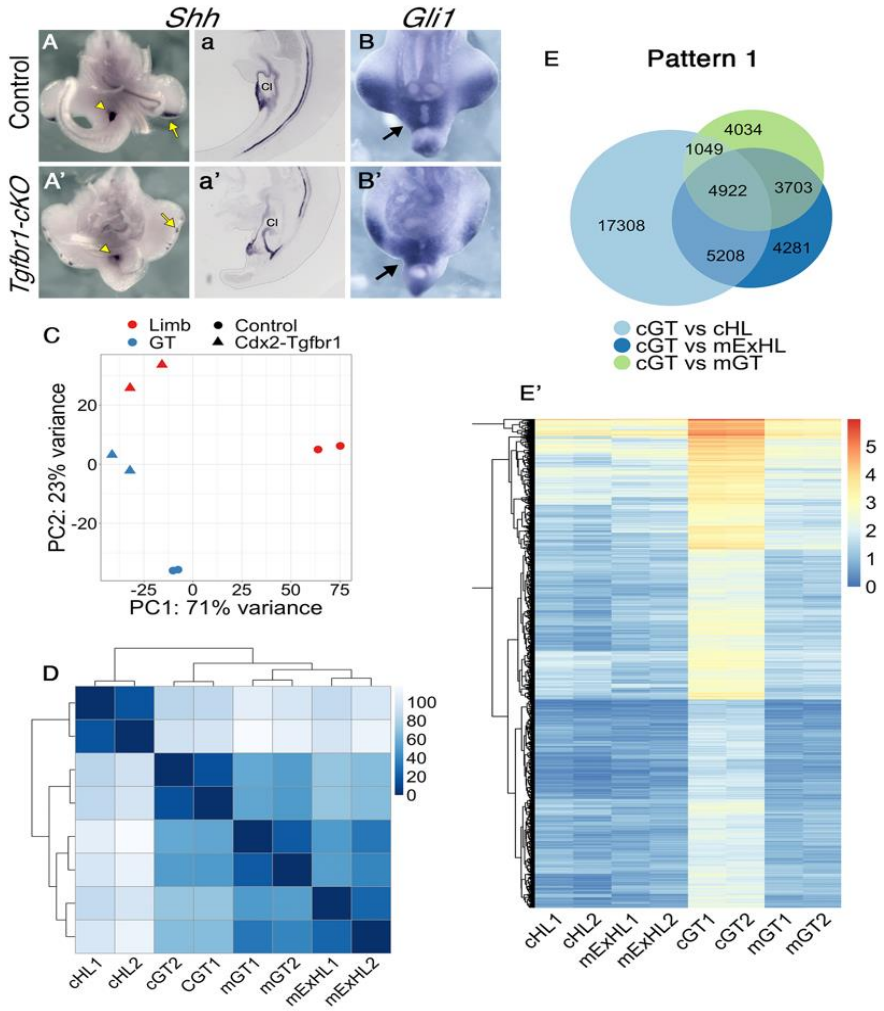

Figure 4-5. Tgfbr1 regulates the chromatin landscape in the pericloacal region. A–B'. The pericloacal mesenchyme of *Tgfbr1-cKO* embryos responds to Shh signaling from the cloacal endoderm. *Shh* expression in E11.5 control (A, a) and *Tgfbr1-cKO* (A', a') embryos. (A, A') show ventral views of the stained embryos: (a, a') show sagittal sections through cloacal (Cl) region. Gli1 expression in E10.5 control (B) and *Tgfbr1-cKO* (B') embryos. **C.** PCA analysis reveals closer proximity of the chromatin accessibility pattern of the *Tgfbr1-cKO* extra hindlimb to that of *Tgfbr1-cKO* and control GT than to the control hindlimb. **D.** Distance heatmap of the chromatin accessibility patterns showing that the *Tgfbr1-cKO* extra hindlimb clusters closer to mutant and control GT than to control limb. **E-E'** Chromatin regions following pattern 1. (E) Venn diagram showing interception of the regions tested more accessible in control GT than in other tissues by pairwise comparisons [FDR<0.001, logFC>1.5]. (E') Heatmap showing log2 normalized counts across samples of the regions following pattern 1. cHL: control hindlimb; mExHL: mutant extra hindlimb; cGT: control GT; mGT: mutant GT.

downregulation of the GT markers in the mutant embryos resulted from the cells becoming refractory to Shh. Alternatively, the *Tgfbr1-cKO* phenotype indicates

that Tgfbr1 signaling regulates how the pericloacal mesoderm respond to Shh and possibly other factors regulating the development of this tissue. Several studies using *in vitro* systems suggest that Tgf-β signaling nuclear effectors SMADs can act as chromatin remodelers to regulate gene expression (Coda et al., 2017; Ross et al., 2006). Therefore, we questioned whether the absence of *Tgfbr1* caused changes in the chromatin profile of the pericloacal mesenchyme cells. We thus obtained ATAC-seq profiles from *Tgfbr1-cKO* extra hindlimbs and GT and compared them with those from control hindlimbs and GT at E11.25.

Despite its limb identity, the chromatin accessibility pattern of the *Tgfbr1-cKO* extra hindlimb clustered closer to the mutant and control GTs than to control limb, further supporting its pericloacal origin (Figure *4-5*C, D). Therefore, despite their GT-like chromatin state, the extra hindlimb progenitor cells lost capacity to respond to GT forming signals from cloacal endoderm and acquired instead limb characteristics.

While the majority of accessible regions in the extra hindlimb follow the GT pattern, some genomic regions elude this tendency. We identified two accessibility patterns suggestive of their involvement in the control of cell fate decisions of the pericloacal mesoderm.

Pattern 1 included 4922 regions that in control tissues were accessible in the GT but not in the hindlimb, and that lost accessibility in the tissues from *Tgfbr1-cKO* embryos (Figure *4-5*E, E'). These elements could represent enhancers involved in the activation of genes expressed in the pericloacal region of wild type embryos but inactive in the *Tgfbr1-cKO* mutants. Pattern 2 contained 2013 chromatin regions representing elements that in control embryos were accessible in the hindlimb but not in the GT and became accessible in the extra hindlimb of the mutant embryos (Figure *4-7*A, A'). These elements could be involved in activating the limb program in the pericloacal mesoderm of *Tgfbr1-cKO* embryos.

We identified pattern 1 elements within the *Tbx5*, *Isl1* and *Wnt5a* genomic regions, three of the pericloacal mesoderm markers down-regulated in the

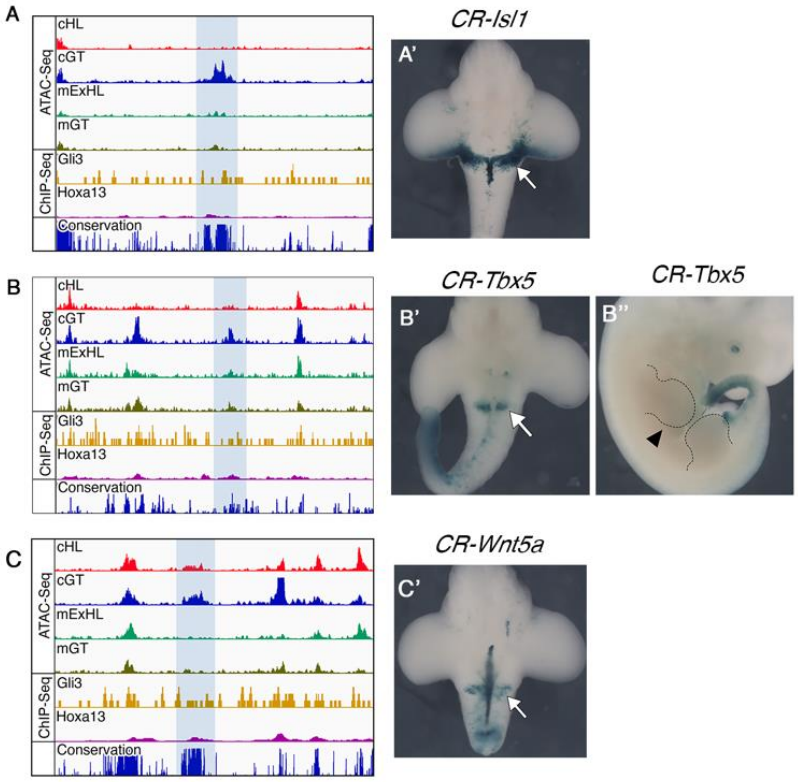

Figure 4-6. Genomic regions following Pattern 1. A-C. ATAC-seq tracks showing accessible chromatin in control GT, but not in other samples in regions 24 kb downstream of the *Isl1* TSS (A), 93 kb upstream of the *Tbx5* TSS (B), and 93 kb upstream of the *Wnt5a* TSS (C). The regions highlighted with the blue shade are characterized by high conservation level among placental animals (bottom track). **A'-C'.** The highlighted elements drive *β-galactosidase* expression in the GT region (white arrows). Hoxa13 and Gli3 ChiP-Seq tracks from forelimb buds (GSE81356 and GSE133710, respectively) are shown in yellow and magenta, respectively. CR: conserved region.

pericloacal region of *Tgfbr1-cKO* mutants (Figure *4-6*A-C). These elements mapped to highly conserved areas, suggesting their possible involvement in regulatory processes. When tested using a transgenic reporter assay, one of the elements associated with *Tbx5* showed activity in the pericloacal region (n=6/14, Figure *4-6*B'). Interestingly, it did not activate overt forelimb expression (Figure *4-6*B"), the major expression domain of this gene, further indicating specificity for the pericloacal region. Similarly, the element identified downstream of *Isl1* also reproduced to a large extent *Isl1* expression in the GT

when tested in transgenic reporter assays (n=5/12, Figure *4-6*A'). An element associated with *Wnt5a* was also able to activate expression in the GT, although much less frequently as the other elements (n=2/18, Figure *4-6*C'). This element was also active in the tail, but it did not promote expression in the hindlimb. Together, these observations are consistent with these elements indeed representing enhancers potentially involved in the expression of the relevant genes in the pericloacal area.

We found pattern 2 elements in regions associated with genes playing essential roles during the earliest stages of limb development, which could thus play a relevant role in promoting limb fates from the pericloacal mesoderm (Figure *4-4*A, A'). As for pattern 1 elements, these regions were also highly conserved among vertebrates. We found pattern 2 elements in the *Fgf10* genomic region (Figure *4-7*B), a gene activated in the mesenchyme adjacent to the cloaca entering hindlimb fate in the mutant embryo (Figure *4-4*D, D'). Interestingly, published ChIP-seq data from forelimb buds (Lex et al., 2020; Sheth et al., 2016) showed binding of Gli3 and Hoxa13 to one of this element located within an intronic region of this gene (Figure *4-7*B), indicating that it might respond to Shh and/or Hoxa13 activities in the developing limb buds. The lack of accessibility of this element in the GT of wild type embryos might thus suggest that Tgfbr1 renders this enhancer blind to endodermal Shh and/or the strong pericloacal Hoxa13 (and maybe also Hoxd13) expression consistent with absent *Fgf10* signal at early stages in this tissue. Rather surprisingly, this element failed to generate reporter activity in transgenic embryos (n=10). We still do not understand whether this reflects real lack of activity or the absence of proper genomic context for their activity.

Another pattern 2 element was located within the *Lmn1* locus, matching the position of one of the enhancers (element 7 in (Malkmus et al., 2021)) controlling *Grem1* in the limb buds, responding to Shh activity from the ZPA. In wild type embryos *Grem1* expression cannot be detected in the pericloacal mesoderm or in the GT (Figure *4-8*B), indicating that in the pericloacal

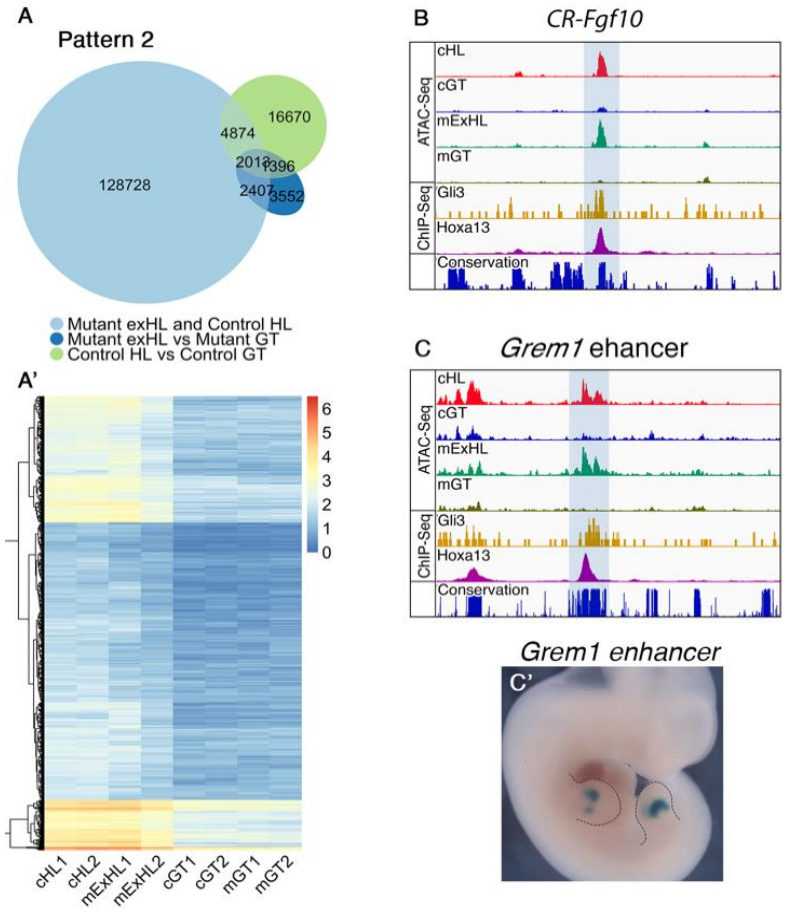

Figure 4-7. A fraction of limb enhancers gain accessibility in pericloacal mesenchyme of the *Tgfbr1-cKO* embryos. A. Venn diagram showing interception between the regions more accessible in mutant extra limb than in mutant GT [FDR<0.001, logFC>1.5] and more accessible in control hindlimb than in control GT [FDR<0.001, logFC>1.5], but at the same time not differentially accessible between mutant extra hindlimb and control hindlimb [FDR>0.01, logFC<0.5]. **A'.** Heatmap showing log2 normalized counts from genomic regions following pattern 2 across the samples. **B.** A region located within intron 1 of the *Fgf10* gene (highlighted with a blue shadow), is accessible in the hindlimb samples of the control and Tgfbr1-cKO embryos, but not in GT samples. ChIP data from forelimb buds show that this genomic region is bound by Hoxa13 and Gli3. **C.** ATAC-Seq profiles showing a *Grem1* enhancer that gains accessibility in the mutant extra hindlimb (highlighted with the blue shadow). Also shown are ChiP-Seq tracks of ChIP seq data from wild type forelimbs for Gli3 (yellow) and Hoxa13 (magenta) ((GSE81356 and GSE133710, respectively), as well as the conservation in placental mammals. **C'.** *β-galactosidase* expression driven by the *Grem1* enhancer using a transgenic reporter assay (n=2/8) (limbs outlined with the dashed line). CR: conserved region.

mesoderm Tgfbr1 might render them inaccessible to activation by endodermal Shh. The gain of accessibility of element 7 in the extra hindlimb thus suggests

that in the absence of Tgfbr1 the pericloacal mesoderm could become responsive to the endodermal Shh, activating *Grem1* expression. In situ hybridization analyses were consistent with this hypothesis, as *Grem1* was detected in the caudal-most end of the expanded hindlimb next to the endoderm (Figure *4-8*B').

It has been shown that Grem1 can regenerate a functional AER (Panman et al., 2006). Moreover, *Grem1* exclusion from the most anterior and posterior regions of the limb bud is associated with the BMP-dependent regulation of the antero-posterior limits of AER (Farin et al., 2013; Nissim et al., 2006). Therefore, activation of this gene in the pericloacal mesenchyme could contribute to the AER extension into the pericloacal mesoderm in *Tgfbr1-cKO* embryos as indicated by *Fgf8* expression. Overexpression of *Grem1* in GT region, alone or together with early limb bud factor *Fgf10,* however, was not sufficient to induce development of ectopic limb buds (data not shown). This likely indicates that in the presence of the globally unchanged chromatin profile these factors are unable to divert the pericloacal mesenchyme cells from entering their normal GT developmental route.

Accessibility of ZRS in the limb bud requires Tgfbr1 activity.

Rather surprisingly, *Grem1* expression was strongly reduced or absent throughout the mesoderm of the extended hindlimb bud of *Tgfbr1-cKO* embryos (Figure *4-8*B'). *Grem1* expression in the limb depends on Shh activity from ZPA (Malkmus et al., 2021; Zúñiga et al., 2004) suggesting that the absent *Grem1* expression resulted from the abnormal *Shh* expression observed in the hindlimb buds of *Tgfbr1-cKO* mutants (Figure *4-5*A, A'). Consistently, *Gli1* expression was maintained in the native hindlimb and pericloacal mesenchyme of the *Tgfbr1-cKO* embryos but excluded from the extra hindlimb (Figure *4-5*B, B'). *Shh* expression in the ZPA is under the control of the ZRS, an enhancer element within an intron of the *Lmbr1* gene. As expected, this region was accessible in the wild type hindlimbs (Figure *4-8*C). However, it was in a locked configuration

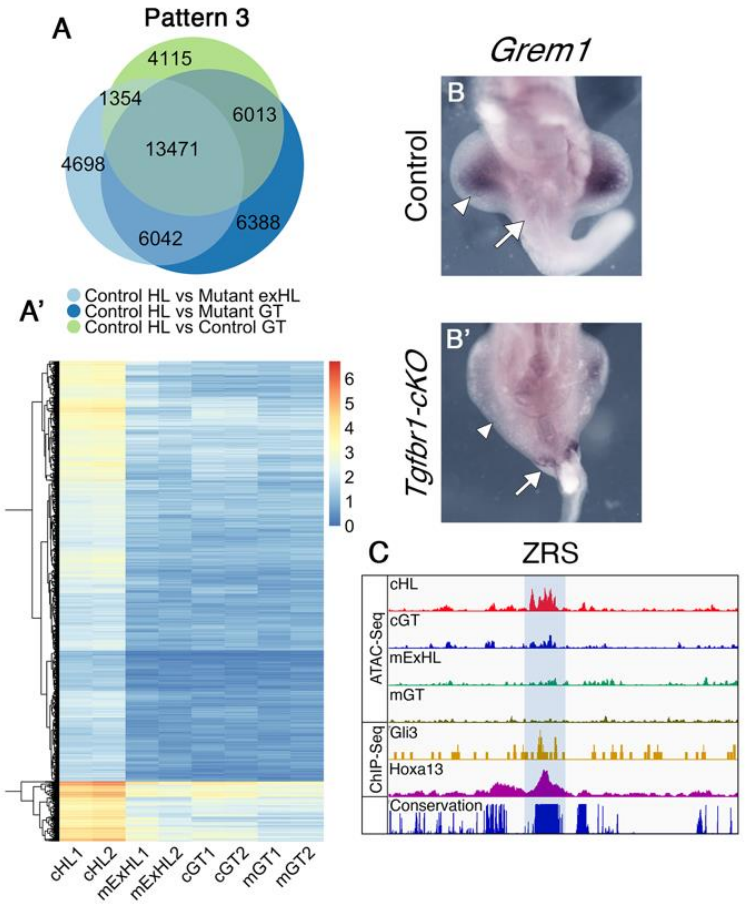

Figure 4-8. Tgfbr1 confers accessibly of the limb specific enhancers. A. Venn diagram showing interception between regions tested more accessible in control hindlimb than in other tissues by pairwise comparisons [FDR<0.001, logFC>1.5]. **B.** Heatmap showing log2 normalized counts for the chromatin regions following pattern 3 across samples. **B, B'.** *Grem1* expression in E10.5 wild type (B) or *Tgfbr1-cKO* (B') embryos showing the absence of pericloacal expression in wild type embryos and ectopic activation in the caudal-most region of the pericloacal mesoderm of the mutant embryo (white arrow). *Grem1* is expressed in the developing limb bud of the control embryo, but it is almost non detectable in the developing limb buds of the mutant embryo (white arrowheads). **C.** ATAC-seq data through the ZRS (highlighted with the blue shadow), showing that it is accessible in the control limb but not in any of the other samples. cHL: control hindlimb; mExHL: mutant extra hindlimb; cGT: control GT; mGT: mutant GT.

in the wild type GT (Figure *4-8*C), consistent with the absence of the *Shh* expression in the pericloacal mesoderm or the GT, despite the presence of relevant activators of this enhancer, like Hand2, Hoxa13 and Hoxd13, in these

tissues. Remarkably, this region was also non-accessible in the extra hindlimb bud of *Tgfbr1-cKO* embryos (Figure *4-8*C), consistent with the abnormal *Shh* expression in this region. Therefore, Tgfbr1 seems to influence *Shh* expression in the limb buds by regulating the accessibility of the ZRS. Interestingly, this enhancer is part of an additional pattern (pattern 3) consisting of elements requiring *Tgfbr1* activity to become accessible in the limb bud. Analysis of the ATAC-seq data revealed that 13471 elements fitting the criteria of this pattern (Figure *4-8*A, A'). The complementary tissue specificities of patterns 1 and 3 indicates context dependency for Tgfbr1 activity in the modulation of genomic configuration.

DISCUSSION

Hindlimbs and external genitalia both belong to the trunk terminal unit. These two structures share induction mechanisms at the caudal-most part of the trunk, which are conserved among vertebrate clades (Dias et al., 2020; Jurberg et al., 2013; Matsubara et al., 2017). From studies in squamates it has been proposed that ancestrally external genitalia derive from the hindlimb primordium (Tschopp et al., 2014). Here we show that the mammalian pericloacal mesenchyme is a plastic tissue, which retains limb forming potential. Tgfbr1 is a factor controlling GT versus hindlimb fate decisions by acting on the genomic regulatory landscape, whereby modulating cellular response to common inductive signals, like Shh. Indeed, dUE expressing *Shh* have been shown to induce growth of the limb structures when presented to the receptive limb mesenchymal cells (Perriton et al., 2002). How the same factor produces different morphological outcomes depending on the context remained an open question. Our findings demonstrate that a subset of gene regulatory regions confers tissue specific response to Shh signaling, and possibly to other factors. These regions, regulated by the Tgfbr1, serve two main purposes in the pericloacal mesenchyme: to grant activation of the genes required for GT growth, and to avert activation of the limb specific genes.

An important finding from our work is that Tgfbr1 controls pericloacal mesoderm plasticity by modulating its regulatory landscape. It has been reported that BMP signaling can affect the chromatin status of Smad-responsive enhancers by interacting with chromatin remodelers, eventually rendering these regulatory elements competent to convey the Smad transcriptional activity (Coda et al., 2017; Dahle et al., 2010; Ross et al., 2006; Xi et al., 2011, 2008). What we have observed in the pericloacal/hindlimb region does not easily fit within this mechanism. For instance, for the *Grem1* enhancer 7 ChIP-seq analyses failed to detect Smad4 binding on limb tissues, where *Grem1* is normally expressed (Malkmus et al., 2021). In addition, we failed to detect enrichment of Smad binding to enhancers rendered accessible by *Tgfbr1* using a HINT-ATAC transcription factor footprinting analysis on the ATAC-seq profiles (Li et al., 2019). Even considering the limitations of the bioinformatic approach, these observations suggest that effectors of the Tgbfr1/BMP signaling pathways are not among the main regulators of the activity of those elements. Consistent with this, Smads have so far not been identified among the factors involved in the activation of the ZRS enhancer. Our data suggest a general model according to which Tgfbr1 signaling acts in a pioneer-like activity, determining the accessibility of regulatory elements to patterning transcription factors.

Loss of the Tgfbr1 from the posterior trunk, after its requirement to induce hindlimb buds and GT has been fulfilled, changes response of the pericloacal mesenchymal cells to the dUE derived Shh signaling from GT-like to limb-like. Particularly, early expression of *Grem1* in lateral pericloacal mesenchyme counteracts BMP inhibition of the FGF factors (Farin et al., 2013; Lopez-Rios et al., 2012) in the posterior limb bud and perturbs AER spatial organization extending its posterior limit. Together with the altered competence of the pericloacal mesenchyme, this leads to its recruitment to the elongated posteriorly AER and formation of the ectopic hindlimbs. Due to the extra hindlimb bud's small size, the inhibitory effect of the Fgf8 from extended AER on *Grem1* (Verheyden and Sun, 2008) is spread throughout the entire extra

hindlimb mesenchyme. This, together with intermittent *Shh* pattern, likely explains the early *Grem1* downregulation in the extra hindlimb bud.

Some features of *Tgfbr1* deficient embryos phenocopy compound mutants of Tgf-β family members, displaying redundancy between the ligands. For example, *Tgfβ1/Tgfβ2* compound mutants exhibit failure of the midline closure (Dünker and Krieglstein, 2002). *Gdf11* KO and *Gdf8/Gdf11* double KO fetuses lack one or both kidneys, another feature also present in the *Tgfbr1-cKO* mutants (McPherron et al., 2009). Our data thus indicate that these ligands' activity is mediated by Tgfbr1. Whether forelimb duplication of the *Gdf8/Gdf11* double mutants is caused by mechanism similar to one in the hindlimbs of the *Tgfbr1-cKO* remains unclear. However, the reported penetrance of this phenotype is much lower in the *Gdf8/Gdf11* double mutants than in *Tgfbr1-cKO* fetuses.

In squamates, contrary to mouse, hindlimbs are more akin to GT than to the forelimbs by their transcriptome (Tschopp et al., 2014). Similarly, the extra hindlimb of the *Tgfbr1-cKO* share more similarities with the chromatin landscape of GT than with the native hindlimb. Therefore, we propose that Tgfbr1 might play a role in evolutionary divergence between the hindlimbs and GT observed in mammals. Our findings show that Tgfbr1 ensures tissue specific response in the hindlimb and GT primordial tissue to common inductive signals. This specificity is granted by regulation of the chromatin conformation at specific regulatory regions. This is a novel function of Tgfbr1 as a modulator of response to other signaling pathways, which sheds light on the complicated issue of the context-dependent signaling specificity.

Acknowledgements

We would like to thank the members of the Mallo lab, especially Ana Casaca for continuous support at different stages of this project, the IGC mouse facility for their help with animal housing, genomics facility for helping with the ATAC-seq procedures and advanced imaging facility, especially Gabriel Martins, for help with image acquisition and analysis. This project was funded by

Fundação para a Ciência e a Tecnologia (FCT) grants PTDC/BIA-BID/30254/2017 to MM, PTDC/BII-BTI/32375/2017 to GGM, and PhD fellowships PD/BD/128437/2017 to AL and PD/BD/128426/2017 to AD, by the PhD fellowship 36/8l-D/21 from Fundação Calouste Gulbenkian to AK, and the research infrastructures PPBI-POCI-01-0145-FEDER-022122 to the Advanced Imaging Facility, and Congento LISBOA-01-0145-FEDER-022170 to the animal facility, both co-financed by Lisboa Lisboa 2020/FEDER and FCT (Portugal).

Chapter 5

GENERAL DISCUSSION

The broad Tgf-β signaling family is involved in multiple developmental and pathological processes. This work was aimed to advance our understanding of the Gdf11/Tgfbr1 signaling regulatory mechanisms in a specific developmental process, namely the trunk to tail transition. The combination of transcriptomic, genetic, and genomic approaches utilized in this study helped to uncover some of aspects of the Gdf11/Tgfbr1 regulatory mechanisms. Excitingly, our studies revealed novel functions of Tgfbr1 in hindlimb and GT morphogenesis with possible implications in the regulation of crosstalk between signaling pathways and in evolution.

Tgf-β and cellular mechanisms of tail bud formation.

The leading role of Gdf11 signaling in the process of trunk to tail transition was reported more than two decades ago (McPherron et al., 1999). Subsequent studies identified Tgfbr1 as the type I receptor mediating Gdf11 signaling in this developmental context (Andersson et al., 2006). Considering the redundancy between Gdf11 and other Tgf-β ligands, particularly Gdf8 (McPherron et al., 2009), elimination of the signaling by the genetic KO of the receptor ought to elucidate the role of this signaling pathway in the process of the trunk to tail transition.

Although *Tgfbr1* null mutants (*Tgfbr1-KO*) were first generated and described twenty-two years ago (Larsson et al., 2001), evaluating its axial phenotype proved to be challenging due their early embryonic lethality. Nonetheless, we took advantage of the ability of *Tgfbr1-KO* embryos to survive unlit the E9.5 and undergo the process of turning. During that time wild type embryos form their tail bud and establish the tail axial extension niche. Our genetic experiments revealed that *Tgfbr1-KO* embryos were unable to undergo the trunk to tail transition and form a functional tail bud. Tail bud formation requires NMCs relocation from the NBS in the epiblast to the CNH. RNA-seq analysis of the wild type embryos undergoing the trunk to tail transition

reported in chapter 2 and in the published studies (Dias et al., 2020; Gouti et al., 2017) show that such reorganization requires changes in the composition of cell adhesion molecules. Analysis of differentially expressed cell adhesion marker genes suggests that cells relocating from the NSB to CNH undergo EMT as they downregulate epithelial markers, including *Chd1, Krt19, Col4a1* and *Epcam*, and upregulate some mesenchymal markers, e.g., *Snai1* and *Vim* (Chapter 2, (Dias et al., 2020)). It must be noted, however, that we observed reorganization in the adhesion molecules composition rather than replacement of epithelial markers with the mesenchymal ones, as tail bud samples maintain many, and even upregulate some, epithelial markers. This observation is in line with the idea that the tail bud axial progenitors retain some epithelial properties along with their differentiation potential as discussed in (Aires et al., 2019; Jurberg et al., 2013).

Analysis of several EMT markers shows that in the *Tgfbr1-KO* embryos the EMT associated with the trunk to tail transition is compromised. Particularly, at E9.5 the axial progenitor region of the *Tgfbr1-KO* embryos retains significant levels of Cdh1 and Epcam, and do not display levels of Cdh2 and Vim resembling those in the wild type controls. Interestingly, our analysis of E9.5 *Gdf11-KO* tailbud transcriptome does not show changes in the expression of these markers compared to controls. This observation is particularly interesting when considering the differences between the tailbud phenotypes of the *Gdf11-KO* and *Tgfbr1-KO* embryos. *Gdf11*expression in the tailbud is required for successful relocation of the progenitors to the CNH (Aires et al., 2019; Jurberg et al., 2013). *Gdf11-KO* tails are characterized by the presence of an ectopic endodermal pocked containing the mix of the mesodermal cells and cells expressing NMCs markers, proposed to be the remnants of the unresolved epiblast (Aires et al., 2016). We didn't observe anything alike in the *Tgfbr1-KO* tailbud. Moreover, we noted a significant decrease of all the tailbud mesodermal markers tested in the mutants. This possibly reflects the aggravated progenitor relocation phenotype in the *Tgfbr1-KO* compared to the *Gdf11-KO* embryos: while in the *Gdf11* mutants

progenitors are "lost on their way" to CNH, in *Tgfbr1* KO progenitors are just unable to undergo EMT and delaminate from the NSB.

Tgfbr1 and development of the caudal trunk.

Establishing the axial extension niche for the tail growth is one of the components of the trunk to tail transition. Termination of trunk development by induction of its most caudal derivatives is another one. *Tgfbr1-KO* embryos are unable to form hindlimbs, the cloacal widening, or the GT. Interestingly, the GT was proposed to have, at least partially, tailbud origin in mouse (Tschopp et al., 2014). Whether absence of GT in *Tgfbr1-KO* embryos is a secondary effect of their inability to form the tail bud or is it due to failure to activate downstream regulators remains to be elucidated.

Anterior-posterior patterning along the main body axis has been associated with the appropriate expression of the corresponding *Hox* gene paralogue groups (PG) (Wellik, 2007). Indeed, the trunk to tail transition is concurrent with the activation of posterior *Hox* genes. Furthermore, Gdf11 (chapter 2 of this work, (Andersson et al., 2006; Gaunt et al., 2013; Jurberg et al., 2013; Mcpherron et al., 1999; Szumska et al., 2008)) and Tgfbr1 (Dias et al., 2020) have been shown to be involved in the activation of the *Hox* genes of PGs 9 to 13. Interestingly, however, neither gain of function (Carapuço et al., 2005; Jurberg et al., 2013; Vinagre et al., 2010), nor loss of function (Koyama et al., 2010; Wellik and Capecchi, 2003) experiments were able to reveal a major regulatory role of the posterior *Hox* genes in the induction of trunk to tail transition landmarks, like the hindlimbs. *Isl1*, on the other hand, is required to induce the hindlimbs (Kawakami et al., 2011), and seemingly the GT (Kaku et al., 2013). *Isl1* overexpression in the axial tissues is sufficient to anticipate the trunk to tail transition in mouse embryos (Jurberg et al., 2013). It has been proposed that *Isl1* expression in the caudal LMP and in the pericloacal mesenchyme is under the control of *Gdf11* (Jurberg et al., 2013). Analysis of *Isl1* expression in *Tgfbr1-KO* embryos presented in chapter 3 of the thesis supports this idea.

Interestingly, while reportedly regulated by the *Foxf1* in different tissues, including trunk posterior ventral mesoderm and allantois (Kang et al., 2009), *Isl1* expression is absent from *Tgfbr1* mutants despite the strong upregulation of *Foxf1* in their caudal end, suggesting that it requires additional activators. Analysis of the *Isl1-KO* embryos – a matter of ongoing research in the lab – will help dissecting regulatory mechanisms of different components of the trunk to tail transition and to clarify the relationships between *Isl1* and *Tgfbr1* in the induction of the hindlimbs and GT.

The phenotype of the *Tgfbr1-KO* embryos reveals the complexity of coordinated events required for the trunk to tail transition. When the wild type embryo undergoes turning, the allantois is positioned along the ventral side of the embryo anteriorly to the pericloacal mesenchyme, and thus can be used as a reference to mark the end of the trunk. *Tgfbr1-KO* embryos are able to turn and to relocate their allantois. Therefore, in the absence of hindlimbs the allantois could indicate the posterior border of the trunk. However, morphological and gene expression analyses of the *Tgfbr1-KO* embryos presented in chapter 3 showed that their trunks do not terminate near the connection with the allantois and trunk structures, including LPM, IM, coelomic cavity and dorsal aortae, extend to the very tip of the embryo. At the same time, tissues in the caudal-most part of the mutant embryos were severely disorganized, with cells intercalating in the neighboring tissues. This was particularly evident for the splanchnic LPM marker *Foxf1* and the marker of the newly formed endoderm *Apela*.

The pattern of *Foxf1* expression is particularly interesting. Regulation of *Foxf1* expression is different in the trunk, there it is under the regulation of HH signaling from the endoderm, and in the caudal most part of the epiblast, where it is HH-independent (Astorga and Carlsson, 2007; Tsiairis and McMahon, 2009). This region later contributes to ventral posterior mesoderm (Wymeersch et al., 2019, 2016), which, in turn, was shown to contribute to pericloacal mesenchyme in mouse (Tschopp et al., 2014). Consequently, *Foxf1* expressing pericloacal mesenchymal cells possibly derive from the posterior ventral mesenchyme

rather than from splanchnic LPM. It is possible, therefore, that intermingled Foxf1-positive cells are prospective pericloacal cells trapped in ectopic trunk tissue. Similarly, Apela-positive endodermal cells are trapped in ectopic LPM instead of becoming incorporated into the gut tube.

Finally, the *Tgfbr1-cKO* phenotype shows requirement of this receptor after the trunk to tail transition, for proper patterning of all major aspects of the caudal trunk. The pleiotropic phenotype of *Tgfbr1-cKO* mutants reveals that this receptor is shared by multiple Tgf-β ligands. For example, the omphalocele phenotype was also observed in Tgf-β2/Tgf-β3 double mutants (Dünker and Krieglstein, 2002), indicating that Tgfbr1 might mediate Tgf-β2 and Tgf-β3 activity in the body wall. The absence of kidneys and of the rectal portion of the gut most likely results from the absence of Gdf11/Gdf8 activity (McPherron et al., 2009; Szumska et al., 2008). The most striking phenotype of *Tgfbr1-cKO* mutants is the duplication of their hindlimbs. It must be noted that in our experimental setup the forelimb was not targeted by Cre recombinase, and therefore expression of *Tgfbr1* was unaffected. *Gdf11/Gdf8* double mutants are characterized by a similar forelimb duplication (hindlimbs are small and deformed in the mutants, but no duplication has been reported), thought the phenotype is much less penetrant (McPherron et al., 2009). The two phenotypes might share some common mechanisms. However, we do not anticipate them to be identical due to different tissue contexts. The ectopic hindlimbs of the *Tgfbr1-cKO* embryos are formed from the pericloacal mesenchyme recruited to the extended hindlimb field. We show that the pericloacal mesenchyme ability to engage in limb development is caused by change in the enhancer regulatory landscape. We also suggest that the altered response of pericloacal mesenchyme to inductive signals from the cloaca largely contributes to the phenotype, particularly in regard to degenerated GT.

Interplay of signaling pathways and chromatin regulation.

Cell populations in the developing embryo are exposed to multiple simultaneous inputs from different signaling pathways and transcription factors. Results presented in this work showed how Gdf11/Tgfbr1 signaling influences the activity of other signaling pathways. Wnt and RA signaling have been shown to differently regulate axial progenitor differentiation, Wnt3a promoting mesodermal fates, while RA activates neural differentiation (Gouti et al., 2017; Jurberg et al., 2013; Takada et al., 1994). In *Gdf11* mutants tail bud axial progenitors favor neural over mesodermal fates, maybe due to the downregulation of the RA degrading enzyme *Cyp26a1* and of *Wnt3a* (Aires et al., 2019; Jurberg et al., 2013). We also observe this tendency in the tail bud of *Tgfbr1-KO* embryos, consistent with Tgfbr1 mediating Gdf11-dependent regulation of these genes. Notably, in chapter 2 we report many components of Wnt and other signaling pathways among the differentially expressed genes in the *Gdf11* mutant tail bud right after the trunk to tail transition. Differential gene expression in the mutants may be direct consequence of reduced activation of the intracellular effectors (indeed, Smad2 phosphorylation was reduced in *Gdf11* KO progenitors region at E9.5 [Irma Varela-Lasheras, unpublished]), or a secondary effect of the mutant's phenotype.

Regulation of gene expression is one of the modes of the Gdf11/Tgfbr1 control of the activity of other signaling pathways. In chapter 4 we describe an alternative way of Tgfbr1-dependent modulation of the Shh signaling regulatory output. We show that Tgfbr1 adjusts the tissue response to Shh and probably other factors common to the hindlimb and GT by regulating the chromatin accessibility landscape. This regulation results in the formation of morphologically and functionally very different structures, despite the many common regulatory inputs.

The Tgf-β ability to act on chromatin was previously studied in several different contexts. A recent study using ATAC-seq proposed that *Eomes* activation during ESCs differentiation into definitive endoderm is mediated, at

least partially, by enhancers gaining accessibility upon Smad2/3 binding (Simon et al., 2017). Indeed, Smad proteins have been shown to be able to bind not only to accessible, acetylated chromatin, but also to heterochromatin, where they changed its conformation by recruiting chromatin remodeling complexes. Thereby, interaction of Smad proteins with H3K27me3 demethylase Jmjd3 (Dahle et al., 2010), TRIM33 protein displacing the chromatin compacting factor HP1γ (Xi et al., 2011), helicase SMARCA4 (Coda et al., 2017), and histone acetyltransferases CBP/EP300 (Janknecht et al., 1998) have been reported. Notably, all these studies were performed *in vitro* and mostly are related to Activin/Nodal signaling. Furthermore, studies listed above describe molecular mechanisms of regulation for the Tgf-β/Smad target genes. The phenomenon described in chapter 4, on the other hand, is the example of the Tgf-β signaling influencing gene expression indirectly, by creating permissive o restrictive environments for other regulators. Moreover, our bioinformatic TF footprinting analysis failed to identify enrichment for Smad2/3 proteins in the differentially assessable peaks, suggesting an alternative mechanism. Direct evaluation of Smad2/3 binding to the genome of the GT would be required to clarify their involvement in the regulatory process. A recent study in murine mammary gland epithelial cells showed widespread changes of chromatin accessibility upon Tgf-β treatment, modeling the EMT condition. Interestingly, ATAC-seq footprints for Smad3 and Smad4 were found in activated enhancers, but not in the repressed, suggesting different mechanism for Tgf- β dependent activation and repression of chromatin (Guerrero-Martínez et al., 2020). The possibility that Tgfbr1 acts via non-canonical downstream effectors, or Smad1, which can be phosphorylated by Tgfbr1 (Wrighton et al., 2009) and have been shown to remodel chromatin (Adam et al., 2018), cannot be excluded. Additionally, our GO enrichment analysis on DEGs showed histone modifying enzymes and chromatin binding proteins among genes differentially expressed in *Gdf11* mutant tail bud. Expression of specific chromatin remodeling complexes activated by Gdf11/Tgfbr1 signaling could be involved in activation of

chromatin remodeling function, however it does not explain how specific enhancers are targeted.

Finally, it would be interesting to know whether Tgfbr1 dependent chromatin rearrangement is involved in gene regulation in other developmental contexts, for example for posterior *Hox* gene regulation during the trunk to tail transition. Our results showing differential chromatin accessibility in distal enhancer regions during the trunk to tail transition, some associated with posterior *Hox* genes, is in line with this hypothesis. Moreover, the *Hoxd11* enhancer reportedly activated by direct binding of Smad2 (Gaunt et al., 2013) gained accessibility after the trunk to tail transition in our ATAC-seq analysis. A recent study in a murine cell line reports that Tgf-β can co-regulate clusters of genes located in the same topologically associating domain (TAD) by chromatin accessibility changes in the mutual enhancers (Guerrero-Martínez et al., 2020). A similar mode of regulation was described for *HoxA* and *HoxD* clusters located at the boundary of two TADs. During proximal limb development anterior *Hox* genes are activated by regulatory regions in the telomeric TAD, and later, during distal limb development, posterior *Hox* genes are activated by the enhancers located in the centromeric TAD (Fabre et al., 2017; Rodríguez-Carballo et al., 2017). Gdf11/Tgfbr1, therefore, may cumulatively activate posterior *Hox* genes by acting on enhancers located in the respective TAD in the context on antero-posterior patterning.

Evolutionary perspective on Tgfbr1 activity for hindlimb and GT development.

In the course of evolution, body appendages developed as adaptations, including locomotion and internal fertilization among others. Despite the drastically different morphology and functions, vertebrate hindlimbs and GT are often paralleled due to the common regulatory mechanisms and expression of common marker genes (Cohn, 2011).

Indeed, studies in squamates showed that their paired external genitalia develop from the same developmental field as the hindlimb buds (Tschopp et al., 2014). This mode has been proposed to be ancestral and that evolved differently in various tetrapods. For instance, in the chick the two structures develop from the neighboring regions of posterior LPM (Herrera and Cohn, 2014), whereas in the mouse the GT seems to derive from ventral and tailbud mesoderm (Tschopp et al., 2014). Although the mouse hindlimb and GT are more distantly related than those of ancestral squamate species (Tschopp et al., 2014), in chapter 4 we show the existence of remarkable plasticity of their hindlimb and GT precursors.

Our findings reveal a leading role of Tgfbr1 in the regulation of chromatin accessibility to generate distinct and specific responses from the hindlimb and GT primordia to common signals. How neighboring appendages interpret similar regulatory inputs in a tissue-specific manner to engage in different morphogenetic programs have been a longstanding question. Tschopp et al. propose that it is the regulatory influence of the cloaca what triggers GT fates from the mesodermal cells. To support this claim, they show that grafting the cloaca into the chick limb bud changes the expression profile of the neighboring mesenchyme cells to acquire genital-like features. However, it was previously shown that grafts of both snakes and chick cloacal endoderm induce ectopic limb-like structures when grafted to the limb bud (Cohn and Tickle, 1999; Perriton et al., 2002). This, consistently with our findings, shows that hindlimb and GT fates are defined by the intrinsic properties of the mesodermal cells, rather than by nature of inductive signaling source. Our results propose that the cellular response largely depends on the chromatin landscape of regulatory regions. The presence of limb and GT specific enhancer activity in the mouse is in line with this idea (Infante et al., 2015).

Interestingly, the role of *cis*-regulatory elements and their chromatin state in limbs and GT morphogenesis have been studied in an evolutionary context in squamates, particularly in loss of limbs in snakes. While sequences of many limb and common limb/GT enhancers diverged in snakes and lost their TF-binding

sites (Leal and Cohn, 2016; Roscito et al., 2018) or were co-opted for GT-only expression (Guerreiro et al., 2016; Infante et al., 2015), it is admitted that a large proportion of limb specific enhancers are conserved in snakes (Infante et al., 2015; Roscito et al., 2018). This is possibly explained by pleiotropy of many *cis*-regulatory regions. Therefore, different level of regulation might take place, thereby conserved regulatory sequences would be rendered inaccessible in the tissues there their activity is not required. In line with this idea, it has been shown in the limbed lizard *Anolis*, that most of conserved GT specific enhancers are deprived of active chromatin marks (Infante et al., 2015).

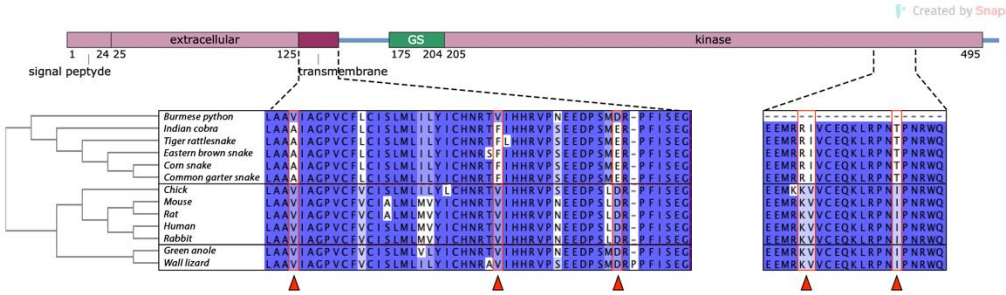

Figure 5-1. Tgfbr1 protein sequence alignments result for 13 vertebrates species. Alignment and phylogram was made with ClustalW2.

It would be interesting to know whether Tgfbr1 might be involved in the regulation of appendage development in an evolutionary context, like the loss of limbs in snakes. Such loss of limbs has been attributed to mutations in ZRS, leading to transient *Shh* expression, or loss of expression (Kvon et al., 2016; Leal and Cohn, 2016). Despite that *Tgfbr1-cKO* embryos form fairly well-developed limbs including autopod, we show that Tgfbr1 is required to make ZRS accessible to induce adequate level of *Shh* expression. Moreover, in the mouse, the *Shh* mutant limb phenotype mainly concerns the autopod (Litingtung et al., 2002). Therefore, while *Shh* admittedly plays a role in limb loss in snakes, there must be additional factors contributing to this phenotype.

Analysis of the Tgfbr1 protein sequence in six snake species (including one python), two lizard species, chicken and four mammalian species, reveled some

amino acid differences correlating with presence/absence of limbs (Figure 5-1). First of all, lizard Tgfbr1 sequence clustered closer to other limbed vertebrates than to snakes, despite their phylogenetic proximity. The extracellular domain of the receptor is very variable in all analyzed species; the GS and kinase domains, on the contrary, are characterized by very high conservation level, and the transmembrane domain shows an intermediate pattern. Interestingly, three amino acid changes in the transmembrane domain were present in five advanced snake species, characterized by complete loss of limbs, but not in python, which retains vestigial limbs (red arrowheads in Figure 5-1). Additionally, we identified three amino acid changes in advanced snakes (python proteins sequence is truncated earlier in kinase domain) in the C-terminal part of otherwise highly conserved kinase domain (red arrowheads in Figure 5-1). To understand whether Tgfbr1 is indeed involved in the regulation of limb/GT fate in snakes will require direct genetic evaluation by either knocking in snake Tgfbr1 coding sequence in the mouse endogenous locus, or by introduction of some serpentine mutations into the mouse gene.

In conclusion

In this work we studied multifaceted regulatory mechanisms under the control of Tgf-β signaling in the contexts of trunk to tail transition and caudal trunk development. Generation of the total and conditional knock outs of the Gdf11 membrane receptor Tgfbr1 allowed us to research multiple functions of this signaling in development. We show that while in the *Gdf11-KO* embryos the trunk to tail transition is delayed, total ablation of the signaling in *Tgfbr1-KO* blocks most aspects of the transition. Furthermore, the phenotype of the *Tgfbr1-cKO* embryos and fetuses revealed a novel role of this receptor as regulator of tissue plasticity. Here we show for the first time *in vivo* that Tgf-β signaling is not only directly involved in the regulation of morphogenic processes, but also modulates tissue response to other regulators. Our work opens prospects for

further research. Identifying the mechanism of Tgfbr1 activity on the chromatin landscape and whether similar mechanisms operate in different developmental processes could shed light on mechanisms of context dependent response to signaling inputs. Finally, this work evokes considerations regarding the possible role of Tgfbr1, and Tgf-β signaling in general, in the evolution of diverse phenotypes of vertebrate body appendages.

REFERENCES

Abu-Abed, S., Dollé, P., Metzger, D., Beckett, B., Chambon, P., Petkovich, M., 2001. The retinoic acid-metabolizing enzyme, CYP26A1, is essential for normal hindbrain patterning, vertebral identity, and development of posterior structures. Genes Dev. 15, 226–240. https://doi.org/10.1101/gad.855001

Adam, R.C., Yang, H., Ge, Y., Lien, W.-H., Wang, P., Zhao, Y., Polak, L., Levorse, J., Baksh, S.C., Zheng, D., Fuchs, E., 2018. Temporal Layering of Signaling Effectors Drives Chromatin Remodeling during Hair Follicle Stem Cell Lineage Progression. Cell Stem Cell 22, 398-413.e7. https://doi.org/10.1016/j.stem.2017.12.004

Afgan, E., Baker, D., van den Beek, M., Blankenberg, D., Bouvier, D., Čech, M., Chilton, J., Clements, D., Coraor, N., Eberhard, C., Grüning, B., Guerler, A., Hillman-Jackson, J., Von Kuster, G., Rasche, E., Soranzo, N., Turaga, N., Taylor, J., Nekrutenko, A., Goecks, J., 2016. The Galaxy platform for accessible, reproducible and collaborative biomedical analyses: 2016 update. Nucleic Acids Res. 44, W3–W10. https://doi.org/10.1093/nar/gkw343

Agarwal, P., Wylie, J.N., Galceran, J., Arkhitko, O., Li, C., Deng, C., Grosschedl, R., Bruneau, B.G., 2003. *Tbx5* is essential for forelimb bud initiation following patterning of the limb field in the mouse embryo. Development 130, 623–633. https://doi.org/10.1242/dev.00191

Agrotis, A., Condron, M., Bobik, A., 2000. Alternative splicing within the TGF-β type I receptor gene (ALK-5) generates two major functional isoforms in vascular smooth muscle cells. FEBS Lett. 467, 128–132. https://doi.org/10.1016/S0014-5793(00)01132-7

Ahn, K., Mishina, Y., Hanks, M.C., Behringer, R.R., Bryan Crenshaw, E., 2001. BMPR-IA signaling is required for the formation of the apical ectodermal ridge and dorsal-ventral patterning of the limb. Development 128, 4449–4461.

Aires, R., de Lemos, L., Nóvoa, A., Jurberg, A.D., Mascrez, B., Duboule, D., Mallo, M., 2019. Tail Bud Progenitor Activity Relies on a Network Comprising Gdf11, Lin28, and Hox13 Genes. Dev. Cell 48, 383-395.e8. https://doi.org/10.1016/j.devcel.2018.12.004

Aires, R., Dias, A., Mallo, M., 2018. Deconstructing the molecular mechanisms shaping the vertebrate body plan. Curr. Opin. Cell Biol. 55, 81–86. https://doi.org/10.1016/j.ceb.2018.05.009

Aires, R., Jurberg, A.D., Leal, F., Nóvoa, A., Cohn, M.J., Mallo, M., 2016. Oct4 Is a Key Regulator of Vertebrate Trunk Length Diversity. Dev. Cell 38, 262–274. https://doi.org/10.1016/j.devcel.2016.06.021

Akiyama, R., Kawakami, H., Wong, J., Oishi, I., Nishinakamura, R., Kawakami, Y., 2015. Sall4-Gli3 system in early limb progenitors is essential for the

development of limb skeletal elements. Proc. Natl. Acad. Sci. 112, 5075–5080. https://doi.org/10.1073/pnas.1421949112

Ali, I.H.A., Brazil, D.P., 2014. Bone morphogenetic proteins and their antagonists: current and emerging clinical uses: Targeting BMPs in human disease. Br. J. Pharmacol. 171, 3620–3632. https://doi.org/10.1111/bph.12724

Amack, J.D., 2021. Cellular dynamics of EMT: lessons from live in vivo imaging of embryonic development. Cell Commun. Signal. 19, 79. https://doi.org/10.1186/s12964-021-00761-8

Amin, S., Neijts, R., Simmini, S., van Rooijen, C., Tan, S.C., Kester, L., van Oudenaarden, A., Creyghton, M.P., Deschamps, J., 2016. Cdx and T Brachyury Co-activate Growth Signaling in the Embryonic Axial Progenitor Niche. Cell Rep. 17, 3165–3177. https://doi.org/10.1016/j.celrep.2016.11.069

Andersson, O., Reissmann, E., Ibáñez, C.F., 2006. Growth differentiation factor 11 signals through the transforming growth factor-beta receptor ALK5 to regionalize the anterior-posterior axis. EMBO Rep. 7, 831–7. https://doi.org/10.1038/sj.embor.7400752

Andrews, S., 2010. FastQC: A Quality Control Tool for High Throughput Sequence Data [Online]. Available online at: http://www.bioinformatics.babraham.ac.uk/projects/fastqc/.

Armfield, B.A., Cohn, M.J., 2021. Single cell transcriptomic analysis of external genitalia reveals complex and sexually dimorphic cell populations in the early genital tubercle. Dev. Biol. 477, 145–154. https://doi.org/10.1016/j.ydbio.2021.05.014

Astorga, J., Carlsson, P., 2007. Hedgehog induction of murine vasculogenesis is mediated by Foxf1 and Bmp4. Development 134, 3753–3761. https://doi.org/10.1242/dev.004432

Attardi, A., Fulton, T., Florescu, M., Shah, G., Muresan, L., Lenz, M.O., Lancaster, C., Huisken, J., van Oudenaarden, A., Steventon, B., 2019. Correction: Neuromesodermal progenitors are a conserved source of spinal cord with divergent growth dynamics (doi: 10.1242/dev.166728). Development 146, dev175620. https://doi.org/10.1242/dev.175620

Balmer, S., Nowotschin, S., Hadjantonakis, A.K., 2016. Notochord morphogenesis in mice: Current understanding and open questions. Dev. Dyn. 245, 547–557. https://doi.org/10.1002/dvdy.24392

Bandyopadhyay, A., Tsuji, K., Cox, K., Harfe, B.D., Rosen, V., Tabin, C.J., 2006. Genetic Analysis of the Roles of BMP2, BMP4, and BMP7 in Limb Patterning and Skeletogenesis. PLoS Genet. 2, e216. https://doi.org/10.1371/journal.pgen.0020216

Bardot, E.S., Hadjantonakis, A.-K., 2020. Mouse gastrulation: Coordination of tissue patterning, specification and diversification of cell fate. Mech. Dev. 163, 103617. https://doi.org/10.1016/j.mod.2020.103617

Barnett, D.W., Garrison, E.K., Quinlan, A.R., Strömberg, M.P., Marth, G.T., 2011. BamTools: a C++ API and toolkit for analyzing and managing BAM files. Bioinformatics 27, 1691–1692. https://doi.org/10.1093/bioinformatics/btr174

Barrow, J.R., Thomas, K.R., Boussadia-Zahui, O., Moore, R., Kemler, R., Capecchi, M.R., McMahon, A.P., 2002. Ectodermal *Wnt3/β-catenin* signaling is required for the establishment and maintenance of the apical ectodermal ridge. Genes Dev. 17, 394–409. https://doi.org/10.1101/gad.1044903

Bell, S.M., Schreiner, C.M., Waclaw, R.R., Campbell, K., Pottert, S.S., Scottt, W.J., 2003. Sp8 is crucial for limb outgrowth and neuropore closure. Proc. Natl. Acad. Sci. U. S. A. 100, 12195–12200. https://doi.org/10.1073/pnas.2134310100

Bénazet, J.-D., Bischofberger, M., Tiecke, E., Gonçalves, A., Martin, J.F., Zuniga, A., Naef, F., Zeller, R., 2009. A Self-Regulatory System of Interlinked Signaling Feedback Loops Controls Mouse Limb Patterning. Science 323, 1050–1053. https://doi.org/10.1126/science.1168755

Bénazet, J.D., Pignatti, E., Nugent, A., Unal, E., Laurent, F., Zeller, R., 2012. Smad4 is required to induce digit ray primordia and to initiate the aggregation and differentiation of chondrogenic progenitors in mouse limb buds. Development 139, 4250–4260. https://doi.org/10.1242/DEV.084822

Benazet, J.-D., Zeller, R., 2013. Dual requirement of ectodermal *Smad4* during AER formation and termination of feedback signaling in mouse limb buds: SMAD4 Functions in the Limb Bud AER. genesis 1–7. https://doi.org/10.1002/dvg.22412

Ben-Haim, N., Lu, C., Guzman-Ayala, M., Pescatore, L., Mesnard, D., Bischofberger, M., Naef, F., Robertson, E.J., Constam, D.B., 2006. The Nodal Precursor Acting via Activin Receptors Induces Mesoderm by Maintaining a Source of Its Convertases and BMP4. Dev. Cell 11, 313–323. https://doi.org/10.1016/j.devcel.2006.07.005

Binagui-Casas, A., Dias, A., Guillot, C., Metzis, V., Saunders, D., 2021. Building consensus in neuromesodermal research: Current advances and future biomedical perspectives. Curr. Opin. Cell Biol. 73, 133–140. https://doi.org/10.1016/j.ceb.2021.08.003

Boulet, A.M., Capecchi, M.R., 2012. Signaling by FGF4 and FGF8 is required for axial elongation of the mouse embryo. Dev. Biol. 371, 235–245. https://doi.org/10.1016/j.ydbio.2012.08.017

Boulet, A.M., Moon, A.M., Arenkiel, B.R., Capecchi, M.R., 2004. The roles of Fgf4 and Fgf8 in limb bud initiation and outgrowth. Dev. Biol. 273, 361–372. https://doi.org/10.1016/j.ydbio.2004.06.012

Brazil, D.P., Church, R.H., Surae, S., Godson, C., Martin, F., 2015. BMP signalling: agony and antagony in the family. Trends Cell Biol. 25, 249–264. https://doi.org/10.1016/j.tcb.2014.12.004

Brogna, S., Wen, J., 2009. Nonsense-mediated mRNA decay (NMD) mechanisms. Nat. Struct. Mol. Biol. 16, 107–113. https://doi.org/10.1038/nsmb.1550

Buenrostro, J.D., Wu, B., Chang, H.Y., Greenleaf, W., 2016. ATAC-seq: A Method for Assaying Chromatin Accessibility Genome-Wide. Curr Protoc Mol Biol 48, 1197–1222. https://doi.org/10.1249/MSS.0000000000000901.Physical

Cai, C.-L., Liang, X., Shi, Y., Chu, P.-H., Pfaff, S.L., Chen, J., Evans, S., 2003. Isl1 Identifies a Cardiac Progenitor Population that Proliferates Prior to Differentiation and Contributes a Majority of Cells to the Heart. Dev. Cell 5, 877–889. https://doi.org/10.1016/S1534-5807(03)00363-0

Cambray, N., Wilson, V., 2007. Two distinct sources for a population of maturing axial progenitors. Dev. Camb. Engl. 134, 2829–40. https://doi.org/10.1242/dev.02877

Cambray, N., Wilson, V., 2002. Axial progenitors with extensive potency are localised to the mouse chordoneural hinge. Development 129, 4855–4866. https://doi.org/10.1242/dev.129.20.4855

Capdevila, J., Tsukui, T., Esteban, C.R., Zappavigna, V., Belmonte, J.C.I., 1999. Control of Vertebrate Limb Outgrowth by the Proximal Factor Meis2 and Distal Antagonism of BMPs by Gremlin. Mol. Cell 4, 839–849. https://doi.org/10.1016/S1097-2765(00)80393-7

Capellini, T.D., Di Giacomo, G., Salsi, V., Brendolan, A., Ferretti, E., Srivastava, D., Zappavigna, V., Selleri, L., 2006. *Pbx1/Pbx2* requirement for distal limb patterning is mediated by the hierarchical control of Hox gene spatial distribution and *Shh* expression. Development 133, 2263–2273. https://doi.org/10.1242/dev.02395

Carapuço, M., Nóvoa, A., Bobola, N., Mallo, M., 2005. *Hox* genes specify vertebral types in the presomitic mesoderm. Genes Dev. 19, 2116–2121. https://doi.org/10.1101/gad.338705

Chapman, D.L., Garvey, N., Hancock, S., Alexiou, M., Agulnik, S.I., Gibson-Brown, J.J., Cebra-Thomas, J., Bollag, R.J., Silver, L.M., Papaioannou, V.E., 1996. Expression of the T-box family genes,Tbx1-Tbx5, during early mouse development. Dev. Dyn. 206, 379–390. https://doi.org/10.1002/(SICI)1097-0177(199608)206:4<379::AID-AJA4>3.0.CO;2-F

Charité, J., McFadden, D.G., Olson, E.N., 2000. The bHLH transcription factor dHAND controls *Sonic hedgehog* expression and establishment of the zone of polarizing activity during limb development. Development 127, 2461–2470. https://doi.org/10.1242/dev.127.11.2461

Chawengsaksophak, K., De Graaff, W., Rossant, J., Deschamps, J., Beck, F., 2004. *Cdx2* is essential for axial elongation in mouse development. Proc. Natl. Acad. Sci. 101, 7641–7645. https://doi.org/10.1073/pnas.0401654101

Chen, H., Johnson, R.L., 2002. Interactions between dorsal-ventral patterning genes lmx1b, engrailed-1 and wnt-7a in the vertebrate limb. Int. J. Dev. Biol. 46, 937–941. https://doi.org/10.1387/ijdb.12455631

Chen, H., Lun, Y., Ovchinnikov, D., Kokubo, H., Oberg, K.C., Pepicelli, C.V., Gan, L., Lee, B., 1998. Limb and kidney defects in Lmx1b mutant mice suggest an involvement of LMX18 in human nail patella syndrome 19, 5.

Chiang, C., Litingtung, Y., Lee, E., Young, K.E., Corden, J.L., Westphal, H., Beachy, P.A., 1996. Cyclopia and defective axial patterning in mice lacking Sonic hedgehog gene function. Nature 383, 407–413. https://doi.org/10.1038/383407a0

Ching, S.T., Infante, C.R., Du, W., Sharir, A., Park, S., Menke, D.B., Klein, O.D., 2018. Isl1 mediates mesenchymal expansion in the developing external genitalia via regulation of Bmp4, Fgf10 and Wnt5a. Hum. Mol. Genet. 27, 107–119. https://doi.org/10.1093/HMG/DDX388

Chiu, H.S., Szucsik, J.C., Georgas, K.M., Jones, J.L., Rumballe, B.A., Tang, D., Grimmond, S.M., Lewis, A.G., Aronow, B.J., Lessard, J.L., Little, M.H., 2010. Comparative gene expression analysis of genital tubercle development reveals a putative appendicular Wnt7 network for the epidermal differentiation. Dev. Biol. 344, 1071–1087. https://doi.org/10.1016/j.ydbio.2010.05.495

Chiu, W.T., Charney Le, R., Blitz, I.L., Fish, M.B., Li, Y., Biesinger, J., Xie, X., Cho, K.W.Y., 2014. Genome-wide view of TGFβ/Foxh1 regulation of the early mesendoderm program. Development 141, 4537–4547. https://doi.org/10.1242/dev.107227

Choi, K.-S., Lee, C., Maatouk, D.M., Harfe, B.D., 2012. Bmp2, Bmp4 and Bmp7 Are Co-Required in the Mouse AER for Normal Digit Patterning but Not Limb Outgrowth. PLoS ONE 7, e37826. https://doi.org/10.1371/journal.pone.0037826

Coda, D.M., Gaarenstroom, T., East, P., Patel, H., Miller, D.S.J., Lobley, A., Matthews, N., Stewart, A., Hill, C.S., 2017. Distinct modes of SMAD2 chromatin binding and remodeling shape the transcriptional response to NODAL/Activin signaling. eLife 6, 1–31. https://doi.org/10.7554/eLife.22474

Coda, D.M., Patel, H., Gori, I., Gaarenstroom, T.E., Song, O.-R., Howell, M., Hill, C.S., 2022. A network of transcription factors governs the dynamics of NODAL/Activin transcriptional responses. J. Cell Sci. 135, jcs259972. https://doi.org/10.1242/jcs.259972

Cohn, M.J., 2011. Development of the external genitalia: Conserved and divergent mechanisms of appendage patterning. Dev. Dyn. 240, 1108–1115. https://doi.org/10.1002/dvdy.22631

Cohn, M.J., Tickle, C., 1999. Developmental basis of limblessness and axial patterning in snakes. Nature 399, 474–479. https://doi.org/10.1038/20944

Crossley, P.H., Martin, G.R., 1995. The mouse *Fgf8* gene encodes a family of polypeptides and is expressed in regions that direct outgrowth and patterning in the developing embryo. Development 121, 439–451. https://doi.org/10.1242/dev.121.2.439

Cygan, J.A., Johnson, R.L., McMahon, A.P., 1997. Novel regulatory interactions revealed by studies of murine limb pattern in Wnt-7a and En-1 mutants. Development 124, 5021–5032. https://doi.org/10.1242/dev.124.24.5021

Daane, J.M., Downs, K.M., 2011. Hedgehog signaling in the posterior region of the mouse gastrula suggests manifold roles in the fetal-umbilical connection and posterior morphogenesis. Dev. Dyn. 240, 2175–2193. https://doi.org/10.1002/dvdy.22711

Dahle, Ø., Kumar, A., Kuehn, M.R., 2010. Nodal Signaling Recruits the Histone Demethylase Jmjd3 to Counteract Polycomb-Mediated Repression at Target Genes. Sci. Signal. 3. https://doi.org/10.1126/scisignal.2000841

David, C.J., Massagué, J., 2018. Contextual determinants of TGFβ action in development, immunity and cancer. Nat. Rev. Mol. Cell Biol. 19, 419–435. https://doi.org/10.1038/s41580-018-0007-0

Davis, C.A., Joyner, A.L., 1988. Expression patterns of the homeo box-containing genes En-1 and En-2 and the proto-oncogene int-1 diverge during mouse development. Genes Dev. 2, 1736–1744. https://doi.org/10.1101/gad.2.12b.1736

Deimling, S.J., Lau, K., Hui, C., Hopyan, S., 2018. Genetic interaction between Gli3 and Ezh2 during limb pattern formation. Mech. Dev. 151, 30–36. https://doi.org/10.1016/j.mod.2018.05.002

Delgado, I., Giovinazzo, G., Temiño, S., Gauthier, Y., Balsalobre, A., Drouin, J., Torres, M., 2021. Control of mouse limb initiation and antero-posterior patterning by Meis transcription factors. Nat. Commun. 12, 3086. https://doi.org/10.1038/s41467-021-23373-9

Delgado, I., López-Delgado, A.C., Roselló-Díez, A., Giovinazzo, G., Cadenas, V., Fernández-de-Manuel, L., Sánchez-Cabo, F., Anderson, M.J., Lewandoski, M., Torres, M., 2020. Proximo-distal positional information encoded by an Fgf-regulated gradient of homeodomain transcription factors in the vertebrate limb. Sci. Adv. 6, eaaz0742. https://doi.org/10.1126/sciadv.aaz0742

Derynck, R., Budi, E.H., 2019. Specificity, versatility, and control of TGF-β family signaling. Sci. Signal. 12, eaav5183. https://doi.org/10.1126/scisignal.aav5183

Deschamps, J., Duboule, D., 2017. Embryonic timing, axial stem cells, chromatin dynamics, and the Hox clock. Genes Dev. 31, 1406–1416. https://doi.org/10.1101/gad.303123.117

Dias, A., Lozovska, A., Wymeersch, F.J., Nóvoa, A., Binagui-Casas, A., Sobral, D., Martins, G.G., Wilson, V., Mallo, M., 2020. A Tgfbr1/Snai1-dependent developmental module at the core of vertebrate axial elongation. eLife 9, 1–28. https://doi.org/10.7554/eLife.56615

Dias, A., Martins, G.G., Lopes, A., Mallo, M., 2021. Three and Four-Dimensional Visualization and Analysis Approaches to Study Vertebrate Axial Elongation and Segmentation. J. Vis. Exp. 62086. https://doi.org/10.3791/62086

Divate, M., Cheung, E., 2018. GUAVA: A graphical user interface for the analysis and visualization of ATAC-seq data. Front. Genet. 9, 1–10. https://doi.org/10.3389/fgene.2018.00250

Dobreva, M.P., Pereira, P.N.G., Deprest, J., Zwijsen, A., 2010. On the origin of amniotic stem cells: of mice and men. Int. J. Dev. Biol. 54, 761–777. https://doi.org/10.1387/ijdb.092935md

Downs, K.M., Rodriguez, A.M., 2020. The mouse fetal-placental arterial connection: A paradigm involving the primitive streak and visceral endoderm with implications for human development. Wiley Interdiscip. Rev. Dev. Biol. 9. https://doi.org/10.1002/wdev.362

Duboc, V., Logan, M.P.O., 2011. Pitx1 is necessary for normal initiation of hindlimb outgrowth through regulation of Tbx4 expression and shapes hindlimb morphologies via targeted growth control. Development 138, 5301–5309. https://doi.org/10.1242/dev.074153

Dünker, N., Krieglstein, K., 2002. Tgfβ2-/-Tgfβ3-/- double knockout mice display severe midline fusion defects and early embryonic lethality. Anat. Embryol. (Berl.) 206, 73–83. https://doi.org/10.1007/s00429-002-0273-6

Echelard, Y., Epstein, D.J., St-Jacques, B., Shen, L., Mohler, J., McMahon, J.A., McMahon, A.P., 1993. Sonic hedgehog, a member of a family of putative signaling molecules, is implicated in the regulation of CNS polarity. Cell 75, 1417–1430. https://doi.org/10.1016/0092-8674(93)90627-3

Economides, K.D., Zeltser, L., Capecchi, M.R., 2003. Hoxb13 mutations cause overgrowth of caudal spinal cordand tail vertebrae. Dev. Biol. 256, 317–330. https://doi.org/10.1016/S0012-1606(02)00137-9

Eden, E., Navon, R., Steinfeld, I., Lipson, D., Yakhini, Z., 2009. GOrilla: a tool for discovery and visualization of enriched GO terms in ranked gene lists. BMC Bioinformatics 10, 48. https://doi.org/10.1186/1471-2105-10-48

El Shahawy, M., Reibring, C.-G., Hallberg, K., Neben, C.L., Marangoni, P., Harfe, B.D., Klein, O.D., Linde, A., Gritli-Linde, A., 2019. Sonic Hedgehog Signaling Is Required for Cyp26 Expression during Embryonic Development. Int. J. Mol. Sci. 20, 2275. https://doi.org/10.3390/ijms20092275

Fabre, P.J., Leleu, M., Mormann, B.H., Lopez-Delisle, L., Noordermeer, D., Beccari, L., Duboule, D., 2017. Large scale genomic reorganization of topological domains at the HoxD locus. Genome Biol. 18, 149. https://doi.org/10.1186/s13059-017-1278-z

Farin, H.F., Lüdtke, T.H.-W., Schmidt, M.K., Placzko, S., Schuster-Gossler, K., Petry, M., Christoffels, V.M., Kispert, A., 2013. Tbx2 Terminates Shh/Fgf Signaling in the Developing Mouse Limb Bud by Direct Repression of Gremlin1. PLoS Genet. 9, e1003467. https://doi.org/10.1371/journal.pgen.1003467

Fazilaty, H., Rago, L., Kass Youssef, K., Ocaña, O.H., Garcia-Asencio, F., Arcas, A., Galceran, J., Nieto, M.A., 2019. A gene regulatory network to control EMT programs in development and disease. Nat. Commun. 10, 5115. https://doi.org/10.1038/s41467-019-13091-8

Feenstra, J.M., Kanaya, K., Pira, C.U., Hoffman, S.E., Eppey, R.J., Oberg, K.C., 2012. Detection of genes regulated by Lmx1b during limb dorsalization: Lmx1b regulated genes in limb dorsalization. Dev. Growth Differ. 54, 451–462. https://doi.org/10.1111/j.1440-169X.2012.01331.x

Feng, J., Liu, T., Qin, B., Zhang, Y., Liu, X.S., 2012. Identifying ChIP-seq enrichment using MACS. Nat. Protoc. 7, 1728–1740. https://doi.org/10.1038/nprot.2012.101

Fernandez-Teran, M., Ros, M.A., Mariani, F.V., 2013. Evidence that the limb bud ectoderm is required for survival of the underlying mesoderm. Dev. Biol. 381, 341–352. https://doi.org/10.1016/j.ydbio.2013.06.032

Fromental-Ramain, C., Warot, X., Messadecq, N., LeMeur, M., Dolle, P., Chambon, P., 1996. Hoxa-13 and Hoxd-13 play a crucial role in the patterning of the limb autopod. Development 122, 2997–3011. https://doi.org/10.1242/dev.122.10.2997

Frum, T., Ralston, A., 2015. Cell signaling and transcription factors regulating cell fate during formation of the mouse blastocyst. Trends Genet. 31, 402–410. https://doi.org/10.1016/j.tig.2015.04.002

Funayama, N., Sato, Y., Matsumoto, K., Ogura, T., Takahashi, Y., 1999. Coelom formation: Binary decision of the lateral plate mesoderm is controlled by the ectoderm, Development.

Galli, A., Robay, D., Osterwalder, M., Bao, X., Bénazet, J.-D., Tariq, M., Paro, R., Mackem, S., Zeller, R., 2010. Distinct Roles of Hand2 in Initiating Polarity and Posterior Shh Expression during the Onset of Mouse Limb Bud Development. PLoS Genet. 6, e1000901. https://doi.org/10.1371/journal.pgen.1000901

Gamer, L.W., Cox, K.A., Small, C., Rosen, V., 2001. Gdf11 Is a Negative Regulator of Chondrogenesis and Myogenesis in the Developing Chick Limb. Dev. Biol. 229, 407–420. https://doi.org/10.1006/dbio.2000.9981

Gao, B., Ajima, R., Yang, W., Li, C., Song, H., Anderson, M.J., Liu, R.R., Lewandoski, M.B., Yamaguchi, T.P., Yang, Y., 2018. Coordinated directional outgrowth and pattern formation by integration of Wnt5a and Fgf signaling in planar cell polarity. Development dev.163824. https://doi.org/10.1242/dev.163824

Gaunt, S.J., George, M., Paul, Y.L., 2013. Direct activation of a mouse Hoxd11 axial expression enhancer by Gdf11/Smad signalling. Dev. Biol. 383, 52–60. https://doi.org/10.1016/j.ydbio.2013.08.025

Gouti, M., Delile, J., Stamataki, D., Wymeersch, F.J., Huang, Y., Kleinjung, J., Wilson, V., Briscoe, J., 2017. A Gene Regulatory Network Balances Neural and Mesoderm Specification during Vertebrate Trunk Development. Dev. Cell 41, 243-261.e7. https://doi.org/10.1016/j.devcel.2017.04.002

Gredler, M.L., Patterson, S.E., Seifert, A.W., Cohn, M.J., 2020. Foxa1 and Foxa2 orchestrate development of the urethral tube and division of the embryonic

cloaca through an autoregulatory loop with Shh. Dev. Biol. 465, 23–30. https://doi.org/10.1016/j.ydbio.2020.06.009

Gros, J., Hu, J.K.-H., Vinegoni, C., Feruglio, P.F., Weissleder, R., Tabin, C.J., 2010. WNT5A/JNK and FGF/MAPK Pathways Regulate the Cellular Events Shaping the Vertebrate Limb Bud. Curr. Biol. 20, 1993–2002. https://doi.org/10.1016/j.cub.2010.09.063

Gros, J., Tabin, C.J., 2014. Vertebrate limb bud formation is initiated by localized epithelial-to-mesenchymal transition. Science 343, 1253–1256. https://doi.org/10.1126/science.1248228

Gu, W.X.W., Kania, A., 2010. Identification of genes controlled by LMX1B in E13.5 mouse limbs. Dev. Dyn. 239, 2246–2255. https://doi.org/10.1002/dvdy.22357

Guerreiro, I., Gitto, S., Novoa, A., Codourey, J., Nguyen Huynh, T.H., Gonzalez, F., Milinkovitch, M.C., Mallo, M., Duboule, D., 2016. Reorganisation of Hoxd regulatory landscapes during the evolution of a snake-like body plan. eLife 5, e16087. https://doi.org/10.7554/eLife.16087

Guerrero-Martínez, J.A., Ceballos-Chávez, M., Koehler, F., Peiró, S., Reyes, J.C., 2020. TGFβ promotes widespread enhancer chromatin opening and operates on genomic regulatory domains. Nat. Commun. 11, 6196. https://doi.org/10.1038/s41467-020-19877-5

Guillot, C., Djeffal, Y., Michaut, A., Rabe, B., Pourquié, O., 2021. Dynamics of primitive streak regression controls the fate of neuromesodermal progenitors in the chicken embryo. eLife 10, e64819. https://doi.org/10.7554/eLife.64819

Guo, G., Huss, M., Tong, G.Q., Wang, C., Li Sun, L., Clarke, N.D., Robson, P., 2010. Resolution of Cell Fate Decisions Revealed by Single-Cell Gene Expression Analysis from Zygote to Blastocyst. Dev. Cell 18, 675–685. https://doi.org/10.1016/j.devcel.2010.02.012

Harada, M., Omori, A., Nakahara, C., Nakagata, N., Akita, K., Yamada, G., 2015. Tissue-specific roles of FGF signaling in external genitalia development: FGFRS AND EXTERNAL GENITALIA DEVELOPMENT. Dev. Dyn. 244, 759–773. https://doi.org/10.1002/dvdy.24277

Haraguchi, R., Motoyama, J., Sasaki, H., Satoh, Y., Miyagawa, S., Nakagata, N., Moon, A., Yamada, G., 2007. Molecular analysis of coordinated bladder and urogenital organ formation by Hedgehog signaling. Dev. Camb. Engl. 134, 525–33. https://doi.org/10.1242/dev.02736

Haraguchi, R., Suzuki, K., Murakami, R., Sakai, M., Kamikawa, M., Kengaku, M., Sekine, K., Kawano, H., Kato, S., Ueno, N., Yamada, G., 2000. Molecular analysis of external genitalia formation: the role of fibroblast growth factor (Fgf) genes during genital tubercle formation. Development 127, 2471–2479. https://doi.org/10.1242/dev.127.11.2471

Haro, E., Delgado, I., Junco, M., Yamada, Y., Mansouri, A., Oberg, K.C., Ros, M.A., 2014. Sp6 and Sp8 Transcription Factors Control AER Formation and Dorsal-

Ventral Patterning in Limb Development. PLoS Genet. 10. https://doi.org/10.1371/journal.pgen.1004468

Haro, E., Watson, B.A., Feenstra, J.M., Tegeler, L., Pira, C.U., Mohan, S., Oberg, K.C., 2017. Lmx1b-targeted *cis* -regulatory modules involved in limb dorsalization. Development dev.146332. https://doi.org/10.1242/dev.146332

Hassan, A.S., Hou, J., Wei, W., Hoodless, P.A., 2010. Expression of two novel transcripts in the mouse definitive endoderm. Gene Expr. Patterns 10, 127–134. https://doi.org/10.1016/j.gep.2010.02.001

Hayashi, S., Suzuki, H., Takemoto, T., 2021. The nephric mesenchyme lineage of intermediate mesoderm is derived from Tbx6-expressing derivatives of neuro-mesodermal progenitors via BMP-dependent Osr1 function. Dev. Biol. 478, 155–162. https://doi.org/10.1016/j.ydbio.2021.07.006

Heldin, C.-H., Moustakas, A., 2016. Signaling Receptors for TGF-β Family Members. Cold Spring Harb. Perspect. Biol. 8, a022053. https://doi.org/10.1101/cshperspect.a022053

Herrera, A.M., Cohn, M.J., 2014. Embryonic origin and compartmental organization of the external genitalia. Sci. Rep. 4, 6896. https://doi.org/10.1038/srep06896

Hill, C.S., 2018. Spatial and temporal control of NODAL signaling. Curr. Opin. Cell Biol. 51, 50–57. https://doi.org/10.1016/j.ceb.2017.10.005

Hinck, A.P., Mueller, T.D., Springer, T.A., 2016. Structural Biology and Evolution of the TGF-β Family. Cold Spring Harb. Perspect. Biol. 8, a022103. https://doi.org/10.1101/cshperspect.a022103

Ho, D.M., Yeo, C.Y., Whitman, M., 2010. The role and regulation of GDF11 in Smad2 activation during tailbud formation in the Xenopus embryo. Mech. Dev. 127, 485–495. https://doi.org/10.1016/j.mod.2010.08.004

Hoodless, P.A., Pye, M., Chazaud, C., Labbé, E., Attisano, L., Rossant, J., Wrana, J.L., 2001. *FoxH1* (*Fast*) functions to specify the anterior primitive streak in the mouse. Genes Dev. 15, 1257–1271. https://doi.org/10.1101/gad.881501

Huang, Y.C., Chen, F., Li, X., 2016. Clarification of mammalian cloacal morphogenesis using high-resolution episcopic microscopy. Dev. Biol. 409, 106–113. https://doi.org/10.1016/j.ydbio.2015.10.018

Huelsken, J., Vogel, R., Brinkmann, V., Erdmann, B., Birchmeier, C., Birchmeier, W., 2000. Requirement for ␣L-Catenin in Anterior-Posterior Axis Formation in Mice. J. Cell Biol. 148.

Hui, C., Joyner, A.L., 1993. A mouse model of Greig cephalo–polysyndactyly syndrome: the extra–toesJ mutation contains an intragenic deletion of the Gli3 gene. Nat. Genet. 3, 241–246. https://doi.org/10.1038/ng0393-241

Infante, C.R., Mihala, A.G., Park, S., Wang, J.S., Johnson, K.K., Lauderdale, J.D., Menke, D.B., 2015. Shared Enhancer Activity in the Limbs and Phallus and Functional Divergence of a Limb-Genital cis-Regulatory Element in Snakes. Dev. Cell 35, 107–119. https://doi.org/10.1016/j.devcel.2015.09.003

Inman, K.E., Downs, K.M., 2007. The murine allantois: emerging paradigms in development of the mammalian umbilical cord and its relation to the fetus. genesis 45, 237–258. https://doi.org/10.1002/dvg.20281

Itou, J., Kawakami, H., Quach, T., Osterwalder, M., Evans, S.M., Zeller, R., Kawakami, Y., 2012. Islet1 regulates establishment of the posterior hindlimb field upstream of the Hand2-Shh morphoregulatory gene network in mouse embryos. Dev. Camb. Engl. 139, 1620–1629. https://doi.org/10.1242/DEV.073056

Janknecht, R., Wells, N.J., Hunter, T., 1998. TGF-β-stimulated cooperation of Smad proteins with the coactivators CBP/p300. Genes Dev. 12, 2114–2119. https://doi.org/10.1101/gad.12.14.2114

Javed, A., Bae, J.-S., Afzal, F., Gutierrez, S., Pratap, J., Zaidi, S.K., Lou, Y., van Wijnen, A.J., Stein, J.L., Stein, G.S., Lian, J.B., 2008. Structural Coupling of Smad and Runx2 for Execution of the BMP2 Osteogenic Signal. J. Biol. Chem. 283, 8412–8422. https://doi.org/10.1074/jbc.M705578200

Jinek, M., Chylinski, K., Fonfara, I., Hauer, M., Doudna, J.A., Charpentier, E., 2012. A Programmable Dual-RNA–Guided DNA Endonuclease in Adaptive Bacterial Immunity. Science 337, 816–821. https://doi.org/10.1126/science.1225829

Johnson, M.H., Ziomek, C.A., 1981. Induction of polarity in mouse 8-cell blastomeres: Specificity, geometry, and stability. J. Cell Biol. 91, 303–308. https://doi.org/10.1083/jcb.91.1.303

Jones, C.M., Lyons, K.M., Hogan, B.L.M., 1991. Involvement of *Bone Morphogenetic Protein-4* (BMP-4) and *Vgr-1* in morphogenesis and neurogenesis in the mouse. Development 111, 531–542. https://doi.org/10.1242/dev.111.2.531

Jurberg, A.D., Aires, R., Varela-Lasheras, I., Nóvoa, A., Mallo, M., 2013. Switching axial progenitors from producing trunk to tail tissues in vertebrate embryos. Dev. Cell 25, 451–462. https://doi.org/10.1016/j.devcel.2013.05.009

Kajioka, D., Suzuki, K., Nakada, S., Matsushita, S., Miyagawa, S., Takeo, T., Nakagata, N., Yamada, G., 2019. Bmp4 is an essential growth factor for the initiation of genital tubercle (GT) outgrowth. Congenit. Anom. 60, 15–21. https://doi.org/10.1111/cga.12326

Kaku, Y., Ohmori, T., Kudo, K., Fujimura, S., Suzuki, K., Evans, S.M., Kawakami, Y., Nishinakamura, R., 2013. *Islet1* Deletion Causes Kidney Agenesis and Hydroureter Resembling CAKUT. J. Am. Soc. Nephrol. 24, 1242–1249. https://doi.org/10.1681/ASN.2012050528

Kang, J., Nathan, E., Xu, S.M., Tzahor, E., Black, B.L., 2009. Isl1 is a direct transcriptional target of Forkhead transcription factors in second heart field-derived mesoderm. Dev. Biol. 334, 513–522. https://doi.org/10.1016/j.ydbio.2009.06.041

Kawakami, Y., Capdevila, J., Büscher, D., Itoh, T., Esteban, C.R., Belmonte, J.C.I., 2001. WNT Signals Control FGF-Dependent Limb Initiation and AER

Induction in the Chick Embryo. Cell 104, 891–900. https://doi.org/10.1016/S0092-8674(01)00285-9

Kawakami, Y., Esteban, C.R., Matsui, T., Rodríguez-León, J., Kato, S., Belmonte, J.C.I., 2004. *Sp8* and *Sp9* , two closely related *buttonhead* -like transcription factors, regulate *Fgf8* expression and limb outgrowth in vertebrate embryos. Development 131, 4763–4774. https://doi.org/10.1242/dev.01331

Kawakami, Y., Marti, M., Kawakami, H., Itou, J., Quach, T., Johnson, A., Sahara, S., O'Leary, D.D.M., Nakagawa, Y., Lewandoski, M., Pfaff, S., Evans, S.M., Belmonte, J.C.I., 2011. Islet1-mediated activation of the β-catenin pathway is necessary for hindlimb initiation in mice. Development 138, 4465–4473. https://doi.org/10.1242/dev.065359

Kengaku, M., Capdevila, J., Rodriguez-Esteban, C., De La Peña, J., Johnson, R.L., Belmonte, J.C.I., Tabin, C.J., 1998. Distinct WNT Pathways Regulating AER Formation and Dorsoventral Polarity in the Chick Limb Bud. Science 280, 1274–1277. https://doi.org/10.1126/science.280.5367.1274

Khokha, M.K., Hsu, D., Brunet, L.J., Dionne, M.S., Harland, R.M., 2003. Gremlin is the BMP antagonist required for maintenance of Shh and Fgf signals during limb patterning. Nat. Genet. 34, 303–307. https://doi.org/10.1038/ng1178

Kim, Y.S., Bedzhov, I., 2022. Mechanisms of formation and functions of the early embryonic cavities. Semin. Cell Dev. Biol. 131, 110–116. https://doi.org/10.1016/j.semcdb.2022.04.020

Kmita, M., Tarchini, B., Zàkàny, J., Logan, M., Tabin, C.J., Duboule, D., 2005. Early developmental arrest of mammalian limbs lacking HoxA/HoxD gene function. Nature 435, 1113–1116. https://doi.org/10.1038/nature03648

Kondo, T., Zákány, J., Innis, J.W., Duboule, D., 1997. Of fingers, toes and penises. Nature 390, 29–29. https://doi.org/10.1038/36234

Koyama, E., Yasuda, T., Minugh-Purvis, N., Kinumatsu, T., Yallowitz, A.R., Wellik, D.M., Pacifici, M., 2010. *Hox11* genes establish synovial joint organization and phylogenetic characteristics in developing mouse zeugopod skeletal elements. Development 137, 3795–3800. https://doi.org/10.1242/dev.053447

Koyano-Nakagawa, N., Gong, W., Das, S., Theisen, J.W.M., Swanholm, T.B., Van Ly, D., Dsouza, N., Singh, B.N., Kawakami, H., Young, S., Chen, K.Q., Kawakami, Y., Garry, D.J., 2022. Etv2 regulates enhancer chromatin status to initiate Shh expression in the limb bud. Nat. Commun. 13, 4221. https://doi.org/10.1038/s41467-022-31848-6

Kuijper, S., Feitsma, H., Sheth, R., Korving, J., Reijnen, M., Meijlink, F., 2005. Function and regulation of Alx4 in limb development: Complex genetic interactions with Gli3 and Shh. Dev. Biol. 285, 533–544. https://doi.org/10.1016/j.ydbio.2005.06.017

Kulakovskiy, I.V., Vorontsov, I.E., Yevshin, I.S., Sharipov, R.N., Fedorova, A.D., Rumynskiy, E.I., Medvedeva, Y.A., Magana-Mora, A., Bajic, V.B., Papatsenko,

D.A., Kolpakov, F.A., Makeev, V.J., 2018. HOCOMOCO: towards a complete collection of transcription factor binding models for human and mouse via large-scale ChIP-Seq analysis. Nucleic Acids Res. 46, D252–D259. https://doi.org/10.1093/nar/gkx1106

Kumar, A., Lualdi, M., Lyozin, G.T., Sharma, P., Loncarek, J., Fu, X.-Y., Kuehn, M.R., 2015. Nodal signaling from the visceral endoderm is required to maintain Nodal gene expression in the epiblast and drive DVE/AVE migration. Dev. Biol. 400, 1–9. https://doi.org/10.1016/j.ydbio.2014.12.016

Kvon, E.Z., Kamneva, O.K., Melo, U.S., Barozzi, I., Osterwalder, M., Mannion, B.J., Tissières, V., Pickle, C.S., Plajzer-Frick, I., Lee, E.A., Kato, M., Garvin, T.H., Akiyama, J.A., Afzal, V., Lopez-Rios, J., Rubin, E.M., Dickel, D.E., Pennacchio, L.A., Visel, A., 2016. Progressive Loss of Function in a Limb Enhancer during Snake Evolution. Cell 167, 633-642.e11. https://doi.org/10.1016/j.cell.2016.09.028

Kwon, G.S., Viotti, M., Hadjantonakis, A.-K., 2008. The Endoderm of the Mouse Embryo Arises by Dynamic Widespread Intercalation of Embryonic and Extraembryonic Lineages. Dev. Cell 15, 509–520. https://doi.org/10.1016/j.devcel.2008.07.017

Langmead, B., Salzberg, S.L., 2012. Fast gapped-read alignment with Bowtie 2. Nat. Methods 9, 357–359. https://doi.org/10.1038/nmeth.1923

Larsson, J., 2022. eulerr: Area-Proportional Euler and Venn Diagrams with Ellipses. R package version 7.0.0, https://CRAN.R-project.org/package=eulerr.

Larsson, J., Goumans, M.J., Sjöstrand, L.J., Van Rooijen, M.A., Ward, D., Levéen, P., Xu, X., Ten Dijke, P., Mummery, C.L., Karlsson, S., 2001. Abnormal angiogenesis but intact hematopoietic potential in TGF-β type I receptor-deficient mice. EMBO J. 20, 1663–1673. https://doi.org/10.1093/emboj/20.7.1663

Leal, F., Cohn, M.J., 2016. Loss and Re-emergence of Legs in Snakes by Modular Evolution of Sonic hedgehog and HOXD Enhancers. Curr. Biol. 26, 2966–2973. https://doi.org/10.1016/j.cub.2016.09.020

Lee, Y.J., McPherron, A., Choe, S., Sakai, Y., Chandraratna, R.A., Lee, S.J., Oh, S.P., 2010. Growth differentiation factor 11 signaling controls retinoic acid activity for axial vertebral development. Dev. Biol. 347, 195–203. https://doi.org/10.1016/j.ydbio.2010.08.022

Lettice, L.A., 2003. A long-range Shh enhancer regulates expression in the developing limb and fin and is associated with preaxial polydactyly. Hum. Mol. Genet. 12, 1725–1735. https://doi.org/10.1093/hmg/ddg180

Lewandoski, M., Sun, X., Martin, G.R., 2000. Fgf8 signalling from the AER is essential for normal limb development. Nat. Genet. 26, 460–463. https://doi.org/10.1038/82609

Lex, R.K., Ji, Z., Falkenstein, K.N., Zhou, W., Henry, J.L., Ji, H., Vokes, S.A., 2020. GLI transcriptional repression regulates tissue-specific enhancer activity in

response to Hedgehog signaling. eLife 9, e50670. https://doi.org/10.7554/eLife.50670

Lex, R.K., Zhou, W., Ji, Z., Falkenstein, K.N., Schuler, K.E., Windsor, K.E., Kim, J.D., Ji, H., Vokes, S.A., 2022. GLI transcriptional repression is inert prior to Hedgehog pathway activation. Nat. Commun. 13, 808. https://doi.org/10.1038/s41467-022-28485-4

Li, D., Sakuma, R., Vakili, N.A., Mo, R., Puviindran, V., Deimling, S., Zhang, X., Hopyan, S., Hui, C., 2014. Formation of Proximal and Anterior Limb Skeleton Requires Early Function of Irx3 and Irx5 and Is Negatively Regulated by Shh Signaling. Dev. Cell 29, 233–240. https://doi.org/10.1016/j.devcel.2014.03.001

Li, Q., Lewandowski, J.P., Powell, M.B., Norrie, J.L., Cho, S.H., Vokes, S.A., 2014. A Gli silencer is required for robust repression of gremlin in the vertebrate limb bud. Development 141, 1906–1914. https://doi.org/10.1242/dev.104299

Li, Z., Schulz, M.H., Look, T., Begemann, M., Zenke, M., Costa, I.G., 2019. Identification of transcription factor binding sites using ATAC-seq. Genome Biol. 20, 45. https://doi.org/10.1186/s13059-019-1642-2

Liao, Y., Smyth, G.K., Shi, W., 2014. featureCounts: an efficient general purpose program for assigning sequence reads to genomic features. Bioinformatics 30, 923–930. https://doi.org/10.1093/bioinformatics/btt656

Lin, C., Yin, Y., Bell, S.M., Veith, G.M., Chen, H., Huh, S.H., Ornitz, D.M., Ma, L., 2013. Delineating a Conserved Genetic Cassette Promoting Outgrowth of Body Appendages. PLoS Genet. 9, 1–12. https://doi.org/10.1371/journal.pgen.1003231

Lin, C., Yin, Y., Long, F., Ma, L., 2008. Tissue-specific requirements of β-catenin in external genitalia development. Development 135, 2815–2825. https://doi.org/10.1242/dev.020586

Lin, C., Yin, Y., Veith, G.M., Fisher, A.V., Long, F., Ma, L., 2009. Temporal and spatial dissection of Shh signaling in genital tubercle development. Development 136, 3959–3967. https://doi.org/10.1242/dev.039768

Lin, Y.-T., Wu, K.-J., 2020. Epigenetic regulation of epithelial-mesenchymal transition: focusing on hypoxia and TGF-β signaling. J. Biomed. Sci. 27, 39. https://doi.org/10.1186/s12929-020-00632-3

Litingtung, Y., Li, Y., Fallon, J.F., Chiang, C., 2002. Shh and Gli3 are dispensable for limb skeleton formation but regulate digit number and identity. Nature 418, 979–983. https://doi.org/10.1038/nature01033

Liu, J.-P., 2006. The function of growth/differentiation factor 11 (Gdf11) in rostrocaudal patterning of the developing spinal cord. Development 133, 2865–2874. https://doi.org/10.1242/dev.02478

Liu, L., Suzuki, K., Nakagata, N., Mihara, K., Matsumaru, D., Ogino, Y., Yashiro, K., Hamada, H., Liu, Z., Evans, S.M., Mendelsohn, C., Yamada, G., 2011. Retinoic acid signaling regulates Sonic hedgehog and bone morphogenetic protein signalings during genital tubercle development. Birth Defects Res. B. Dev. Reprod. Toxicol. n/a-n/a. https://doi.org/10.1002/bdrb.20344

Liu, P., Wakamiya, M., Shea, M.J., Albrecht, U., Behringer, R.R., Bradley, A., 1999. Requirement for Wnt3 in vertebrate axis formation. Nat. Genet. 22, 361–365. https://doi.org/10.1038/11932

Logan, M., Simon, H.-G., Tabin, C., 1998. Differential regulation of T-box and homeobox transcription factors suggests roles in controlling chick limb-type identity. Development 125, 2825–2835. https://doi.org/10.1242/dev.125.15.2825

Lopez-Rios, J., Speziale, D., Robay, D., Scotti, M., Osterwalder, M., Nusspaumer, G., Galli, A., Holländer, G.A., Kmita, M., Zeller, R., 2012. GLI3 Constrains Digit Number by Controlling Both Progenitor Proliferation and BMP-Dependent Exit to Chondrogenesis. Dev. Cell 22, 837–848. https://doi.org/10.1016/j.devcel.2012.01.006

Love, M.I., Huber, W., Anders, S., 2014. Moderated estimation of fold change and dispersion for RNA-seq data with DESeq2. Genome Biol. 15, 550. https://doi.org/10.1186/s13059-014-0550-8

Lu, P., Minowada, G., Martin, G.R., 2005. Increasing *Fgf4* expression in the mouse limb bud causes polysyndactyly and rescues the skeletal defects that result from loss of *Fgf8* function. Development 133, 33–42. https://doi.org/10.1242/dev.02172

Lu, P., Yu, Y., Perdue, Y., Werb, Z., 2008. The apical ectodermal ridge is a timer for generating distal limb progenitors. Development 135, 1395–1405. https://doi.org/10.1242/dev.018945

Mahlapuu, M., Ormestad, M., Enerback, S., Carlsson, P., 2001. The forkhead transcription factor Foxf1 is required for differentiation of extra-embryonic and lateral plate mesoderm. Dev. Camb. Engl. 128, 155–166.

Mahmood, R., Bresnick, J., Hornbruch, A., Mahony, C., Morton, N., Colquhoun, K., Martin, P., Lumsden, A., Dickson, C., Mason, I., 1995. A role for FGF-8 in the initiation and maintenance of vertebrate limb bud outgrowth. Curr. Biol. 5, 797–806. https://doi.org/10.1016/S0960-9822(95)00157-6

Maître, J.L., Niwayama, R., Turlier, H., Nedelec, F., Hiiragi, T., 2015. Pulsatile cell-autonomous contractility drives compaction in the mouse embryo. Nat. Cell Biol. 17, 849–855. https://doi.org/10.1038/ncb3185

Malkmus, J., Ramos Martins, L., Jhanwar, S., Kircher, B., Palacio, V., Sheth, R., Leal, F., Duchesne, A., Lopez-Rios, J., Peterson, K.A., Reinhardt, R., Onimaru, K., Cohn, M.J., Zuniga, A., Zeller, R., 2021. Spatial regulation by multiple Gremlin1 enhancers provides digit development with cis-regulatory robustness and evolutionary plasticity. Nat. Commun. 12, 5557. https://doi.org/10.1038/s41467-021-25810-1

Marcil, A., Dumontier, É., Chamberland, M., Camper, S.A., Drouin, J., 2003. *Pitx1* and *Pitx2* are required for development of hindlimb buds. Development 130, 45–55. https://doi.org/10.1242/dev.00192

Mariani, F.V., Ahn, C.P., Martin, G.R., 2008. Genetic evidence that FGFs have an instructive role in limb proximal–distal patterning. Nature 453, 401–405. https://doi.org/10.1038/nature06876

Martin, M., 2011. Cutadapt removes adapter sequences from high-throughput sequencing reads. EMBnet.journal 17, 10. https://doi.org/10.14806/ej.17.1.200

Martinez-Hackert, E., Sundan, A., Holien, T., 2021. Receptor binding competition: A paradigm for regulating TGF-β family action. Cytokine Growth Factor Rev. 57, 39–54. https://doi.org/10.1016/j.cytogfr.2020.09.003

Martins, G.G., Lopes, A., Pereira, H., Martins, N.P., Munck, S., Swoger, J., 2021. Optical projection tomography, in: Imaging Modalities for Biological and Preclinical Research: A Compendium, Volume 1. IOP Publishing, p. I.2.f-1. https://doi.org/10.1088/978-0-7503-3059-6ch12

Maska, E.L., Cserjesi, P., Hua, L.L., Garstka, M.E., Brody, H.M., Morikawa, Y., 2010. A Tlx2-Cre mouse line uncovers essential roles for hand1 in extraembryonic and lateral mesoderm. genesis 48, 479–484. https://doi.org/10.1002/dvg.20644

Massagué, J., 2012. TGFβ signalling in context. Nat. Rev. Mol. Cell Biol. 13, 616–30. https://doi.org/10.1038/nrm3434

Masuya, H., Sagai, T., Wakana, S., Moriwaki, K., Shiroishi, T., 1995. A duplicated zone of polarizing activity in polydactylous mouse mutants. Genes Dev. 9, 1645–1653. https://doi.org/10.1101/gad.9.13.1645

Matsubara, Y., Hirasawa, T., Egawa, S., Hattori, A., Suganuma, T., Kohara, Y., Nagai, T., Tamura, K., Kuratani, S., Kuroiwa, A., Suzuki, T., 2017. Anatomical integration of the sacral-hindlimb unit coordinated by GDF11 underlies variation in hindlimb positioning in tetrapods. Nat. Ecol. Evol. 1, 1392–1399. https://doi.org/10.1038/s41559-017-0247-y

Matsumaru, D., Murashima, A., Fukushima, J., Senda, S., Matsushita, S., Nakagata, N., Miyajima, M., Yamada, G., 2015. Systematic stereoscopic analyses for cloacal development: The origin of anorectal malformations. Sci. Rep. 5, 13943. https://doi.org/10.1038/srep13943

McPherron, A.C., Huynh, T.V., Lee, S.J., 2009. Redundancy of myostatin and growth/differentiation factor 11 function. BMC Dev. Biol. 9, 1–9. https://doi.org/10.1186/1471-213X-9-24

Mcpherron, A.C., Lawler, A.M., Lee, S., 1999. Regulation of anterior / posterior patterning of the axial skeleton by growth / differentiation factor 11. Nature 22, 1–5.

McQueen, C., Towers, M., 2020. Establishing the pattern of the vertebrate limb. Development 147, dev177956. https://doi.org/10.1242/dev.177956

Mercader, N., Leonardo, E., Azpiazu, N., Serrano, A., Morata, G., Martínez-A, C., Torres, M., 1999. Conserved regulation of proximodistal limb axis development by Meis1/Hth. Nature 402, 425–429. https://doi.org/10.1038/46580

Mercader, N., Selleri, L., Criado, L.M., Pallares, P., Parras, C., Cleary, M.L., Torres, M., 2009. Ectopic Meis1 expression in the mouse limb bud alters P-D patterning in a Pbx1-independent manner. Int. J. Dev. Biol. 53, 1483–1494. https://doi.org/10.1387/ijdb.072430nm

Mesnard, D., Guzman-Ayala, M., Constam, D.B., 2006. Nodal specifies embryonic visceral endoderm and sustains pluripotent cells in the epiblast before overt axial patterning. Development 133, 2497–2505. https://doi.org/10.1242/dev.02413

Minguillon, C., Del Buono, J., Logan, M.P., 2005. Tbx5 and Tbx4 Are Not Sufficient to Determine Limb-Specific Morphologies but Have Common Roles in Initiating Limb Outgrowth. Dev. Cell 8, 75–84. https://doi.org/10.1016/j.devcel.2004.11.013

Miyagawa, S., Harada, M., Matsumaru, D., Tanaka, K., Inoue, C., Nakahara, C., Haraguchi, R., Matsushita, S., Suzuki, K., Nakagata, N., Ng, R.C.-L., Akita, K., Lui, V.C.-H., Yamada, G., 2014. Disruption of the temporally regulated cloaca endodermal β-catenin signaling causes anorectal malformations. Cell Death Differ. 21, 990–997. https://doi.org/10.1038/cdd.2014.21

Miyagawa, S., Moon, A., Haraguchi, R., Inoue, C., Harada, M., Nakahara, C., Suzuki, K., Matsumaru, D., Kaneko, T., Matsuo, I., Yang, L., Taketo, M.M., Iguchi, T., Evans, S.M., Yamada, G., 2009. Dosage-dependent hedgehog signals integrated with Wnt/β-catenin signaling regulate external genitalia formation as an appendicular program. Development 136, 3969–3978. https://doi.org/10.1242/dev.039438

Moon, A.M., Boulet, A.M., Capecchi, M.R., 2000. Normal limb development in conditional mutants of *Fgf4*. Development 127, 989–996. https://doi.org/10.1242/dev.127.5.989

Moustakas, A., Heldin, C.H., 2009. The regulation of TGFβ signal transduction. Development 136, 3699–3714. https://doi.org/10.1242/dev.030338

Mullen, A.C., Orlando, D.A., Newman, J.J., Lovén, J., Kumar, R.M., Bilodeau, S., Reddy, J., Guenther, M.G., Dekoter, R.P., Young, R.A., 2011. Master transcription factors determine cell-type-specific responses to TGF-β signaling. Cell 147, 565–576. https://doi.org/10.1016/j.cell.2011.08.050

Naiche, L.A., Papaioannou, V.E., 2003. Loss of Tbx4 blocks hindlimb development and affects vascularization and fusion of the allantois. Development 130, 2681–2693. https://doi.org/10.1242/dev.00504

Nakashima, M., Toyono, T., Akamine, A., Joyner, A., 1999. Expression of growth/differentiation factor 11, a new member of the BMP/TGFβ superfamily during mouse embryogenesis. Mech. Dev. 80, 185–189. https://doi.org/10.1016/S0925-4773(98)00205-6

Nelson, C.E., Morgan, B.A., Burke, A.C., Laufer, E., DiMambro, E., Murtaugh, L.C., Gonzales, E., Tessarollo, L., Parada, L.F., Tabin, C., 1996. Analysis of Hox gene expression in the chick limb bud. Development 122, 1449–1466. https://doi.org/10.1242/dev.122.5.1449

Nelson, L.T., Rakshit, S., Sun, H., Wellik, D.M., 2008. Generation and expression of a *Hoxa11eGFP* targeted allele in mice. Dev. Dyn. 237, 3410–3416. https://doi.org/10.1002/dvdy.21756

Newton, A.H., Williams, S.M., Major, A.T., Smith, C.A., 2022. Cell lineage specification and signalling pathway use during development of the lateral plate mesoderm and forelimb mesenchyme. Development 149, dev200702. https://doi.org/10.1242/dev.200702

Ng, R.C.-L., Matsumaru, D., Ho, A.S.-H., Garcia-Barceló, M.-M., Yuan, Z.-W., Smith, D., Kodjabachian, L., Tam, P.K.-H., Yamada, G., Lui, V.C.-H., 2014. Dysregulation of Wnt inhibitory factor 1 (Wif1) expression resulted in aberrant Wnt-β-catenin signaling and cell death of the cloaca endoderm, and anorectal malformations. Cell Death Differ. 21, 978–989. https://doi.org/10.1038/cdd.2014.20

Nishimoto, S., Logan, M.P.O., 2016. Subdivision of the lateral plate mesoderm and specification of the forelimb and hindlimb forming domains. Semin. Cell Dev. Biol. 49, 102–108. https://doi.org/10.1016/j.semcdb.2015.11.011

Nissim, S., Hasso, S.M., Fallon, J.F., Tabin, C.J., 2006. Regulation of Gremlin expression in the posterior limb bud. Dev. Biol. 299, 12–21. https://doi.org/10.1016/j.ydbio.2006.05.026

Niswander, L., Jeffrey, S., Martin, G.R., Tickle, C., 1994. A positive feedback loop coordinates growth and patterning in the vertebrate limb. Nature 371, 609–612. https://doi.org/10.1038/371609a0

Norrie, J.L., Lewandowski, J.P., Bouldin, C.M., Amarnath, S., Li, Q., Vokes, M.S., Ehrlich, L.I.R., Harfe, B.D., Vokes, S.A., 2014. Dynamics of BMP signaling in limb bud mesenchyme and polydactyly. Dev. Biol. 393, 270–281. https://doi.org/10.1016/j.ydbio.2014.07.003

Nowotschin, S., Setty, M., Kuo, Y.Y., Liu, V., Garg, V., Sharma, R., Simon, C.S., Saiz, N., Gardner, R., Boutet, S.C., Church, D.M., Hoodless, P.A., Hadjantonakis, A.K., Pe'er, D., 2019. The emergent landscape of the mouse gut endoderm at single-cell resolution. Nature 569, 361–367. https://doi.org/10.1038/s41586-019-1127-1

Oh, S.P., Li, E., 1997. The signaling pathway mediated by the type IIB activin receptor controls axial patterning and lateral asymmetry in the mouse. Genes Dev. 11, 1812–1826. https://doi.org/10.1101/gad.11.14.1812

Oishi, I., Suzuki, H., Onishi, N., Takada, R., Kani, S., Ohkawara, B., Koshida, I., Suzuki, K., Yamada, G., Schwabe, G.C., Mundlos, S., Shibuya, H., Takada, S., Minami, Y., 2003. The receptor tyrosine kinase Ror2 is involved in non-canonical Wnt5a/JNK signalling pathway: Role of Ror2 in Wnt5a signalling pathway. Genes Cells 8, 645–654. https://doi.org/10.1046/j.1365-2443.2003.00662.x

Olivera-Martinez, I., Harada, H., Halley, P.A., Storey, K.G., 2012. Loss of FGF-Dependent Mesoderm Identity and Rise of Endogenous Retinoid Signalling Determine Cessation of Body Axis Elongation. PLoS Biol. 10. https://doi.org/10.1371/journal.pbio.1001415

Osterwalder, M., Speziale, D., Shoukry, M., Mohan, R., Ivanek, R., Kohler, M., Beisel, C., Wen, X., Scales, S.J., Christoffels, V.M., Visel, A., Lopez-Rios, J., Zeller, R., 2014. HAND2 targets define a network of transcriptional regulators that compartmentalize the early limb bud mesenchyme. Dev. Cell 31, 345–357. https://doi.org/10.1016/j.devcel.2014.09.018

Ovchinnikov, D.A., Selever, J., Wang, Y., Chen, Y.-T., Mishina, Y., Martin, J.F., Behringer, R.R., 2006. BMP receptor type IA in limb bud mesenchyme regulates distal outgrowth and patterning. Dev. Biol. 295, 103–115. https://doi.org/10.1016/j.ydbio.2006.03.013

Pajni-Underwood, S., Wilson, C.P., Elder, C., Mishina, Y., Lewandoski, M., 2007. BMP signals control limb bud interdigital programmed cell death by regulating FGF signaling. Development 134, 2359–2368. https://doi.org/10.1242/dev.001677

Panman, L., Galli, A., Lagarde, N., Michos, O., Soete, G., Zuniga, A., Zeller, R., 2006. Differential regulation of gene expression in the digit forming area of the mouse limb bud by SHH and gremlin 1/FGF-mediated epithelial-mesenchymal signalling. Development 133, 3419–3428. https://doi.org/10.1242/dev.02529

Park, H.L., Bai, C., Platt, K.A., Matise, M.P., Beeghly, A., Hui, C.C., Nakashima, M., Joyner, A.L., 2000. Mouse Gli1 mutants are viable but have defects in SHH signaling in combination with a Gli2 mutation. Development 127, 1593–1605. https://doi.org/10.1242/dev.127.8.1593

Paul Oh, S., Yeo, C.Y., Lee, Y., Schrewe, H., Whitman, M., Li, E., 2002. Activin type IIA and IIB receptors mediate Gdf11 signaling in axial vertebral patterning. Genes Dev. 16, 2749–2754. https://doi.org/10.1101/gad.1021802

Peng, G., Suo, S., Cui, G., Yu, F., Wang, R., Chen, J., Chen, S., Liu, Z., Chen, G., Qian, Y., Tam, P.P.L., Han, J.-D.J., Jing, N., 2019. Molecular architecture of lineage allocation and tissue organization in early mouse embryo. Nature 572, 528–532. https://doi.org/10.1038/s41586-019-1469-8

Penington, E.C., Hutson, J.M., 2002. The urethral plate - Does it grow into the genital tubercle or within it? BJU Int. 89, 733–739. https://doi.org/10.1046/j.1464-410X.2002.02656.x

Pérez-Gómez, R., Haro, E., Fernández-Guerrero, M., Bastida, M.F., Ros, M.A., 2018. Role of Hox genes in regulating digit patterning. Int. J. Dev. Biol. 62, 797–805. https://doi.org/10.1387/ijdb.180200mr

Perriton, C.L., Powles, N., Chiang, C., Maconochie, M.K., Cohn, M.J., 2002. Sonic hedgehog Signaling from the Urethral Epithelium Controls External Genital Development. Dev. Biol. 247, 26–46. https://doi.org/10.1006/dbio.2002.0668

Pollard, K.S., Hubisz, M.J., Rosenbloom, K.R., Siepel, A., 2010. Detection of nonneutral substitution rates on mammalian phylogenies. Genome Res. 20, 110–121. https://doi.org/10.1101/gr.097857.109

Prummel, K.D., Hess, C., Nieuwenhuize, S., Parker, H.J., Rogers, K.W., Kozmikova, I., Racioppi, C., Brombacher, E.C., Czarkwiani, A., Knapp, D., Burger, S., Chiavacci, E., Shah, G., Burger, A., Huisken, J., Yun, M.H., Christiaen, L., Kozmik, Z., Müller, P., Bronner, M., Krumlauf, R., Mosimann, C., 2019. A conserved regulatory program initiates lateral plate mesoderm emergence across chordates. Nat. Commun. 10. https://doi.org/10.1038/s41467-019-11561-7

Prummel, K.D., Nieuwenhuize, S., Mosimann, C., 2020. The lateral plate mesoderm. Dev. Camb. 147. https://doi.org/10.1242/dev.175059

Qiu, Q., Chen, H., Johnson, R.L., 2009. *Lmx1b* -expressing cells in the mouse limb bud define a dorsal mesenchymal lineage compartment. genesis 47, 224–233. https://doi.org/10.1002/dvg.20430

Quinlan, A.R., Hall, I.M., 2010. BEDTools: a flexible suite of utilities for comparing genomic features. Bioinformatics 26, 841–842. https://doi.org/10.1093/bioinformatics/btq033

Ramírez, F., Dündar, F., Diehl, S., Grüning, B.A., Manke, T., 2014. deepTools: a flexible platform for exploring deep-sequencing data. Nucleic Acids Res. 42, W187–W191. https://doi.org/10.1093/nar/gku365

Riddle, R.D., Johnson, R.L., Laufer, E., Tabin, C., 1993. Sonic hedgehog mediates the polarizing activity of the ZPA. Cell 75, 1401–1416. https://doi.org/10.1016/0092-8674(93)90626-2

Rivera-Pérez, J.A., Magnuson, T., 2005. Primitive streak formation in mice is preceded by localized activation of Brachyury and Wnt3. Dev. Biol. 288, 363–371. https://doi.org/10.1016/j.ydbio.2005.09.012

Robertson, E.J., 2014. Dose-dependent Nodal/Smad signals pattern the early mouse embryo. Semin. Cell Dev. Biol. 32, 73–79. https://doi.org/10.1016/j.semcdb.2014.03.028

Robinson, M.D., McCarthy, D.J., Smyth, G.K., 2009. edgeR : a Bioconductor package for differential expression analysis of digital gene expression data. Bioinformatics 26, 139–140. https://doi.org/10.1093/bioinformatics/btp616

Robinton, D.A., Chal, J., Lummertz da Rocha, E., Han, A., Yermalovich, A.V., Oginuma, M., Schlaeger, T.M., Sousa, P., Rodriguez, A., Urbach, A., Pourquié, O., Daley, G.Q., 2019. The Lin28/let-7 Pathway Regulates the Mammalian Caudal Body Axis Elongation Program. Dev. Cell 48, 396-405.e3. https://doi.org/10.1016/j.devcel.2018.12.016

Rodriguez, A.M., Downs, K.M., 2017. Visceral endoderm and the primitive streak interact to build the fetal-placental interface of the mouse gastrula. Dev. Biol. 432, 98–124. https://doi.org/10.1016/j.ydbio.2017.08.026

Rodriguez, A.M., Jin, D.X., Wolfe, A.D., Mikedis, M.M., Wierenga, L., Hashmi, M.P., Viebahn, C., Downs, K.M., 2017. Brachyury drives formation of a distinct vascular branchpoint critical for fetal-placental arterial union in the mouse

gastrula. Dev. Biol. 425, 208–222. https://doi.org/10.1016/j.ydbio.2017.03.032

Rodríguez-Carballo, E., Lopez-Delisle, L., Zhan, Y., Fabre, P.J., Beccari, L., El-Idrissi, I., Huynh, T.H.N., Ozadam, H., Dekker, J., Duboule, D., 2017. The *HoxD* cluster is a dynamic and resilient TAD boundary controlling the segregation of antagonistic regulatory landscapes. Genes Dev. 31, 2264–2281. https://doi.org/10.1101/gad.307769.117

Ros, M.A., López-Martínez, A., Simandl, B.K., Rodriguez, C., Izpisúa Belmonte, J.C., Dahn, R., Fallon, J.F., 1996. The limb field mesoderm determines initial limb bud anteroposterior asymmetry and budding independent of *sonic hedgehog* or apical ectodermal gene expressions. Development 122, 2319–2330. https://doi.org/10.1242/dev.122.8.2319

Roscito, J.G., Sameith, K., Parra, G., Langer, B.E., Petzold, A., Moebius, C., Bickle, M., Rodrigues, M.T., Hiller, M., 2018. Phenotype loss is associated with widespread divergence of the gene regulatory landscape in evolution. Nat. Commun. 9, 4737. https://doi.org/10.1038/s41467-018-07122-z

Ross, S., Cheung, E., Petrakis, T.G., Howell, M., Kraus, W.L., Hill, C.S., 2006. Smads orchestrate specific histone modifications and chromatin remodeling to activate transcription. EMBO J. 25, 4490–4502. https://doi.org/10.1038/sj.emboj.7601332

Sasaki, H., 2015. Position- and polarity-dependent Hippo signaling regulates cell fates in preimplantation mouse embryos. Semin. Cell Dev. Biol. 47–48, 80–87. https://doi.org/10.1016/j.semcdb.2015.05.003

Satoh, Y., Haraguchi, R., Tracy, ·, Wright, J., Mansour, S.L., Partanen, J., Hajihosseini, M.K., Eswarakumar, V.P., Lonai, P., Yamada, G., 2004. Regulation of external genitalia development by concerted actions of FGF ligands and FGF receptors. Anat Embryol 208, 479–486. https://doi.org/10.1007/s00429-004-0419-9

Saunders, J.W., 1948. The proximo-distal sequence of origin of the parts of the chick wing and the role of the ectoderm. J. Exp. Zool. 108, 363–403. https://doi.org/10.1002/jez.1401080304

Scheibner, K., Schirge, S., Burtscher, I., Büttner, M., Sterr, M., Yang, D., Böttcher, A., Ansarullah, Irmler, M., Beckers, J., Cernilogar, F.M., Schotta, G., Theis, F.J., Lickert, H., 2021. Epithelial cell plasticity drives endoderm formation during gastrulation. Nat. Cell Biol. 23, 692–703. https://doi.org/10.1038/s41556-021-00694-x

Seifert, A.W., Bouldin, C.M., Choi, K.S., Harfe, B.D., Cohn, M.J., 2009a. Multiphasic and tissue-specific roles of sonic hedgehog in cloacal septation and external genitalia development. Development 136, 3949–3957. https://doi.org/10.1242/dev.042291

Seifert, A.W., Harfe, B.D., Cohn, M.J., 2008. Cell lineage analysis demonstrates an endodermal origin of the distal urethra and perineum. Dev. Biol. 318, 143–152. https://doi.org/10.1016/j.ydbio.2008.03.017

Seifert, A.W., Yamaguchi, T., Cohn, M.J., 2009b. Functional and phylogenetic analysis shows that *Fgf8* is a marker of genital induction in mammals but is not required for external genital development. Development 136, 2643–2651. https://doi.org/10.1242/dev.036830

Sekine, K., Ohuchi, H., Fujiwara, M., Yamasaki, M., Yoshizawa, T., Sato, T., Yagishita, N., Matsui, D., Koga, Y., Itoh, N., Kato, S., 1999. Fgf10 is essential for limb and lung formation. Nat. Genet. 21, 138–141. https://doi.org/10.1038/5096

Selever, J., Liu, W., Lu, M.F., Behringer, R.R., Martin, J.F., 2004. Bmp4 in limb bud mesoderm regulates digit pattern by controlling AER development. Dev. Biol. 276, 268–279. https://doi.org/10.1016/j.ydbio.2004.08.024

Sharma, R., Shafer, M.E.R., Bareke, E., Tremblay, M., Majewski, J., Bouchard, M., 2017. Bmp signaling maintains a mesoderm progenitor cell state in the mouse tailbud. Development dev.149955. https://doi.org/10.1242/dev.149955

Shen, M.M., 2007. Nodal signaling: developmental roles and regulation. Development 134, 1023–1034. https://doi.org/10.1242/dev.000166

Sheth, R., Barozzi, I., Langlais, D., Osterwalder, M., Nemec, S., Carlson, H.L., Stadler, H.S., Visel, A., Drouin, J., Kmita, M., 2016. Distal Limb Patterning Requires Modulation of cis-Regulatory Activities by HOX13. Cell Rep. 17, 2913–2926. https://doi.org/10.1016/j.celrep.2016.11.039

Simon, C.S., Downes, D.J., Gosden, M.E., Telenius, J., Higgs, D.R., Hughes, J.R., Costello, I., Bikoff, E.K., Robertson, E.J., 2017. Functional characterisation of cis-regulatory elements governing dynamic *Eomes* expression in the early mouse embryo. Development dev.147322. https://doi.org/10.1242/dev.147322

So, P.L., Danielian, P.S., 1999. Cloning and expression analysis of a mouse gene related to Drosophila odd-skipped. Mech. Dev. 84, 157–160. https://doi.org/10.1016/S0925-4773(99)00058-1

Soshnikova, N., Zechner, D., Huelsken, J., Mishina, Y., Behringer, R.R., Taketo, M.M., Crenshaw, E.B., Birchmeier, W., 2003. Genetic interaction between Wnt/β-catenin and BMP receptor signaling during formation of the AER and the dorsal-ventral axis in the limb. Genes Dev. 17, 1963–1968. https://doi.org/10.1101/gad.263003

Sridurongrit, S., Larsson, J., Schwartz, R., Ruiz-Lozano, P., Kaartinen, V., 2008. Signaling via the Tgf-β type I receptor Alk5 in heart development. Dev. Biol. 322, 208–218. https://doi.org/10.1016/j.ydbio.2008.07.038

Srinivas, S., Watanabe, T., Lin, C.-S., William, C.M., Tanabe, Y., Jessell, T.M., Costantini, F., 2001. Cre reporter strains produced by targeted insertion of EYFP and ECFP into the ROSA26 locus. BMC Dev. Biol. 1, 4. https://doi.org/10.1186/1471-213X-1-4

Srivastava, D., Thomas, T., Lin, Q., Kirby, M.L., Brown, D., Olson, E.N., 1997. Regulation of cardiac mesodermal and neural crest development by the

bHLH transcription factor, dHAND. Nat. Genet. 16, 154–160. https://doi.org/10.1038/ng0697-154

Stenvers, K.L., Tursky, M.L., Harder, K.W., Kountouri, N., Amatayakul-Chantler, S., Grail, D., Small, C., Weinberg, R.A., Sizeland, A.M., Zhu, H.-J., 2003. Heart and Liver Defects and Reduced Transforming Growth Factor ␤2 Sensitivity in Transforming Growth Factor ␤ Type III Receptor-Deficient Embryos. MOL CELL BIOL 23.

Sun, X., Lewandoski, M., Meyers, E.N., Liu, Y.-H., Maxson, R.E., Martin, G.R., 2000. Conditional inactivation of Fgf4 reveals complexity of signalling during limb bud development. Nat. Genet. 25, 83–86. https://doi.org/10.1038/75644

Suzuki, K., Adachi, Y., Numata, T., Nakada, S., Yanagita, M., 2012. Reduced BMP Signaling Results in Hindlimb Fusion with Lethal Pelvic/Urogenital Organ Aplasia: A New Mouse Model of Sirenomelia. PLoS ONE 7, 43453. https://doi.org/10.1371/journal.pone.0043453

Suzuki, K., Bachiller, D., Chen, Y.P.P., Kamikawa, M., Ogi, H., Haraguchi, R., Ogino, Y., Minami, Y., Mishina, Y., Ahn, K., Crenshaw, E.B., Yamada, G., 2003. Regulation of outgrowth and apoptosis for the terminal appendage: External genitalia: Development by concerted actions of BMP signaling. Development 130, 6209–6220. https://doi.org/10.1242/dev.00846

Szeto, D.P., Rodriguez-Esteban, C., Ryan, A.K., O'Connell, S.M., Liu, F., Kioussi, C., Gleiberman, A.S., Izpisua-Belmonte, J.C., Rosenfeld, M.G., 1999. Role of the Bicoid-related homeodomain factor Pitx1 in specifying hindlimb morphogenesis and pituitary development. Genes Dev. 13, 484–494. https://doi.org/10.1101/gad.13.4.484

Szumska, D., Pieles, G., Essalmani, R., Bilski, M., Mesnard, D., Kaur, K., Franklyn, A., El Omari, K., Jefferis, J., Bentham, J., Taylor, J.M., Schneider, J.E., Arnold, S.J., Johnson, P., Tymowska-Lalanne, Z., Stammers, D., Clarke, K., Neubauer, S., Morris, A., Brown, S.D., Shaw-Smith, C., Cama, A., Capra, V., Ragoussis, J., Constam, D., Seidah, N.G., Prat, A., Bhattacharya, S., 2008. VACTERL/caudal regression/Currarino syndrome-like malformations in mice with mutation in the proprotein convertase *Pcsk5*. Genes Dev. 22, 1465–1477. https://doi.org/10.1101/gad.479408

Tahara, N., Akiyama, R., Theisen, J.W.M., Kawakami, H., Wong, J., Garry, D.J., Kawakami, Y., 2018. Gata6 restricts Isl1 to the posterior of nascent hindlimb buds through Isl1 cis-regulatory modules. Dev. Biol. 434, 74–83. https://doi.org/10.1016/j.ydbio.2017.11.013

Tahara, N., Kawakami, H., Chen, K.Q., Anderson, A., Yamashita Peterson, M., Gong, W., Shah, P., Hayashi, S., Nishinakamura, R., Nakagawa, Y., Garry, D.J., Kawakami, Y., 2019. Sall4 regulates neuromesodermal progenitors and their descendants during body elongation in mouse embryos. Dev. Camb. Engl. 146. https://doi.org/10.1242/dev.177659

Takada, S., Stark, K.L., Shea, M.J., Vassileva, G., McMahon, J.A., McMahon, A.P., 1994. Wnt-3a regulates somite and tailbud formation in the mouse embryo. Genes Dev. 8, 174–189. https://doi.org/10.1101/gad.8.2.174

Takeuchi, J.K., Koshiba-Takeuchi, K., Suzuki, T., Kamimura, M., Ogura, K., Ogura, T., 2003. Tbx5 and Tbx4 trigger limb initiation through activation of the Wnt/Fgf signaling cascade. Development 130, 2729–2739. https://doi.org/10.1242/dev.00474

Tanaka, M., 2016. Developmental mechanism of limb field specification along the anterior-posterior axis during vertebrate evolution. J. Dev. Biol. 4, 18. https://doi.org/10.3390/jdb4020018

Tanaka, M., 2013. Molecular and evolutionary basis of limb field specification and limb initiation. Dev. Growth Differ. 55, 149–163. https://doi.org/10.1111/dgd.12017

Tarchini, B., Duboule, D., Kmita, M., 2006. Regulatory constraints in the evolution of the tetrapod limb anterior–posterior polarity. Nature 443, 985–988. https://doi.org/10.1038/nature05247

Tickle, C., Summerbell, D., Wolpert, L., 1975. Positional signalling and specification of digits in chick limb morphogenesis. Nature 254, 199–202. https://doi.org/10.1038/254199a0

Tonegawa, A., Funayama, N., Ueno, N., Takahashi, Y., 1997. Mesodermal subdivision along the mediolateral axis in chicken controlled by different concentrations of BMP-4. Development 124, 1975–1984.

Tortelote, G.G., Hernández-Hernández, J.M., Quaresma, A.J.C., Nickerson, J.A., Imbalzano, A.N., Rivera-Pérez, J.A., 2013. Wnt3 function in the epiblast is required for the maintenance but not the initiation of gastrulation in mice. Dev. Biol. 374, 164–173. https://doi.org/10.1016/j.ydbio.2012.10.013

Treichel, D., Schöck, F., Jäckle, H., Gruss, P., Mansouri, A., 2003. mBtd is required to maintain signaling during murine limb development. Genes Dev. 17, 2630–2635. https://doi.org/10.1101/gad.274103

Tschopp, P., Sherratt, E., Sanger, T.J., Groner, A.C., Aspiras, A.C., Hu, J.K., Pourquié, O., Gros, J., Tabin, C.J., 2014. A relative shift in cloacal location repositions external genitalia in amniote evolution. Nature 516, 391–394. https://doi.org/10.1038/nature13819

Tsiairis, C.D., McMahon, A.P., 2009. An Hh-Dependent Pathway in Lateral Plate Mesoderm Enables the Generation of Left/Right Asymmetry. Curr. Biol. 19, 1912–1917. https://doi.org/10.1016/j.cub.2009.09.057

Tzouanacou, E., Wegener, A., Wymeersch, F.J., Wilson, V., Nicolas, J.F., 2009. Redefining the Progression of Lineage Segregations during Mammalian Embryogenesis by Clonal Analysis. Dev. Cell 17, 365–376. https://doi.org/10.1016/j.devcel.2009.08.002

Ulgen, E., Ozisik, O., Sezerman, O.U., 2019. pathfindR: An R Package for Comprehensive Identification of Enriched Pathways in Omics Data Through

Active Subnetworks. Front. Genet. 10, 858. https://doi.org/10.3389/fgene.2019.00858

van Rooijen, C., Simmini, S., Bialecka, M., Neijts, R., van de Ven, C., Beck, F., Deschamps, J., 2012. Evolutionarily conserved requirement of Cdx for post-occipital tissue emergence. Development 139, 2576–2583. https://doi.org/10.1242/dev.079848

Verheyden, J.M., Sun, X., 2008. An Fgf/Gremlin inhibitory feedback loop triggers termination of limb bud outgrowth. Nature 454, 638–641. https://doi.org/10.1038/nature07085

Vinagre, T., Moncaut, N., Carapuço, M., Nóvoa, A., Bom, J., Mallo, M., 2010. Evidence for a Myotomal Hox/Myf Cascade Governing Nonautonomous Control of Rib Specification within Global Vertebral Domains. Dev. Cell 18, 655–661. https://doi.org/10.1016/j.devcel.2010.02.011

Walls, J.R., Coultas, L., Rossant, J., Henkelman, R.M., 2008. Three-Dimensional Analysis of Vascular Development in the Mouse Embryo. PLoS ONE 3, 2853. https://doi.org/10.1371/journal.pone.0002853

Wang, C., Wang, J.Y., Borer, J.G., Li, X., 2013. Embryonic Origin and Remodeling of the Urinary and Digestive Outlets. PLoS ONE 8, e55587. https://doi.org/10.1371/journal.pone.0055587

Wang, Q., Li, M., Wu, T., Zhan, L., Li, L., Chen, M., Xie, W., Xie, Z., Hu, E., Xu, S., Yu, G., 2022. Exploring Epigenomic Datasets by ChIPseeker. Curr. Protoc. 2, e585. https://doi.org/10.1002/cpz1.585

Wang, W., Chun, H., Baek, J., Sadik, J.E., Shirazyan, A., Razavi, P., Lopez, N., Lyons, K.M., 2019. The TGFβ type i receptor TGFβRI functions as an inhibitor of BMP signaling in cartilage. Proc. Natl. Acad. Sci. U. S. A. 116, 15570–15579. https://doi.org/10.1073/pnas.1902927116

Wang, Y., Venkatesh, A., Xu, J., Xu, M., Williams, J., Smallwood, P.M., James, A., Nathans, J., 2022. The WNT7A/WNT7B/GPR124/RECK signaling module plays an essential role in mammalian limb development. Development 149, dev200340. https://doi.org/10.1242/dev.200340

Warot, X., Fromental-Ramain, C., Fraulob, V., Chambon, P., Dolle, P., 1997. Gene dosage-dependent effects of the Hoxa-13 and Hoxd-13 mutations on morphogenesis of the terminal parts of the digestive and urogenital tracts. Development 124, 4781–4791. https://doi.org/10.1242/dev.124.23.4781

Watson, B., Feenstra, J., Van Arsdale, J., Rai-Bhatti, K., Kim, D., Coggins, A., Mattison, G., Yoo, S., Steinman, E., Pira, C., Gongol, B., Oberg, K., 2018. LHX2 Mediates the FGF-to-SHH Regulatory Loop during Limb Development. J. Dev. Biol. 6, 13. https://doi.org/10.3390/jdb6020013

Wellik, D.M., 2007. Hox patterning of the vertebrate axial skeleton. Dev. Dyn. 236, 2454–2463. https://doi.org/10.1002/dvdy.21286

Wellik, D.M., Capecchi, M.R., 2003. Hox10 and Hox11 genes are required to globally pattern the mammalian skeleton. Science 301, 363–367. https://doi.org/10.1126/science.1085672

Welscher, P., Fernandez-Teran, M., Ros, M.A., Zeller, R., 2002. Mutual genetic antagonism involving GLI3 and dHAND prepatterns the vertebrate limb bud mesenchyme prior to SHH signaling. Genes Dev. 16, 421–426. https://doi.org/10.1101/gad.219202

Wijgerde, M., Karp, S., McMahon, J., McMahon, A.P., 2005. Noggin antagonism of BMP4 signaling controls development of the axial skeleton in the mouse. Dev. Biol. 286, 149–157. https://doi.org/10.1016/j.ydbio.2005.07.016

Williams, M., Burdsal, C., Periasamy, A., Lewandoski, M., Sutherland, A., 2012. Mouse primitive streak forms in situ by initiation of epithelial to mesenchymal transition without migration of a cell population. Dev. Dyn. 241, 270–283. https://doi.org/10.1002/dvdy.23711

Williams, T.M., 2005. Group 13 HOX proteins interact with the MH2 domain of R-Smads and modulate Smad transcriptional activation functions independent of HOX DNA-binding capability. Nucleic Acids Res. 33, 4475–4484. https://doi.org/10.1093/nar/gki761

Wilson, V., Olivera-Martínez, I., Storey, K.G., 2009. Stem cells, signals and vertebrate body axis extension. Development 136, 2133–2133. https://doi.org/10.1242/dev.039172

Wrighton, K.H., Lin, X., Yu, P.B., Feng, X.-H., 2009. Transforming Growth Factor β Can Stimulate Smad1 Phosphorylation Independently of Bone Morphogenic Protein Receptors. J. Biol. Chem. 284, 9755–9763. https://doi.org/10.1074/jbc.M809223200

Wymeersch, F.J., Huang, Y., Blin, G., Cambray, N., Wilkie, R., Wong, F.C.K., Wilson, V., 2016. Position-dependent plasticity of distinct progenitor types in the primitive streak. eLife 5, 1–28. https://doi.org/10.7554/eLife.10042

Wymeersch, F.J., Skylaki, S., Huang, Y., Watson, J.A., Economou, C., Marek-Johnston, C., Tomlinson, S.R., Wilson, V., 2019. Transcriptionally dynamic progenitor populations organised around a stable niche drive axial patterning. Development dev.168161. https://doi.org/10.1242/dev.168161

Xi, Q., He, W., Zhang, X.H.-F., Le, H.-V., Massagué, J., 2008. Genome-wide Impact of the BRG1 SWI/SNF Chromatin Remodeler on the Transforming Growth Factor β Transcriptional Program. J. Biol. Chem. 283, 1146–1155. https://doi.org/10.1074/jbc.M707479200

Xi, Q., Wang, Z., Zaromytidou, A.-I., Zhang, X.H.-F., Chow-Tsang, L.-F., Liu, J.X., Kim, H., Barlas, A., Manova-Todorova, K., Kaartinen, V., Studer, L., Mark, W., Patel, D.J., Massagué, J., 2011. A Poised Chromatin Platform for TGF-β Access to Master Regulators. Cell 147, 1511–1524. https://doi.org/10.1016/j.cell.2011.11.032

Yamada, G., Suzuki, K., Haraguchi, R., Miyagawa, S., Satoh, Y., Kamimura, M., Nakagata, N., Kataoka, H., Kuroiwa, A., Chen, Y., 2006. Molecular genetic cascades for external genitalia formation: An emerging organogenesis program. Dev. Dyn. 235, 1738–1752. https://doi.org/10.1002/dvdy.20807

Yamaguchi, T.P., Bradley, A., McMahon, A.P., Jones, S., 1999. A Wnt5a pathway underlies outgrowth of multiple structures in the vertebrate embryo. Development 126, 1211–1223. https://doi.org/10.1242/dev.126.6.1211

Yamamoto, M., Beppu, H., Takaoka, K., Meno, C., Li, E., Miyazono, K., Hamada, H., 2009. Antagonism between Smad1 and Smad2 signaling determines the site of distal visceral endoderm formation in the mouse embryo. J. Cell Biol. 184, 323–334. https://doi.org/10.1083/jcb.200808044

Yamamoto, M., Saijoh, Y., Perea-Gomez, A., Shawlot, W., Behringer, R.R., Ang, S.-L., Hamada, H., Meno, C., 2004. Nodal antagonists regulate formation of the anteroposterior axis of the mouse embryo. Nature 428, 387–392. https://doi.org/10.1038/nature02418

Yang, L., Cai, C.L., Lin, L., Qyang, Y., Chung, C., Monteiro, R.M., Mummery, C.L., Fishman, G.I., Cogen, A., Evans, S., 2006. Isl1 Cre reveals a common Bmp pathway in heart and limb development. Development 133, 1575–1585. https://doi.org/10.1242/dev.02322

Yang, Y., Niswander, L., 1995. Interaction between the signaling molecules WNT7a and SHH during vertebrate limb development: Dorsal signals regulate anteroposterior patterning. Cell 80, 939–947. https://doi.org/10.1016/0092-8674(95)90297-X

Yeh, C.-Y., Huang, W.-H., Chen, H.-C., Meir, Y.-J.J., 2021. Capturing Pluripotency and Beyond. Cells 10, 3558. https://doi.org/10.3390/cells10123558

Young, T., Rowland, J.E., van de Ven, C., Bialecka, M., Novoa, A., Carapuco, M., van Nes, J., de Graaff, W., Duluc, I., Freund, J.-N., Beck, F., Mallo, M., Deschamps, J., 2009. Cdx and Hox Genes Differentially Regulate Posterior Axial Growth in Mammalian Embryos. Dev. Cell 17, 516–526. https://doi.org/10.1016/j.devcel.2009.08.010

Yuan, G., Yang, G., Zheng, Y., Zhu, X., Chen, Z., Zhang, Z., Chen, Y., 2015. The non-canonical BMP and Wnt/β-catenin signaling pathways orchestrate early tooth development. Development 142, 128–139. https://doi.org/10.1242/dev.117887

Zaidi, S.K., Sullivan, A.J., van Wijnen, A.J., Stein, J.L., Stein, G.S., Lian, J.B., 2002. Integration of Runx and Smad regulatory signals at transcriptionally active subnuclear sites. Proc. Natl. Acad. Sci. 99, 8048–8053. https://doi.org/10.1073/pnas.112664499

Zakany, J., Duboule, D., 2007. The role of Hox genes during vertebrate limb development. Curr. Opin. Genet. Dev. 17, 359–366. https://doi.org/10.1016/j.gde.2007.05.011

Zákány, J., Kmita, M., Duboule, D., 2004. A Dual Role for *Hox* Genes in Limb Anterior-Posterior Asymmetry. Science 304, 1669–1672. https://doi.org/10.1126/science.1096049

Zakin, L., Metzinger, C.A., Chang, E.Y., Coffinier, C., De Robertis, E.M., 2008. Development of the vertebral morphogenetic field in the mouse:

Interactions between Crossveinless-2 and Twisted Gastrulation. Dev. Biol. 323, 6–18. https://doi.org/10.1016/j.ydbio.2008.08.019

Zhang, H.T., Hiiragi, T., 2018. Symmetry Breaking in the Mammalian Embryo. Annu. Rev. Cell Dev. Biol. 34, 405–426. https://doi.org/10.1146/annurev-cellbio-100617-062616

Zhou, Z., Xie, J., Lee, D., Liu, Y., Jung, J., Zhou, L., Xiong, S., Mei, L., Xiong, W.-C., 2010. Neogenin Regulation of BMP-Induced Canonical Smad Signaling and Endochondral Bone Formation. Dev. Cell 19, 90–102. https://doi.org/10.1016/j.devcel.2010.06.016

Zhu, J., Nakamura, E., Nguyen, M.-T., Bao, X., Akiyama, H., Mackem, S., 2008. Uncoupling Sonic Hedgehog Control of Pattern and Expansion of the Developing Limb Bud. Dev. Cell 14, 624–632. https://doi.org/10.1016/j.devcel.2008.01.008

Zhu, J., Patel, R., Trofka, A., Harfe, B.D., Mackem, S., 2022. Sonic hedgehog is not a limb morphogen but acts as a trigger to specify all digits in mice. Dev. Cell 57, 2048-2062.e4. https://doi.org/10.1016/j.devcel.2022.07.016

Zhu, X., Huang, S., Zhang, L., Wu, Y., Chen, Y., Tao, Y., Wang, Y., He, S., Shen, S., Wu, J., Li, B., Guo, X., He, L., Ma, G., 2014. Constitutive Activation of Ectodermal β-Catenin Induces Ectopic Outgrowths at Various Positions in Mouse Embryo and Affects Abdominal Ventral Body Wall Closure. PLoS ONE 9, e92092. https://doi.org/10.1371/journal.pone.0092092

Zhu, X., Zhu, H., Zhang, L., Huang, S., Cao, J., Ma, G., Feng, G., He, L., Yang, Y., Guo, X., 2012. Wls-mediated Wnts differentially regulate distal limb patterning and tissue morphogenesis. Dev. Biol. 365, 328–338. https://doi.org/10.1016/j.ydbio.2012.02.019

Zúñiga, A., Haramis, A.-P.G., McMahon, A.P., Zeller, R., 1999. Signal relay by BMP antagonism controls the SHH/FGF4 feedback loop in vertebrate limb buds. Nature 401, 598–602. https://doi.org/10.1038/44157

Zúñiga, A., Michos, O., Spitz, F., Haramis, A.-P.G., Panman, L., Galli, A., Vintersten, K., Klasen, C., Mansfield, W., Kuc, S., Duboule, D., Dono, R., Zeller, R., 2004. Mouse *limb deformity* mutations disrupt a global control region within the large regulatory landscape required for *Gremlin* expression. Genes Dev. 18, 1553–1564. https://doi.org/10.1101/gad.299904

Zuzarte-Luís, V., Montero, J.A., Rodriguez-León, J., Merino, R., Rodríguez-Rey, J.C., Hurlé, J.M., 2004. A new role for BMP5 during limb development acting through the synergic activation of Smad and MAPK pathways. Dev. Biol. 272, 39–52. https://doi.org/10.1016/j.ydbio.2004.04.015

LIST OF FIGUERS

LIST OF BOXES

LIST OF TABLES

LIST OF ABBREVIATIONS

Acvr - Activin A Receptor
AER - Apical Ectodermal Ridge
Alk5 - Activin Receptor-Like Kinase 5
Alx4 - Aristaless-Like Homeobox 4
ANOVA - Analysis of Variance
ATAC-seq - Assay for Transposase-Accessible Chromatin using sequencing
AVE - Anterior Visceral Endoderm
BABB - Benzoic Alcohol:Benzyl Benzoate
BMP - Bone Morphogenetic Protein
Bmpr1 - Bone Morphogenetic Protein Receptor Type 1
BSA - Bovine Serum Albumin
CBP/EP300 - CREB (Cyclic-AMP Response Element Binding Protein) Binding Protein/ E1A Binding Protein of 300 Kda
Cdh1 – Cadherin 1
Cdh2 – Cadherin 2
cDNA – Complementary DNA
Cdx - Caudal Type Homeobox
Cer1 - Cerberus 1
ChIP - Chromatin Immunoprecipitation
cKO – Conditional Knock Out
CNH - Chordo-Neural Hinge
Col4a1 - Collagen Type IV Alpha 1 Chain
CPM - Counts per Million
CR – conserved region
CRISPR - Clustered Regularly Interspaced Short Palindromic Repeats
crRNA - CRISPR RNA
CV2 - Crossveinless 2
Cyp26a1 - Cytochrome P450 Family 26 Subfamily A Member 1
DA - Dorsal Aorta
DAPI - 4′,6-Diamidino-2-Phenylindole
DE - Definitive Endoderm
DEG - Differentially Expressed Gene
Dkk1 - Dickkopf WNT Signaling Pathway Inhibitor 1
DMEM - Dulbecco's Modified Eagle Medium
DMSO - Dimethyl Sulfoxide
DNA - Deoxyribonucleic Acid
dUE - Distal Urethral Epithelium

DVE - Distal Visceral Endoderm
E – Embryonic Day
E-cadherin - Epithelial Cadherin
EDTA - Ethylenediaminetetraacetic Acid
EMT - Epithelial to Mesenchymal Transition
emVE - Embryonic Visceral Endoderm
En1 - Engrailed Homeobox 1
Eomes - Eomesodermin
Epcam - Epithelial Cell Adhesion Molecule
ERK/MAPK - Extracellular Signal-Regulated Kinase/Mitogen-Activated Protein Kinase
ESC - Embryonic Stem Cells
ExE - Extra Embryonic Ectoderm
exVE - Extra-embryonic Visceral Endoderm
FBS – Fetal Bovine Serum
FDR – False Discovery Rate
FGF - Fibroblast Growth Factor
Fgfr - Fibroblast Growth Factor receptor
Fox - Forkhead Box
Gdf - Growth Differentiation Factor
Gli - Glioma-Associated Oncogene Homolog
Gli-A – Gli Activator
Gli3-R – Gli Repressor
GO - Gene Ontology
Grem1 – Gremlin1
gRNA – Guide RNA
GS-domain - Glycine/Serine-Rich Domain
GT - Genital Tubercle
GUAVA - Graphical User interface for the Analysis and Visualization of ATAC-seq data
Hand2 - Heart and Neural Crest Derivatives Expressed 2
HEK 293T - Human Embryonic Kidney 293T
HH - Hedgehog
HINT - Hmm-based IdeNtification of Transcription Factor Footprints
Hox - Homeobox
HP1γ - Heterochromatin Protein 1 Gamma
HRP - Horseradish Peroxidase
ICM - Inner Cell Mass
Ihh – Indian Hedgehog

IM - Intermediate Mesoderm
Irx - Iroquois Homeobox
Isl1 - ISL LIM Homeobox 1
Kb – Kilobase
KEGG - Kyoto Encyclopedia of Genes and Genomes
KO - Knock Out
Krt19 - Keratin 19
Lefty - Left-Right Determination Factor 1
LMP - Lateral Plate Mesoderm
Lmx1b - LIM Homeobox Transcription Factor 1 Beta
Log2FC – Log2 Fold Change
MACS2 - Model-based Analysis of ChIP-seq
mRNA - Messenger RNA
N-cadherin - Neural Cadherin
NBT/BCIP - 5-Bromo-4-Chloro-3-Indolyl-Phosphate/Nitro Blue Tetrazolium
NMC - Neuro-Mesodermal Competent
NMP - Neuro Mesodermal Progenitor
NSB - Node-Streak Border
OPT - Optical Projection Tomography
Osr1 - Odd-Skipped Related Transcription Factor 1
PAM - Protospacer Adjacent Motif
Pax2 - Paired Box 2
PBS - Phosphate-buffered saline
PCA - Principal Component Analysis
PCR - Polymerase Chain Reaction
PFA - Paraformaldehyde
PG - Paralog Group
pH3 – Phosphor Histon 3
Pitx1 - Paired Like Homeodomain 1
PrE - Primitive Endoderm
Prrx1 - Paired Related Homeobox 1
PS - Primitive Streak
Ptch1 - Patched 1
PVDF - Polyvinylidene Fluoride
qPCR – Quantitative PCR
R-SMAD - Receptor Regulated SMAD
RA - Retinoic Acid
RCF - Relative Centrifugal Force
rDA - Recurved Dorsal Aorta

RGM - Repulsive Guidance Molecule
RNA - Ribonucleic acid
RQN - RNA Quality Number
RT-PCR - Reverse Transcription–Polymerase Chain Reaction
Sall4 - Spalt Like Transcription Factor4
SBE - SMAD Binding Element
Shh - Sonic Hedgehog
SMARCA4 - SWI/SNF Related, Matrix Associated, Actin Dependent Regulator of Chromatin, Subfamily A, Member 4
Snai1 - Snail Family Transcriptional Repressor 1
SSC - Saline-Sodium Citrate
ssDNA – Single Stranded DNA
TAD - Topologically Associating Domain
TBS - Tris-Buffered Saline
Tbx - T-Box Transcription Factor
Tbxt - T-Box Transcription Factor T
TE - Trophectoderm
TF - Transcription Factor
Tgf-β - Transforming Growth Factor Beta
Tgfbr1 - Transforming Growth Factor Beta receptor 1
tracRNA - Trans-Activating CRISPR RNA
TRIM33 - Tripartite Motif Containing 33
tRNA – Transport RNA
Tsg - Twisted Gastrulation
TSS – Transcription Start Site
TUNEL - Terminal Deoxynucleotidyl Transferase dUTP Nick End Labeling
UE - Urethral Epithelium
VE - Visceral Endoderm
Vim - Vimentin
VOC - Vessel of Confluence
VST - Variance Stabilizing Transformation
Wif1 - WNT Inhibitory Factor 1
Wnt - Wingless-Related Integration Site
WT – Wild Type
ZPA - Zone of Polarizing Activity
ZRS - ZPA Regulatory Sequence

Apoio financeiro da FCT e do FSE no âmbito do Quadro Comunitário de Apoio, Bolsa no PD/BD/128437/2017

ITQB NOVA, Avenida da República, 2780-157 Oeiras, Portugal | Tel +351 214 469 100 | itqb.unl.pt